FOURTH ORDER SPECTRAL THEORY AND DIFFUSION-DRIVEN INSTABILITY

BY

JOOYEON CHUNG

DISSERTATION

Submitted in partial fulfillment of the requirements
for the degree of Doctor of Philosophy in Mathematics
in the Graduate College of the
University of Illinois at Urbana-Champaign, 2018

Urbana, Illinois

Doctoral Committee:

Professor Lee DeVille, Chair
Professor Richard S. Laugesen, Director of Research
Professor Jared Bronski
Associate Professor Zoi Rapti

ABSTRACT

In Part I, we study the spectrum of the one-dimensional vibrating free rod equation $u^{(4)} - \tau u'' = \mu u$ under tension ($\tau > 0$) or compression ($\tau < 0$). The eigenvalues μ as functions of the tension/compression parameter τ exhibit three distinct types of behavior. In particular, eigenvalue branches in the lower half-plane exhibit a cascading pattern of barely-avoided crossings.

We provide a complete description of the eigenfunctions and eigenvalues by implicitly parameterizing the eigenvalue curves. We also establish properties of the eigenvalue curves such as monotonicity, crossings, asymptotic growth, cascading and phantom spectral lines.

In Part II, we analyze diffusion-driven (Turing) instability of a reaction-diffusion system. The innovation is that we replace the traditional Laplacian diffusion operator with a combination of the fourth order bi-Laplacian operator and the second order Laplacian. We find new phenomena when the fourth order and second order terms are competing, meaning one of them stabilizes the system whereas the other destabilizes it. We characterize Turing space in terms of parameter values in the system, and also find criteria for instability in terms of the domain size and tension parameter.

To my parents and my advisor, for their love and support.

ACKNOWLEDGMENTS

Most results in Part I of this thesis are published in [7], joint with L. Mercredi Chasman. Support from the University of Illinois Research Board award RB17002 is gratefully acknowledged.

TABLE OF CONTENTS

CHAPTER 1

OVERVIEW

The first part of the thesis studies the spectrum of the one-dimensional vibrating free rod under tension and compression. We describe the spectral curves as functions of the tension/compression parameter by implicit parameterization. We also establish properties of the spectral curves such as monotonicity, crossings, asymptotic growth, and a cascading pattern of barely-avoided crossings. The analysis of the spectrum is particularly challenging for the first and second eigenvalue curves under compression (the sub-parabolic region). Most results in the first part of the thesis are published in [7] with L. Mercredi Chasman.

In the second part of the thesis we apply the results of the first part to analyze diffusion-driven (Turing) instability of a reaction-diffusion system in which diffusion is governed by a combination of the fourth order bi-Laplacian and the second order Laplacian. We find new phenomena in the case when the fourth order and second order diffusions are competing, meaning one of them stabilizes the system whereas the other destabilizes it. For instance, this competition leads to negative eigenvalues of the diffusion operator, which was not applicable in the standard Laplacian Turing analysis. Moreover, to refine understanding of the Turing space, we identify a cross-section of Turing space. Finally, we find that having negative eigenvalues for the diffusion operator does not by itself make Turing instability occur, and additional conditions need to be satisfied.

All figures presented in this thesis were created by the author using the programs *Mathematica* and *Matlab*.

Part I

Free rod spectrum under tension and compression

CHAPTER 2

INTRODUCTION TO THE FREE ROD SPECTRUM

This part of the thesis investigates the spectrum of a one-dimensional vibrating free rod under tension or compression, and finds unexpected behaviors in the compressive regime. We may take our domain to be $\Omega = (-1, 1)$; the spectrum of rods of other lengths can be recovered by rescaling.

2.1 Motivation — periodic boundary conditions

The spectrum of the periodic rod problem motivates our investigation of the spectrum of the free rod in the later chapters. The one-dimensional periodic rod eigenvalue problem is

$$u'''' - \tau u'' = \mu u$$

for $-1 < x < 1$, where $u(x)$ is a 2-periodic function on $\mathbb{R}$ and $\tau \in \mathbb{R}$ is called the tension parameter for reasons explained in the next section. The eigenvalues μ can be computed explicitly as

$$\mu_l^{\text{per}}(\tau) = (l\pi)^4 + \tau(l\pi)^2, \quad l \geq 0,$$

where eigenfunctions can be taken as the even function $u_{\text{e}}(x) = \cos(l\pi x)$ or the odd function $u_{\text{o}}(x) = \sin(l\pi x)$. Note that all the eigenvalues have multiplicity 2, except for $l = 0$. We illustrate the spectrum in (τ, μ)-plane, as shown in Figure 2.1. For the periodic case, we obtain explicit parameterizations of the spectral curves (straight lines). With a short calculation, we find the parabola $\mu = -(\tau + \pi^2)^2/4$ on which the intersections of consecutive eigenvalue branches lie.

In the first part of the thesis, we will see how the spectrum behaves differently when we change to the free boundary conditions. We see the spectrum of periodic boundary

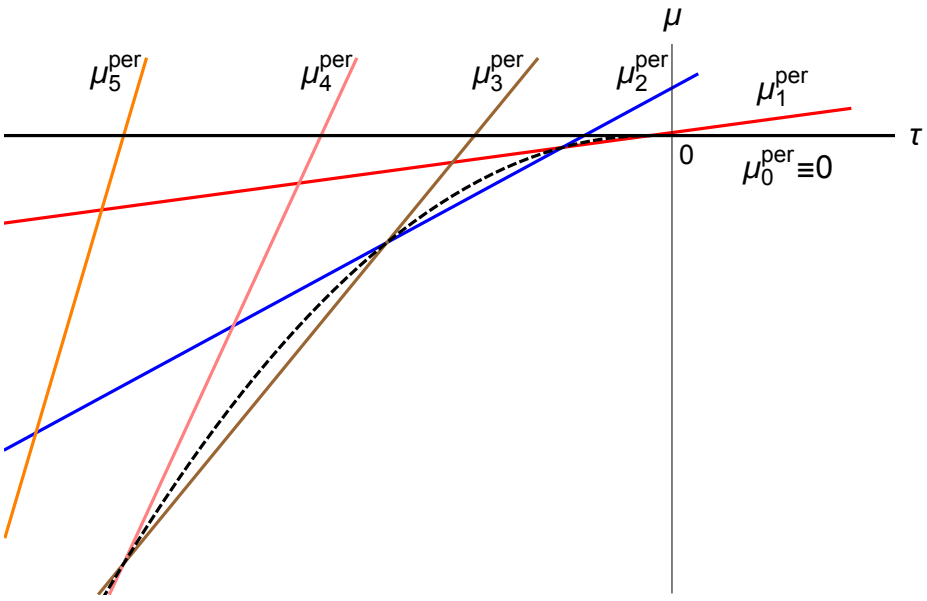

Figure 2.1: Spectrum of $u'''' - \tau u'' = \mu u$ on $(-1, 1)$ with periodic boundary conditions. The dashed curve is the parabola $\mu = -(\tau + \pi^2)^2/4$ on which the intersections of consecutive eigenvalue branches lie. (The figure suggests other patterns too, which the reader could explore.)

conditions and the spectrum of free boundary conditions behave in asymptotically similar way: compare Figure 2.1 and Figure 2.2. For the free boundary conditions, we cannot get an explicit parameterization, so instead we parameterized the spectral curves implicitly. There are actual crossings in the spectrum of periodic boundary conditions, whereas there are barely-avoided crossings along eigenvalue branches for free boundary conditions. A pattern of barely-avoided crossings leads to a pattern of nearly-linear segments. Also, the parabola $\mu = -(\tau + \pi^2)^2/4$ that the periodic spectral lines approximate is the same parabola that is approximated by some of the free rod spectral curves.

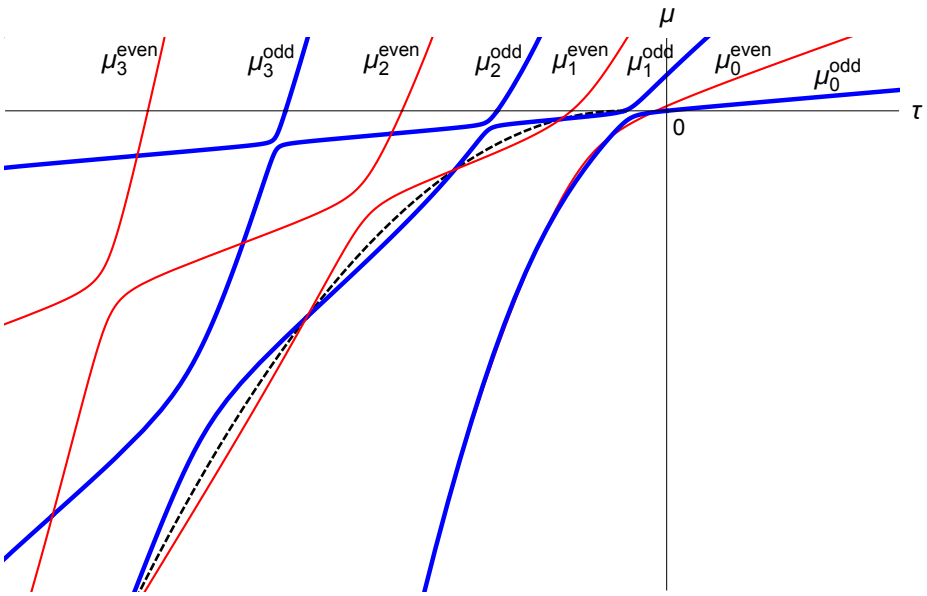

Figure 2.2: Spectrum of $\Delta^2 u - \tau \Delta u = \mu u$ with free boundary conditions. Blue curves (darker) are eigenvalue branches associated with odd eigenfunctions, red curves (lighter) are branches associated with even eigenfunctions. Note the many avoided crossings of the spectral curves. The spectrum is investigated in detail in this part of the thesis.

2.2 Free rod

The eigenvalues μ of the free rod depend on a tension parameter τ (discussed below) and are governed by the differential equation

$$u'''' - \tau u'' = \mu u \tag{2.1}$$

together with the boundary conditions

$$u'' = 0 \qquad \text{at } x = \pm 1, \tag{2.2}$$

$$u''' - \tau u' = 0 \qquad \text{at } x = \pm 1. \tag{2.3}$$

These boundary conditions arise naturally from the minimizers of the rod Rayleigh quotient, which takes the form

$$Q[u] = \frac{\int_{-1}^{1} |u''|^2 + \tau |u'|^2 \, dx}{\int_{-1}^{1} |u|^2 \, dx}. \tag{2.4}$$

It is straightforward to show (see [6]) that the Rayleigh quotient is coercive, and so the free rod eigenvalue problem has a complete discrete spectrum with an orthonormal eigenbasis.

Interpreted physically, the parameter τ represents the tension applied to the ends of the rod. The sign of the tension parameter τ determines whether the rod is under tension ($\tau > 0$) or compression ($\tau < 0$). Positive eigenvalues correspond to a vibrating rod, while $\mu < 0$ indicates the rod is buckling. The case of eigenvalue $\mu = 0$ corresponds to a translational mode.

The spectrum exhibits three types of behavior, shown in Figure 2.3. In the upper half-plane, we observe nearly-linear, non-intersecting eigenvalue branches alternating based on symmetry of the associated eigenfunctions. Behavior in the lower half-plane depends on whether the eigenvalue branches lie above or below the parabola $\mu = -\tau^2/4$, shown more clearly in Figure 2.4. We will refer to this parabola as the **critical parabola**, dividing the lower half-plane into **sub-** and **super-parabolic** regions. Only two spectral curves penetrate the sub-parabolic region, below the critical parabola; we refer to these as the first two buckling branches. Above the critical parabola, we see a pattern of barely-avoided crossings along eigenvalue branches of the same symmetry (called **cascading**), which we discuss further at the end of this chapter. We can also see that the spectrum has predictable asymptotic behavior in this region. We are particularly interested in how the behavior of the eigenvalue curves changes as we move from a vibrational mode ($\mu > 0$) to a buckling mode ($\mu < 0$).

We study the eigenvalues μ_k as functions of the tension parameter τ and consider rods under both tension and compression. In order to completely identify the spectrum, we parameterize the eigenvalue curves for each $\mu_k(\tau)$ for all real values of τ. Different parameterizations are used in three different regions in the (τ, μ)-plane: the upper half-plane, the super-parabolic region (third quadrant above the parabola $\mu = -\tau^2/4$), and the sub-parabolic region (third quadrant below the parabola $\mu = -\tau^2/4$). Note that the fourth quadrant contains no eigenvalues. This is easiest to see from the Rayleigh quotient (2.4), whose numerator is nonnegative when $\tau > 0$.

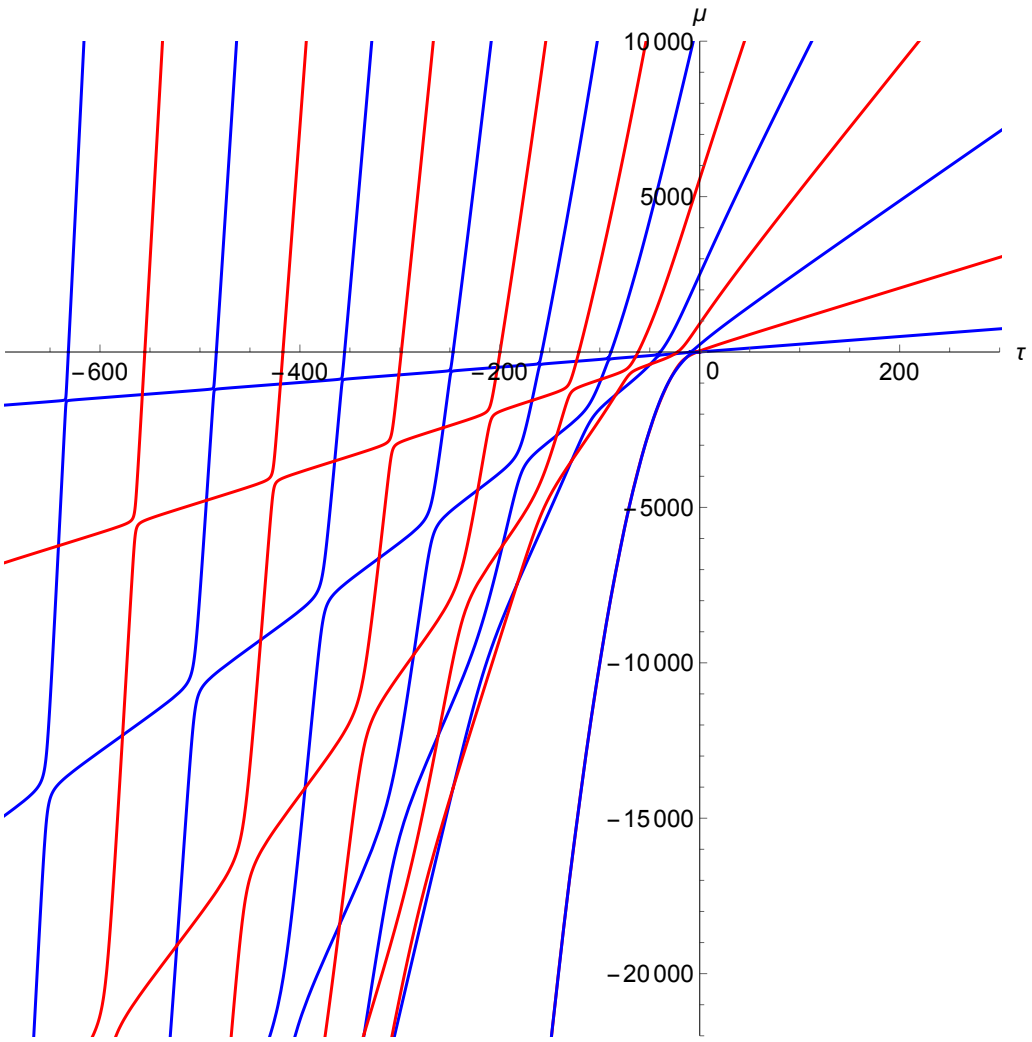

Figure 2.3: Spectrum of the free rod showing behavior under tension ($\tau > 0$) and compression ($\tau < 0$) with vibrational modes ($\mu > 0$) and buckling modes ($\mu < 0$). The spectrum shows repeated cascading behavior in the lower half-plane. Blue curves are eigenvalues associated with odd eigenfunctions; red are associated with even eigenfunctions.

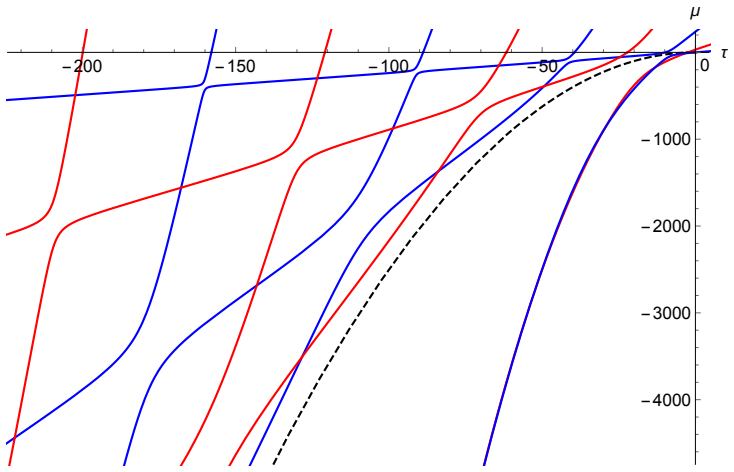

Figure 2.4: Spectral behavior in the lower half-plane. The dashed curve is the critical parabola $\mu = -\tau^2/4$ (not part of the spectrum), which divides two different types of solutions. Cascading occurs above the critical parabola. Below the critical parabola, there are only two eigenvalue curves, which intersect infinitely often (see Figure 6.1 later).

Scaling relation

This part of the thesis focuses on the interval $(-1, 1)$ of length 2. The general interval case can then be obtained from translation and the following scaling relation:

$$\mu_j\big((-R, R), \tau\big) = \frac{1}{R^4}\mu_j\left((-1, 1), R^2\tau\right), \qquad j = 1, 2, 3, \ldots$$

The rod eigenvalue equation can be considered with other boundary conditions. To the best of our knowledge, the spectrum of clamped rod (with $u = u' = 0$ at the endpoints) has not been analyzed in the manner of this part of the thesis.

The structure of the the first part of the thesis is as follows. In Chapter 3, we establish properties of symmetry of the eigenfunctions, and introduce bijections of regions of the (τ, μ)-plane that we will use for our parameterizations of eigenvalue branches. In Chapters 4 and 5, we analyze the eigenvalues in the upper half-plane and super-parabolic region, respectively, by finding eigenvalue conditions for each region and then parameterizing the eigenvalue branches. We also discuss monotonicity, crossing properties, asymptotic growth of the eigenvalue branches, cascading and phantom lines in the spectrum. In Chapter 6, we analyze the eigenvalues in the sub-parabolic region. Our approach to this region differs from the other regions, since our

usual parameterization approach will not work. We find the eigenvalue conditions and describe the behavior of the two eigenvalue branches that lie in this region. In addition, we establish a result involving intersections of a family of parabolas with the eigenvalue branches. We also identify the crossings of the odd and even eigenvalue branches.

2.3 Related literature

The free rod is the one-dimensional case of the free plate. Plate problems are fourth-order analogues of membrane problems, with the bi-Laplacian operator taking the place of the Laplacian. Recall the Laplacian of a function $u(x)$ in n dimension is

$$\Delta u = \nabla \cdot \nabla u = \frac{\partial^2 u}{\partial x_1^2} + \cdots + \frac{\partial^2 u}{\partial x_n^2}, \tag{2.5}$$

and the bi-Laplacian is $\Delta^2 u = \Delta\Delta u$. The bi-Laplacian is more difficult to work with than the Laplacian, as it is fourth-order and lacks some standard properties of the Laplacian. For instance, the maximum principle does not hold for the bi-Laplacian. However, fourth-order problems with appropriate boundary conditions have modeled a number of plates with physically relevant conditions; for instance, Sweers [30] recently gave a survey of sign- and positivity-preserving properties of rod and plate problems with certain boundary conditions.

The literature includes a number of papers on fourth-order eigenvalue problems involving a parameter playing a similar role to our τ. Notable work includes that of Kawohl, Levine, and Velte [15], who considered eigenvalues of a clamped vibrating plate under tension τ:

$$\Delta^2 u - \tau \Delta u = \gamma u$$

with clamped boundary conditions $u = |\nabla u| = 0$ on the boundary. Hence $\tau > 0$ corresponds to tension, and $\tau < 0$ to compression. They proved concavity with respect to the parameter of sums of low eigenvalues. Their paper treats the higher-dimensional case, where much less is known. More recently, Ashbaugh, Benguria, and Mahadevan [2] proved an isoperimetric inequality for the first eigenvalue of the clamped plate under compression for a small range of $\tau < 0$. We expect that in the

one-dimensional clamped rod problem, one could obtain an explicit parameterization of the spectrum and study properties such as cascading and eigenvalue crossings, similar to our work for the free rod problem in this part of the thesis.

Spectral problems with a tension-type parameter result naturally in a family of eigenvalue curves. For example, Grunau [13] considered the related one-dimensional buckling eigenvalue problem $u^{(4)} + au''' = -\lambda u''$ with clamped boundary conditions. He described the spectral curves as functions of the parameter a, and found that in appropriate parameter domains, these curves look different from those for the same equation under Navier boundary conditions.

We do not expect to get an explicit parameterization of eigenvalue curves in the higher-dimensional case, since the spectrum depends on the shape of the plate. However, one can establish relationships between plate and membrane eigenvalues, and between the plate eigenvalues and buckling energies (τ values for $\mu = 0$), in the forms of inequalities. Payne [26] derived such inequalities for both the eigenvalues of the buckling problem and the vibrational eigenvalues for the clamped plate. These include linear (in τ) upper bounds on single vibrational eigenvalues, and linear lower bounds on their sums, with coefficients given by the buckling energies. For the free rod, we observe nearly-linear behavior for all positive (vibrational) eigenvalues (see Chapter 4), with approximate slope given by the free membrane eigenvalues. Linear relationships between free rod eigenvalues and free rod buckling energies also appear in the phantom spectral lines.

Avoided crossings and cascading

The phenomena of avoided crossings and cascading arise in a variety of spectral problems, and have been studied in a number of second-order problems with a parameter. These terms are not well-defined mathematically, although [14] provides a precise definition of avoided crossing in the context of their work, and avoided crossings have long history in quantum mechanics; see [12, pp. 119–121].

The phenomena are generally identified visually, as qualitative properties of the spectrum. We use the term **avoided crossing** if two spectral curves come close together, nearly intersecting, but then veer away sharply. By **cascading**, we mean that as τ increases, a spectral curve exhibits drastic changes in slope at nearly-periodic intervals, with a relatively steady rate of increase between these transition periods.

These regions of alternating steady-then-sharp-increase create a pattern of **phantom spectral lines**, as discussed in Section 5.3 of Chapter 5.

Avoided crossings (also called quasi-crossings) of eigenvalues for a Coulomb centers problem were first studied by Komarov and Slavyanov [17]. To the best of the author's knowledge, the term cascading was first used by Gesztesy *et al.* in [10], which investigated cascading of eigenvalues of a family of Schrödinger eigenvalue problems. Also, avoided crossings and cascading occur in a family of Heun's differential equation problems. For instance, Slavyanov and Veshev [29] showed in 1997 that avoided crossings of a particular family occur periodically with respect to the parameter, and Bay *et al.* [3] calculated avoided crossings of eigenvalue curves of the quartic oscillator of Heun's differential equation and showed dependence of the gap of avoided crossings on asymmetry of the parameter. More recently, in 2007, Hineman and Neuberger [14] considered avoided crossings of eigenvalues of nonlinear second-order PDE's on certain regions and suggested some numerical techniques to solve these problems.

Avoided crossings and cascading are in principle distinct phenomena, but they seem to be connected, since cascading occurs when there is a nearly-periodic pattern of avoided crossings, such as in this part of the thesis.

CHAPTER 3

PRELIMINARIES

In this chapter, we establish two results that will aid our treatment of the spectrum. We prove a result about the symmetry of the eigenfunctions which allows us to assume all eigenfunctions are either odd or even on the open interval $(-1, 1)$, simplifying the solving of the boundary value problem. We then define three bijections of portions of the (τ, μ)-plane, which will allow us to parameterize the spectral curves.

3.1 Reduction to odd and even eigenfunctions

Before embarking on the classification of the eigenvalues, we show that we need only consider odd and even solutions to the eigenvalue equation (2.1).

Note that if $u(x)$ is an eigenfunction satisfying the partial differential equation (2.1) and the boundary conditions (2.2) and (2.3), then by symmetry so is $u(-x)$, with the same eigenvalue μ. The odd and even parts of u can be expressed as

$$u_o(x) = \frac{u(x) - u(-x)}{2} \quad \text{and} \quad u_e(x) = \frac{u(x) + u(-x)}{2}.$$

Thus u_o and u_e are either both solutions of (2.1) with the same eigenvalue, or (in the case that u is purely odd or purely even), one of them is zero everywhere. Because $u(x)$ and $u(-x)$ both satisfy the boundary conditions, u_o and u_e will also satisfy them. Since every eigenfunction is a linear combination of its odd and even parts, it suffices to look only for even and odd eigenfunctions. We will refer to eigenvalues associated with odd and even eigenfunctions as odd and even eigenvalues, respectively.

3.2 Bijections of the plane

In this section, we state and prove the bijections of portions of the (τ, μ)-plane, which will be used in our parameterizations of the eigenvalue curves.

In later chapters, we find the general form of the eigenfunctions by factoring the eigenvalue equation (2.1). The factorization depends on the sign of the eigenvalue μ, and in some cases on the value of τ relative to μ. These differences in factorization correspond to the three different regions (upper half-plane, sub-parabolic, and super-parabolic) of the (τ, μ) plane. In each case, we will use the boundary conditions to precisely identify the form of the eigenfunctions.

Lemma 3.1 (Bijection Lemma)**.** *The following functions are bijective transformations on the indicated sets.*

1. *(Upper half-plane) The function*

$$F_1(a, b) = (-a^2 + b^2, a^2 b^2)$$

maps $\{(a, b) : a, b \geq 0\}$ *onto* $\{(\tau, \mu) : \tau \in \mathbb{R}, \mu \geq 0\}$.

2. *(Super-parabolic region) The function*

$$F_2(a, b) = (-a^2 - b^2, -a^2 b^2)$$

maps $\{(a, b) : a \geq b > 0\}$ *onto* $\{(\tau, \mu) : \tau < 0, -\tau^2/4 \leq \mu < 0\}$.

3. *(Sub-parabolic region) The function*

$$F_3(a, b) = (-2a^2 + 2b^2, -(a^2 + b^2)^2)$$

maps $\{(a, b) : a > b > 0\}$ *onto* $\{(\tau, \mu) : \tau < 0, \mu < -\tau^2/4\}$.

Proof. We construct explicit inverses of our functions as follows:

$$F_1^{-1}(\tau,\mu) = \Big(\sqrt{\frac{\sqrt{\tau^2+4\mu}-\tau}{2}}, \sqrt{\frac{\sqrt{\tau^2+4\mu}+\tau}{2}}\Big),$$
$$F_2^{-1}(\tau,\mu) = \Big(\frac{\sqrt{|\tau|+2\sqrt{|\mu|}}+\sqrt{|\tau|-2\sqrt{|\mu|}}}{2}, \frac{\sqrt{|\tau|+2\sqrt{|\mu|}}-\sqrt{|\tau|-2\sqrt{|\mu|}}}{2}\Big),$$
$$F_3^{-1}(\tau,\mu) = \Big(\frac{\sqrt{-\tau+\sqrt{\tau^2+|\tau^2+4\mu|}}}{2}, \frac{\sqrt{\tau+\sqrt{\tau^2+|\tau^2+4\mu|}}}{2}\Big).$$

Note that F_1^{-1} is well-defined on the region $\{(\tau,\mu) : \tau \in \mathbb{R}, \mu \geq 0\}$, the function F_2^{-1} is well-defined on the region $\{(\tau,\mu) : \tau < 0, -\tau^2/4 \leq \mu < 0\}$, and F_3^{-1} is well-defined on the region $\{(\tau,\mu) : \tau < 0, \mu < -\tau^2/4\}$. Hence all three functions are indeed bijections of the appropriate sets. □

Remark 3.2. It is obvious from the Rayleigh quotient (2.4) for the free rod that there is no negative eigenvalue when $\tau \geq 0$. That is, there are no eigenvalues in the fourth quadrant. For the sake of completeness, however, one could treat the fourth quadrant $\{(\tau,\mu) : \tau \geq 0, \mu \leq 0\}$ in the same way as the other regions. In this case, we would use the bijective transformation

$$F_4(a,b) = (a^2+b^2, -a^2b^2),$$

which maps $\{(a,b) : a \geq b \geq 0\}$ onto $\{(\tau,\mu) : \tau \geq 0, \mu \leq 0\}$. We could then show there is no eigenvalue pair in the fourth quadrant using methods similar to those in the next chapters.

CHAPTER 4

THE UPPER HALF-PLANE

In the next three chapters, beginning with this one, we determine the eigenvalues and eigenfunctions for the free rod and parameterize the spectral curves. We begin with the technically easiest case where the eigenvalue μ is nonnegative. The next chapter treats the more sophisticated case of negative eigenvalues — except for two eigenvalue branches that exhibit different behavior and are treated later, in Chapter 6.

The overall method for each of these three cases is similar: transform the parameters τ and μ to get a convenient form for the eigenfunctions and determine the eigenvalue relationship between the two parameters. In the first two cases, the eigenvalue condition "separates" the parameters, yielding an explicit parameterization. In the third exceptional case, they do not separate, and hence in that case we obtain only an implicit parameterization.

4.1 Eigenfunctions and eigenvalue conditions

We will treat the case of eigenvalue branches lying in the upper half-plane $\{(\tau, \mu) : \tau \in \mathbb{R}, \mu \geq 0\}$, where the eigenvalues are nonnegative. Recall that the eigenvalue equation has the form $u^{(4)} - \tau u'' = \mu u$; then the characteristic equation is $r^4 - \tau r^2 - \mu = 0$. As we will see, the upper half-plane corresponds to the case that the characteristic equation has real and purely-imaginary complex roots. We will identify the eigenfunctions, provide a complete description for the eigenvalues as functions of τ via parameterization, and identify some key properties of the eigenvalue curves.

The starting point for solving the eigenvalue equation is factoring the eigenvalue equation (2.1). When μ is non-negative, regardless of the value of τ, we may factor

the eigenvalue equation as

$$\left(\frac{d^2}{dx^2} + a^2\right)\left(\frac{d^2}{dx^2} - b^2\right) u = 0, \tag{4.1}$$

where $\mu = a^2 b^2$ and $\tau = b^2 - a^2$. We may take a and b to be nonnegative since $\mu \geq 0$.

Lemma 4.1 (Eigenfunctions and eigenvalue conditions)**.** *For all eigenvalues $\mu > 0$ and all $\tau \in \mathbb{R}$, one of the following must hold:*

1. *The eigenvalue μ is associated with an odd eigenfunction u_o of the form $u_o(x) = A\sin(ax) + B\sinh(bx)$, where A and B are nonzero constants, and a and b are nonnegative numbers such that $\mu = a^2 b^2$, $\tau = b^2 - a^2$, and*

$$a^3 \tan a = b^3 \tanh b. \tag{4.2}$$

2. *The eigenvalue μ is associated with an even eigenfunction u_e of the form $u_e(x) = C\cos(ax) + D\cosh(bx)$, where C and D are nonzero constants, and a and b are nonnegative numbers such that $\mu = a^2 b^2$, $\tau = b^2 - a^2$, and*

$$-a^3 \cot a = b^3 \coth b. \tag{4.3}$$

Lemma 4.2 (Zero eigenvalues)**.** *For all $\tau \in \mathbb{R}$, the constant function $u_e(x) \equiv 1$ is an even eigenfunction with eigenvalue $\mu = 0$.*

The eigenvalue $\mu = 0$ has multiplicity two under the following conditions on τ:

1. *$\tau = 0$. In this case, a second eigenfunction can be taken as the odd function $u_o(x) = x$.*

2. *$\tau = -(l\pi)^2$, any $l \in \mathbb{N}$. In this case, a second eigenfunction can be taken as the odd function $u_o(x) = \sin(ax)$.*

3. *$\tau = -(2l-1)^2\pi^2/4$, any $l \in \mathbb{N}$. In this case, a second eigenfunction can be taken as the even function $u_e(x) = \cos(ax)$.*

For all other values of τ, the eigenvalue $\mu = 0$ is simple.

Although we state the $\mu = 0$ case as a separate lemma, we treat both cases $\mu > 0$ and $\mu = 0$ in a single proof below.

Proof. It is easy to see that the constant function $u_e \equiv 1$ satisfies our boundary value problem for all τ and has an associated eigenvalue $\mu = 0$. We look now for non-constant solutions.

Since we are considering $\mu \geq 0$ and $\tau \in \mathbb{R}$, by Lemma 3.1.1, we may factor the eigenvalue equation as (4.1). The characteristic equation then becomes

$$r^4 + (a^2 - b^2)r^2 - a^2b^2 = 0.$$

Since $a, b \geq 0$, the above quartic equation has solutions $r = \pm ia, \pm b$. We must consider four cases, depending on the positivity of a and b.

Case 1: $a > 0$ and $b > 0$. In this case, $\mu = a^2b^2$ is positive and the differential equation has four linearly independent solutions: $e^{\pm iax}$ and $e^{\pm bx}$. Because we need consider only odd and even solutions, we express these solutions instead as the trigonometric functions $\sin(ax)$ and $\cos(ax)$ and hyperbolic trigonometric functions $\sinh(bx)$ and $\cosh(bx)$. Our possible solutions are then linear combinations of these, chosen according to symmetry.

Writing u_o for the odd eigenfunction and u_e for the even, we have

$$\begin{aligned} u_o(x) &= A\sin(ax) + B\sinh(bx), \\ u_e(x) &= C\cos(ax) + D\cosh(bx). \end{aligned}$$

Then by Lemma 3.1.1, the boundary conditions can be expressed in terms of a and b as follows:

$$\begin{cases} u'' = 0 & \text{when } x = \pm 1, \\ u''' + (a^2 - b^2)u' = 0 & \text{when } x = \pm 1. \end{cases}$$

We consider the odd eigenfunction first. We wish to determine which choices of a and b (and hence τ and μ) yield a solution to the boundary value problem. Applying the two boundary conditions yields

$$\begin{cases} Aa^2 \sin a - Bb^2 \sinh b = 0, \\ Aab^2 \cos a - Ba^2 b \cosh b = 0. \end{cases}$$

We require that our linear combination coefficients (A, B) be nontrivial, so the system's determinant must vanish. That is $-a^4 b \sin a \cosh b + ab^4 \cos a \sinh b = 0$. Since

a and b are nonzero, this is equivalent to

$$a^3 \tan a = b^3 \tanh b.$$

This gives us a condition on (a, b) that assures us of an odd solution to the eigenvalue problem.

For the even eigenfunction u_e, applying the boundary conditions gives us

$$\begin{cases} Ca^2 \cos a - Db^2 \cosh b = 0, \\ -Cab^2 \sin a - Da^2 b \sinh b = 0 \end{cases}$$

Once again, to have nontrivial linear combination coefficients (C, D), we require that the system's determinant be zero. That is, $-a^4 b \cos a \sinh b - ab^4 \sin a \cosh b = 0$, or equivalently, since a and b are nonzero,

$$-a^3 \cot a = b^3 \coth b.$$

Case 2: $a = 0$ and $b > 0$. In this case, our eigenvalue $\mu = 0$, and our tension parameter $\tau = b^2$ is positive.

We also note that here $r = 0$ is a double root of the characteristic equation, and so in place of $e^{\pm iax}$, the solutions we consider are e^{0x} and xe^{0x}. The solutions $e^{\pm bx}$ can still be expressed as hyperbolic trigonometric functions, and so when we consider the possible odd and even solutions, we may write

$$\begin{aligned} u_o(x) &= Ax + B \sinh(bx), \\ u_e(x) &= C + D \cosh(bx). \end{aligned}$$

For the odd eigenfunction u_o, applying the boundary conditions gives us

$$\begin{cases} Bb^2 \sinh b = 0, \\ Ab^2 = 0. \end{cases}$$

Since b is positive, there is no nontrivial (A, B) pair in this case, and there are no odd solutions of this form.

For the even eigenfunction u_e, applying the boundary conditions yields

$$\begin{cases} Db^2 \cosh b = 0, \\ 0 = 0. \end{cases}$$

Thus we must take the coefficient $D = 0$, and the only even eigenfunction is the constant solution $u_e(x) = C$.

Case 3: $a > 0$ and $b = 0$. As in the previous case, our eigenvalue $\mu = 0$, but this time $\tau = -a^2$ is negative.

The roots of the characteristic equation are now $r = \pm ia$ and a double root $r = 0$, so for the odd and even eigenfunctions, we obtain

$$\begin{aligned} u_o(x) &= A \sin(ax) + Bx, \\ u_e(x) &= C \cos(ax) + D. \end{aligned}$$

Applying the boundary conditions to the odd eigenfunction u_0 yields

$$\begin{cases} -Aa^2 \sin a = 0, \\ a^2 B = 0. \end{cases}$$

From this, we see that we must take $B = 0$. Therefore, $u_o(x)$ must have the form $A \sin(ax)$ for some $A \neq 0$, and the first boundary condition holds if and only if $\sin a = 0$. Thus $a = l\pi$ for some natural number l, and $\tau = -a^2 = -l^2\pi^2$.

For the even eigenfunction $u_e(x)$, applying the boundary conditions gives us

$$\begin{cases} -Ca^2 \cos a = 0, \\ 0 = 0. \end{cases}$$

Taking $C = 0$ yields the constant eigenfunction, which we have already discussed, so we assume $C \neq 0$ and instead impose the requirement $\cos a = 0$. This yields $a = (2l - 1)\pi/2$ for $l \in \mathbb{N}$, or equivalently $\tau = -(2l - 1)^2\pi^2/4$. For these values of τ, we therefore have an even function $u_e(x) = C \cos(ax)$ with associated eigenvalue $\mu = 0$, as desired.

Case 4: $a = 0$ and $b = 0$. In this case, both our eigenvalue μ and tension parameter τ are zero. Since $r = 0$ is a quadruple root of the characteristic equation, the general

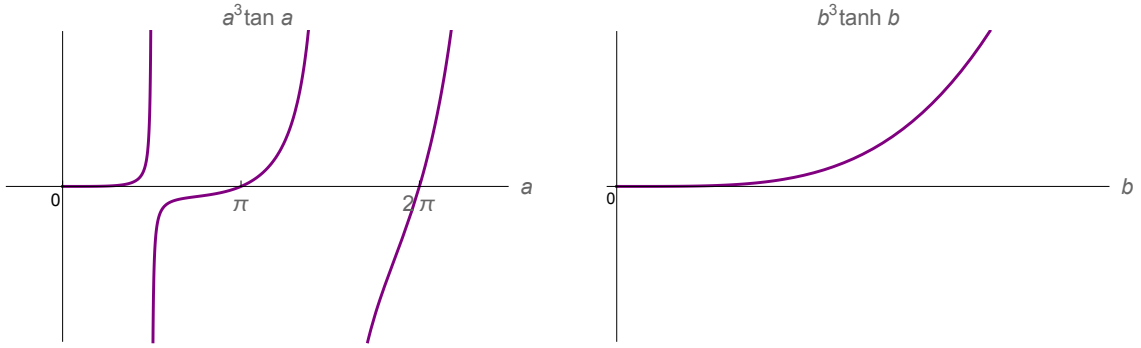

Figure 4.1: Upper half-plane eigenvalue condition $f_{\text{odd}}(a) = g_{\text{odd}}(b)$ (Definition 4.3) allows us to obtain b in terms of a.

solution u is a linear combination of 1, x, x^2, and x^3. As before we only consider odd and even solutions, and write

$$u_o(x) = Ax + Bx^3,$$
$$u_e(x) = C + Dx^2.$$

For the odd eigenfunction u_o, applying the boundary conditions gives us the same condition for both, namely $B = 0$. Therefore, $u_o(x) = Ax$ is an odd eigenfunction in this case.

Applying our boundary conditions to the even eigenfunction u_e yields only $2D = 0$ as a meaningful condition. Therefore, the constant function is the only even eigenfunction in this case. □

4.2 Parameterization of eigenvalue curves in the upper half-plane

Lemma 4.1 allows us to smoothly parameterize the eigenvalue branches lying in the upper half-plane.

Definition 4.3 (Parameterization for the upper half-plane)**.**

1. *(Odd case) Define*

$$f_{\text{odd}}(a) = a^3 \tan a, \quad g_{\text{odd}}(b) = b^3 \tanh b, \qquad \textit{for } a, b \geq 0.$$

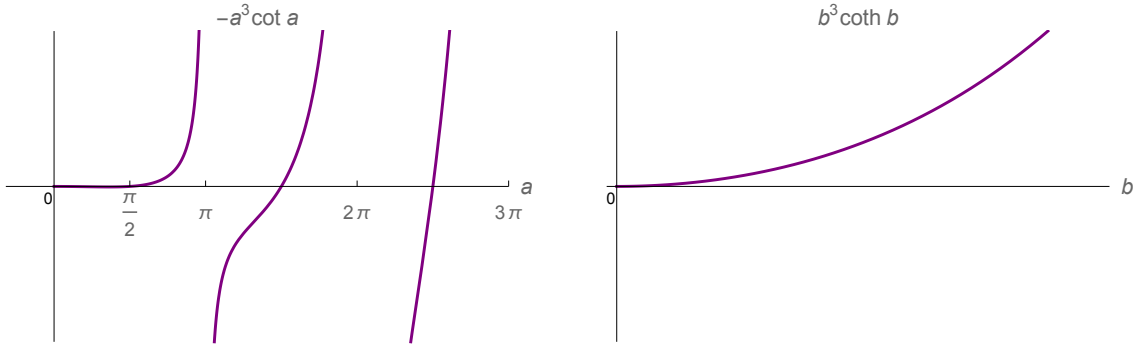

Figure 4.2: Upper half-plane eigenvalue condition $f_{\text{even}}(a) = g_{\text{even}}(b)$ (Definition 4.3) allows us to obtain b in terms of a.

Note that g_{odd} is increasing and hence invertible on its domain. Observe also that f_{odd} is one-to-one when restricted to the intervals $[l\pi, (l+1/2)\pi)$ for integers $l \geq 0$; this restriction is called lth branch of f_{odd}.

For any such l, we define

$$b_{\text{odd}}(a) = g_{\text{odd}}^{-1}(a^3 \tan a), \qquad l\pi \leq a < \left(l + \frac{1}{2}\right)\pi.$$

2. *(Even case) Define*

$$f_{\text{even}}(a) = -a^3 \cot a, \quad g_{\text{even}}(b) = b^3 \coth b, \qquad \text{for } a, b \geq 0.$$

The function g_{even} is increasing and hence invertible (and nonnegative). As before, we identify branches of f_{even} by restricting its domain; since g_{even} is positive, we consider only the positive branches of f_{even}, which are $[(l+1/2)\pi, (l+1)\pi)$ for integers $l \geq 0$. We then define

$$b_{\text{even}}(a) = g_{\text{even}}^{-1}(-a^3 \cot a), \qquad \left(l + \frac{1}{2}\right)\pi \leq a < (l+1)\pi.$$

The graphs of the functions $f_{odd}, g_{odd}, f_{even}$, and g_{even} appear in Figures 4.1 and 4.2.

Theorem 4.4 (Eigenvalues in the upper half-plane)**.** *The eigenvalue curves in the upper half-plane are indexed by $l \geq 0$. For each l there are two curves, according to whether the eigenfunction is odd or even:*

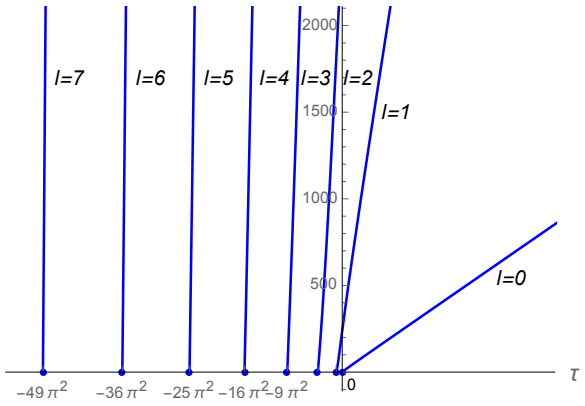

Figure 4.3: The odd eigenvalue branches $\mu_l^{\text{odd}}(\tau)$ in the upper half-plane, for $l = 0, \ldots, 7$ (Theorem 4.4).

1. *Odd (Figure 4.3): The eigenvalue curve* $(\tau, \mu_l^{\text{odd}}) = F_1(a, b_{\text{odd}}(a))$ *is parameterized by* $a \in [l\pi, (l + 1/2)\pi)$.

2. *Even (Figure 4.4): The eigenvalue curve* $(\tau, \mu_l^{\text{even}}) = F_1(a, b_{\text{even}}(a))$ *is parameterized by* $a \in [(l + 1/2)\pi, (l + 1)\pi)$.

3. *Zero eigenvalue: For all* $\tau \in \mathbb{R}$, *the eigenvalue* $\mu = 0$ *has constant eigenfunction (which can be regarded as a translational mode of the rod).*

Proof. This theorem follows immediately from our work for Lemmas 4.1, 4.2 and our definitions in Definition 4.3. □

4.3 Properties of the eigenvalue curves in the upper half-plane

In this section, we state and prove several properties of the eigenvalue branches lying in the upper half-plane. We also state some properties which are clear from numerical investigation but for which we do not have rigorous proof. Our first results, about intersections of eigenvalue branches, follow from our parameterizations.

Proposition 4.5 (Nonintersection of Eigenvalue Curves)**.** *Intersection of eigenvalue branches in the open upper half-plane does not occur. More precisely, for all indices*

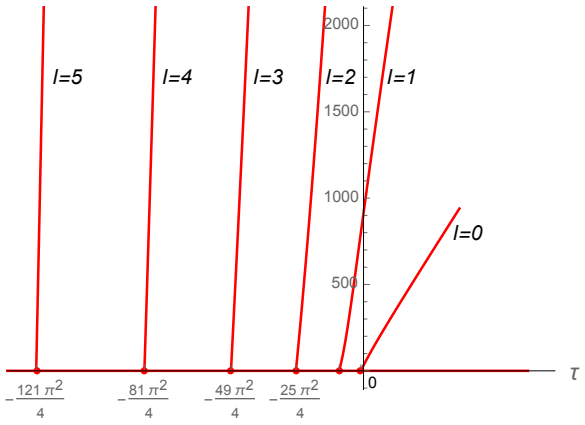

Figure 4.4: The even eigenvalue branches $\mu_l^{\text{even}}(\tau)$ in the upper half-plane, for $l = 0, \ldots, 5$ and the additional zero branch $\mu \equiv 0$ (Theorem 4.4).

l_1, l_2, we have

$$\begin{aligned}
&\mu_{l_2}^{\text{odd}}(\tau) > \mu_{l_1}^{\text{odd}}(\tau) && \text{when } l_2 > l_1 \geq 0 \text{ and } \tau \geq -(l_1\pi)^2,\\
&\mu_{l_2}^{\text{even}}(\tau) > \mu_{l_1}^{\text{even}}(\tau) && \text{when } l_2 > l_1 \geq 0 \text{ and } \tau \geq -\left((l_1 + 1/2)\pi\right)^2,\\
&\mu_{l_2}^{\text{even}}(\tau) > \mu_{l_1}^{\text{odd}}(\tau) && \text{when } l_2 \geq l_1 \geq 0 \text{ and } \tau \geq -(l_1\pi)^2,\\
&\mu_{l_2}^{\text{odd}}(\tau) > \mu_{l_1}^{\text{even}}(\tau) && \text{when } l_2 > l_1 \geq 0 \text{ and } \tau \geq -\left((l_1 + 1/2)\pi\right)^2.
\end{aligned}$$

Proof. By Lemma 3.1.1, since the (a, b) and (τ, μ) pairs are in one-to-one correspondence, we cannot have different (a, b) pairs mapped to the same (τ, μ). Thus the only possible intersections occur when different-symmetry eigenvalues have the same (a, b) values.

Suppose the odd and even eigenvalue curves intersect. At this point, a and b satisfy eigenvalue conditions (4.2) and (4.3) simultaneously:

$$\begin{aligned}
a^3 \tan a &= b^3 \tanh b,\\
-a^3 \cot a &= b^3 \coth b.
\end{aligned}$$

When $b > 0$, we can conclude that both $\tan a$ and $\cot a$ are finite and so multiplication of equations gives $-a^6 = b^6$, which has no solution. When $b = 0$, the conditions $a^3 \tan a = 0$ and $-a^3 \cot a = 0$ are simultaneously satisfied only when $a = 0$. Therefore, (4.2) and (4.3) both hold only when $(a, b) = (0, 0)$, which corresponds to

$(\tau, \mu) = (0, 0)$ that does not belong to the open upper half-plane. □

Proposition 4.6 (Direction of parameterization)**.** *For a fixed $l \geq 0$, the parameterizations of $\mu_l^{\text{odd}}(\tau)$ and $\mu_l^{\text{even}}(\tau)$ in the upper half-plane in Theorem 4.4 travel to the right and upwards. That is, τ and μ are strictly increasing functions of a.*

Proof. For the purpose of this proof, we will show that the eigenvalue curves parameterized according to Theorem 4.4 are exactly those given by Poincaré's min-max characterization

$$\mu_j = \min_{S_j} \max_{u \in S_j} \frac{\int_{-1}^{1} |u''|^2 + \tau |u'|^2 \, dx}{\int_{-1}^{1} |u|^2 \, dx},$$

where S ranges over all j-dimensional subspaces of $H^2((-1, 1))$. Observe that the eigenvalue μ_j is increasing as a function of $\tau \in \mathbb{R}$.

Until now, we have used the terms "eigenvalue curve" and "eigenvalue branch" interchangeably. For the duration of this proof, we will use the former to refer to the parameterized curves, and denote them by $\mu_l^{\text{odd}}(\tau)$ and $\mu_l^{\text{even}}(\tau)$ for $l \geq 0$. The jth eigenvalue branch will mean the set of pairs (τ, μ_j) obtained from the Poincaré principle. Our goal is then to show that each eigenvalue branch corresponds to one of our parameterized curves and vice versa.

We will prove this by considering the inverse functions, that is, we consider τ as a function of μ. Then the eigenvalue curves can be thought of as graphs of functions $\tau_l^{\text{odd}}(\mu)$ and $\tau_l^{\text{even}}(\mu)$ for $l \geq 0$.

For any free rod eigenvalue μ associated with a nonconstant eigenfunction u, the eigenvalue equation (2.1) with free boundary conditions is satisfied for (τ, μ) if and only if $-\tau$ is an eigenvalue for the equation

$$u^{(4)} - \mu u = -(-\tau) u'' \tag{4.4}$$

with boundary conditions arising naturally from the minimizers of the associated Rayleigh quotient (for $-\tau$), which has the form

$$R[v] = \frac{\int_{-1}^{1} |v''|^2 - \mu |v|^2 \, dx}{\int_{-1}^{1} |v'|^2 \, dx}.$$

We take $v \in H^2((-1, 1))$ such that $\int_{-1}^{1} v \, dx = 0$, so that v is not a constant function. Note that (4.4) with $\mu = 0$ is the well-known "buckling eigenvalue" problem.

Fix an index l and consider the lth odd eigenvalue curve, parameterized by $a \in [l\pi, (l+1/2)\pi)$. Recall that our parameterization allows us to consider b as a function of a. We know from the parameterization that $\mu = a^2b^2$ depends smoothly on a with derivative

$$\frac{d\mu}{da} = 2ab^2 + 2a^2b\frac{db}{da}.$$

We also know $\mu = 0$ when $a = l\pi$ and that $\mu \to \infty$ as $a \to (l+1/2)\pi$.

From implicit differentiation of the odd eigenvalue condition (4.2), we obtain

$$\frac{db}{da} = \frac{3a^2 \tan a + a^3 \sec^2 a}{3b^2 \tanh b + b^3(1 - \tanh^2 b)}.$$

The denominator is always positive since $\tanh b < 1$ for all $b > 0$. The numerator is positive for $a \in [l\pi, (l+1/2)\pi)$, and therefore, db/da is positive for all a under consideration. Thus $d\mu/da > 0$, and so we may regard the curve as being parameterized by $\mu \in [0, \infty)$. The argument is similar for the even eigenvalue curves.

Now we write the eigenvalue curves as graphs in the (μ, τ)-plane of the functions

$$\tau = \tau_l^{\text{odd}}(\mu) \qquad \text{or} \qquad \tau = \tau_l^{\text{even}}(\mu),$$

with $\mu \in [0, \infty)$. From Proposition 4.5, we know the ordering of $\tau_l^{\text{odd}}(0)$'s and $\tau_l^{\text{even}}(0)$'s for each $l \geq 0$. In other words,

$$\tau_l^{\text{odd}}(0) > \tau_l^{\text{even}}(0) > \tau_{l+1}^{\text{odd}}(0) > \tau_{l+1}^{\text{even}}(0) > \dots$$

Again from Proposition 4.5, the eigenvalue curves for nonconstant eigenfunctions do not intersect and the ordering at $\mu = 0$ is maintained. That is,

$$\tau_l^{\text{odd}}(\mu) > \tau_l^{\text{even}}(\mu) > \tau_{l+1}^{\text{odd}}(\mu) > \tau_{l+1}^{\text{even}}(\mu) > \dots \quad \forall \mu \in [0, \infty).$$

Therefore, these curves are in fact the eigenvalue branches for the buckling eigenvalues $\tau_1(\mu), \tau_2(\mu), \dots$ of (4.4). So we have

$$\tau_0^{\text{odd}} = \tau_1,$$
$$\tau_0^{\text{even}} = \tau_2,$$
$$\text{etc.}$$

The Rayleigh quotient for (4.4) tells us that the jth eigenvalue $-\tau_j(\mu)$ is decreasing as a function of μ for each j, and so $\tau_j(\mu)$ is increasing as a function of μ. Hence $\tau_l^{\text{odd}}(\mu)$ and $\tau_l^{\text{even}}(\mu)$ are increasing as functions of μ. They are in fact strictly increasing; otherwise, a single τ-value would correspond to a whole interval of μ-values solving the free rod boundary value problem, which is impossible since the spectrum is discrete. Therefore, each eigenvalue curve is strictly increasing for τ as a function of μ. Hence by inverting to get μ as a function of τ, we see that each eigenvalue curve $\mu_l^{\text{odd}}(\tau)$ and $\mu_l^{\text{even}}(\tau)$ are strictly increasing as functions of τ. □

We also list a number of properties of the eigenvalue branches. We proved the first two and the others are not proved, but we could numerically justify. We state only the odd case, since the arguments are similar for the even case.

1. **As l increases, the corresponding eigenvalue branch lies farther to the left.**

   This can easily be seen in Figures 4.3 and 4.4, or by Proposition 4.5.

2. **Vertical intercepts of parameterized eigenvalue curves.** The vertical intercept of the lth eigenvalue branch occurs at $(0, a^4)$, for some a. As $l \to \infty$, we have $a = l\pi + \pi/4 + o(1)$.

   This can be justified algebraically as follows. Vertical intercepts occur when $\tau = 0$, and hence $a = b$. We want values of a such that $a^3 \tan a = a^3 \tanh a$, and so we must have $a = 0$ or $\tan a = \tanh a$. The above $o(1)$ error term for a can be improved with better control on how quickly $\tanh(a) \to 1$ as $a \to \infty$.

3. **The eigenvalue curves become linear in limiting cases.**

   (a) As l increases, the eigenvalue curve looks more like a straight line. This tendency is more pronounced as l increases.

   Proof. (Sketch.) For large values of l, the graph of $y = a^3 \tan a$ becomes quite steep at $a = l\pi$. If a is increased some small amount ε, from $l\pi$ to $l\pi + \varepsilon$, the corresponding b value (see Figure 4.1) increases by a large amount and thus $\tau = -a^2 + b^2$ also increases greatly. Recall μ can be expressed in terms of a and τ as

   $$\mu = a^2\tau + a^4 \qquad \text{where } \tau = -a^2 + b^2.$$

Note that τ is growing quickly while $a^2 = (l\pi)^2 + O(\varepsilon)$ and $a^4 = (l\pi)^4 + O(\varepsilon)$ remain relatively constant, and hence μ is approximately linear as a function of τ for this small range of a values, until a is close to $(l + 1/2)\pi$. □

(b) As τ tends to ∞, the eigenvalue curves converge to straight lines with slopes corresponding to the eigenvalues of a free vibrating string.

The connection between the free rod and free string can most intuitively be seen by considering the Rayleigh quotients. The Rayleigh quotient for the free string is given by

$$Q_s[u] = \frac{\int_{-1}^{1} |u'|^2 \, dx}{\int_{-1}^{1} u^2 \, dx}.$$

If we divide the rod Rayleigh quotient Q (from (2.4)) by τ, the result can be written as

$$\frac{Q[u]}{\tau} = \frac{1}{\tau} \frac{\int_{-1}^{1} |u''|^2 \, dx}{\int_{-1}^{1} u^2 \, dx} + Q_s[u].$$

Note that for a fixed function u and large values of τ, the string Rayleigh quotient dominates. We thus expect the slopes of the eigenvalue curves to approach the eigenvalues of the free string. Although there are complications with the spaces over which we take the infima, this almost-linear relationship between the eigenvalues of the string and the rod can be made rigorous in the case of the first nonzero eigenvalue in all dimensions (see [6]).

In just one dimension, we can make a stronger case by investigating the boundary value problem directly:

Proof. Recall $\tau = -a^2 + b^2$ and $\mu = a^2 b^2 = a^2 \tau + a^4$. Fix l, so that we consider only the lth branch of the eigenvalue curve and of the $a^3 \tan a$ graph. As a increases from $l\pi$ to $(l + 1/2)\pi$, the corresponding b also increases, and hence τ does as well.

Changing our perspective, as $\tau \to \infty$ (and hence $a^3 \tan(a) \to \infty$ along the lth branch), the value of a satisfying the eigenvalue condition approaches $(l + 1/2)\pi$. Thus we can consider a to be nearly constant for large τ, and

so we see that $\mu = a^2\tau + a^4$ is nearly linear in τ, with approximate slope $a^2 \approx (l + 1/2)^2\pi^2$. $\square$

CHAPTER 5

THE LOWER HALF-PLANE: SUPER-PARABOLIC REGION

In this chapter, we address the case of negative eigenvalues whose curves lie above the critical parabola $\mu = -\tau^2/4$ for all $\tau < 0$. We identify the eigenfunctions and derive the eigenvalue conditions from the natural boundary conditions. We also provide a complete description of the eigenvalues as functions of τ via parameterization, and identify some key properties of the eigenvalue curves.

5.1 Eigenvalue conditions in the super-parabolic region

As we will see, the region $\{(\tau, \mu) : \tau < 0, -\tau^2/4 \leq \mu < 0\}$ corresponds to the characteristic equation $r^4 - \tau r^2 - \mu = 0$ having purely imaginary roots. When μ and τ are both negative and satisfy $\mu \geq -\tau^2/4$, we may factor the eigenvalue equation as

$$\left(\frac{d^2}{dx^2} + a^2\right)\left(\frac{d^2}{dx^2} + b^2\right) u = 0, \tag{5.1}$$

where $\mu = -a^2b^2$ and $\tau = -a^2 - b^2$ by Lemma 3.1.2. We may take a and b to be positive since $\mu < 0$.

Lemma 5.1 (Eigenfunctions and eigenvalue conditions)**.** *For all $\tau < 0$ and eigenvalues μ satisfying $-\tau^2/4 \leq \mu < 0$, at least one of the following must hold:*

1. *The eigenvalue μ is associated with an odd eigenfunction u_o of the form $u_o(x) = A\sin(ax) + B\sin(bx)$, where A and B are nonzero constants, and a and b are positive numbers such that $\mu = -a^2b^2$, $\tau = -a^2 - b^2$, and*

$$a^3 \tan a = b^3 \tan b. \tag{5.2}$$

2. *The eigenvalue μ is associated with an even eigenfunction u_e of the form $u_e(x) =$*

$C\cos(ax) + D\cos(bx)$, *where* C *and* D *are nonzero constants, and* a *and* b *are positive numbers such that* $\mu = -a^2b^2$, $\tau = -a^2 - b^2$, *and*

$$a^3 \cot a = b^3 \cot b. \tag{5.3}$$

3. *The eigenvalue* μ *is associated with an even eigenfunction* $u_e(x) = C\cos(ax) + Dx\sin(ax)$, *where* C *and* D *are nonzero constants, and* $a \approx 1.13943$ *satisfies*

$$\sin(2a) = \frac{2a}{3}.$$

This is the only eigenvalue satisfying $\mu = -\tau^2/4$ *and occurs when* $\tau \approx -2.5966$ *and* $\mu \approx -1.6856$.

Proof. Since we are considering those (τ, μ) pairs satisfying $-\tau^2/4 \leq \mu < 0$ and $\tau < 0$, we may factor the eigenvalue equation as (5.1). By Lemma 3.1.2, the boundary conditions can be expressed in terms of a and b as follows:

$$\begin{cases} u'' = 0 & \text{when } x = \pm 1, \\ u''' + (a^2 + b^2)u' = 0 & \text{when } x = \pm 1. \end{cases}$$

From the factorization (5.1), the characteristic equation is

$$r^4 + (a^2 + b^2)r^2 + a^2b^2 = 0.$$

Since $a, b > 0$, the quartic equation has solutions $r = \pm ia, \pm ib$. We must consider two cases, depending on the multiplicities of the roots.

Case 1: $a \neq b$. In this case, the differential equation has four linearly independent solutions: $e^{\pm iax}$ and $e^{\pm ibx}$. Because we have shown that we need consider only odd and even solutions, we express these solutions instead as linear combinations of trigonometric functions, chosen according to symmetry.

Writing u_o for the odd eigenfunction and u_e for the even eigenfunction, we have

$$u_o(x) = A\sin(ax) + B\sin(bx),$$
$$u_e(x) = C\cos(ax) + D\cos(bx).$$

We consider the odd eigenfunction first. We wish to determine which choices of a and

b (and hence τ and μ) yield a solution to the boundary value problem. Applying the two boundary conditions yields

$$\begin{cases} -Aa^2 \sin a - Bb^2 \sin b = 0, \\ -Aab^2 \cos a - Ba^2 b \cos b = 0. \end{cases}$$

We require that our linear combination coefficients (A, B) be nontrivial, so the system's determinant must vanish. Since a and b are nonzero, this is equivalent to

$$a^3 \tan a = b^3 \tan b.$$

For the even eigenfunction u_e, applying the boundary conditions gives us

$$\begin{cases} -Ca^2 \cos a - Db^2 \cos b = 0, \\ Cab^2 \sin a + Da^2 b \sin b = 0, \end{cases}$$

and reasoning as before, we conclude that a, b must satisfy

$$a^3 \cot a = b^3 \cot b.$$

Case 2: $a = b$. In this case, we now have $\tau = -2a^2$ and $\mu = -a^4$, and thus $\mu = -\tau^2/4$. Therefore, this case corresponds to points (τ, μ) on the critical parabola.

Our characteristic equation becomes $r^4 + 2a^2 r^2 + a^4 = 0$, which has two double purely-imaginary roots $r = \pm ia$. Expressing the linearly independent solutions in terms of trigonometric functions, we have $\sin(ax)$, $\cos(ax)$, $x \sin(ax)$, and $x \cos(ax)$. We now have the odd and even eigenfunctions

$$\begin{aligned} u_o(x) &= A \sin(ax) + Bx \cos(ax), \\ u_e(x) &= C \cos(ax) + Dx \sin(ax). \end{aligned}$$

Applying our boundary conditions to the odd eigenfunction, we obtain

$$\begin{cases} -Aa^2 \sin a - 2Ba \sin a - Ba^2 \cos a = 0, \\ -Aa^3 \cos a + Ba^2 \cos a + Ba^3 \sin a = 0. \end{cases}$$

Again we require that our linear combination coefficients be nontrivial, so the system's

determinant must vanish. Thus $-3a^3 \sin a \cos b - a^4 = 0$, and since a is nonzero,

$$\sin(2a) = -\frac{2a}{3}.$$

This equation has no real solutions for $a > 0$, and so there is no odd solution in this case.

For the even eigenfunction u_e, applying the boundary conditions gives us

$$\begin{cases} -Ca^2 \cos a + 2Da \cos a - Da^2 \sin a = 0, \\ Ca^3 \sin a + Da^2 \sin a - Da^3 \cos a = 0. \end{cases}$$

This time, the requirement that (C, D) be nontrivial yields $-3a^3 \sin a \cos b + a^4 = 0$, or equivalently, since a is nonzero,

$$\sin(2a) = \frac{2a}{3}.$$

This equation has only one positive solution, $a \approx 1.13943$. We find our approximate τ and μ values according to $\tau = -2a^2$ and $\mu = -a^4$. Thus we have only one eigenvalue on the critical parabola, corresponding to the above even eigenfunction. □

5.2 Parameterization of eigenvalue curves in the super-parabolic region

Lemma 5.1 allows us to smoothly parameterize the eigenvalue branches lying in the super-parabolic region, mirroring our approach for the upper half-plane. We treat odd and even branches separately.

Parameterization of odd eigenvalue branches

Recall that our odd eigenvalue condition (5.2) can be written as $a^3 \tan a = b^3 \tan b$. With this in mind, we define the functions

$$f_{\text{odd}}(a) = a^3 \tan a, \qquad g_{\text{odd}}(b) = b^3 \tan b, \qquad a, b > 0 \tag{5.4}$$

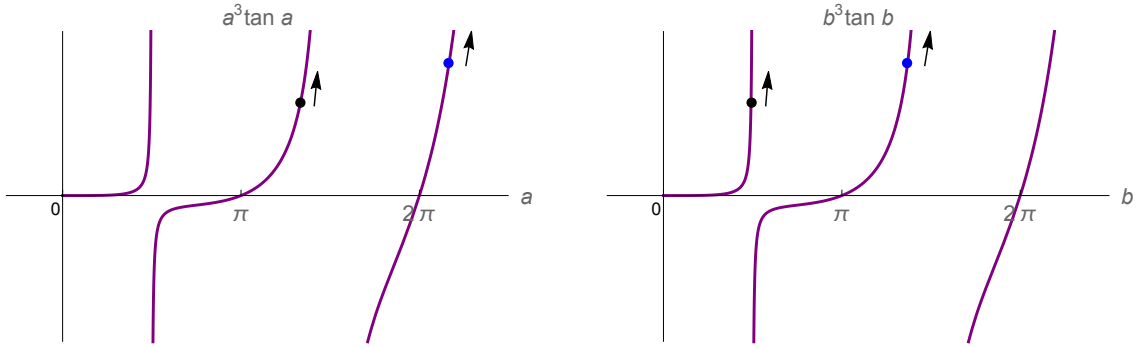

Figure 5.1: By Lemma 5.1 and the definitions of f_{odd} and g_{odd} in (5.4), the odd eigenvalue condition for the super-parabolic region can be written as $f_{\text{odd}}(a) = g_{\text{odd}}(b)$. The points on the above curves illustrate the dependence of a on b for a given branch, that is, $a = a_{l,\text{odd}}(b)$ (defined in (5.5)). The points shown here are on the $l = 1$ branch, and the arrows indicate motion of points as a increases.

Our odd eigenvalues are thus determined by the equation $f_{\text{odd}}(a) = g_{\text{odd}}(b)$, and we wish to express this condition explicitly in the form $a = f_{\text{odd}}^{-1}(g_{\text{odd}}(b))$. However, the function f_{odd} is not one-to-one on $a > 0$, and we have infinitely many choices of restricted domain. This is how our parameterization produces the infinitely many eigenvalue branches that we observe numerically (see, e.g., Figure 2.4).

Definition 5.2 (Parameterization for the super-parabolic region, odd case)**.** *Observe that f_{odd} is one-to-one when restricted to intervals $((j-1/2)\pi, (j+1/2)\pi)]$ for integers $j \geq 1$. Write $R_j f_{\text{odd}}(a)$ for the restriction of f_{odd} to its jth branch, that is,*

$$R_j f_{\text{odd}}(a) = f_{\text{odd}}\Big|_{\left((j-1/2)\pi,(j+1/2)\pi\right]}, \qquad j \geq 1.$$

These functions are bijections from their domains to all of $\mathbb{R}$. Therefore, for each integer $l \geq 1$, we may define a map $f_{\text{odd}}^{-1}(b; l)$ which maps from $b \in (0, \infty)$ to the interval $a \in (l\pi - \pi/2, \infty)$ according to

$$f_{\text{odd}}^{-1}(b; l) = (R_{k+l} f_{\text{odd}})^{-1}(b^3 \tan b), \quad \max\left\{\left(k - \frac{1}{2}\right)\pi, 0\right\} < b \leq \left(k + \frac{1}{2}\right)\pi, \ k \geq 0.$$

To understand this map, notice that $f_{\text{odd}}^{-1}(b; l)$ maps restricted domains of the kth

branch of f_{odd} to the $(k+l)$th branch, i.e.,

$$\left(k\pi - \frac{\pi}{2}, k\pi + \frac{\pi}{2}\right] \mapsto \left((k+l)\pi - \frac{\pi}{2}, (k+l)\pi + \frac{\pi}{2}\right].$$

Finally, we define the composition of the restrictions of f_{odd}^{-1} with $g_{\text{odd}}(b)$:

$$a_{l,\text{odd}}(b) = f_{\text{odd}}^{-1}(b^3 \tan b; l) \quad \text{for } b > 0. \tag{5.5}$$

Figure 5.1 illustrates this relationship across the branches of f_{odd} and g_{odd}.

We now have a family of parameterizations for the branches given by the odd eigenvalue condition (5.2), indexed by integers $l \geq 1$.

Parameterization of even eigenvalue branches

As in the odd case, our goal is to rewrite the even eigenvalue condition (5.3) as $-a^3 \cot a = -b^3 \cot b$ and in an explicit form, providing a parameterization of the eigenvalue branches.

Definition 5.3 (Parameterization for the super-parabolic region, even case)**.** *Define*

$$f_{\text{even}}(a) = -a^3 \cot a, \qquad g_{\text{even}}(b) = -b^3 \cot b, \qquad a, b > 0. \tag{5.6}$$

We also define the numbers a^* (resp. b^*) to be the point where the first branch of f_{even} (resp. g_{even}) obtains its minimum (see Figure 5.3). Observe that f_{even} is one-to-one when restricted to intervals $(j\pi, (j+1)\pi]$ for integers $j \geq 1$, and to $[a^*, \pi]$.

Write $R_j f_{\text{even}}(a)$ for the restriction of f_{even} to its jth branch, that is,

$$R_j f_{\text{even}}(a) = f_{\text{even}}\Big|_{\left(j\pi,(j+1)\pi\right]}, \qquad j \geq 1,$$
$$R_0 f_{\text{even}}(a) = f_{\text{even}}\Big|_{\left[a^*,\pi\right]}.$$

Since these restrictions are invertible, we define the maps $f_{\text{even}}^{-1}(b; l)$ for $l \geq 1$, which map $b \in (0, \infty)$ to $a \in (l\pi, \infty)$ according to

$$f_{\text{even}}^{-1}(b; l) = (R_{k+l} f_{\text{even}})^{-1}(-b^3 \cot b) \quad k\pi < b \leq (k+1)\pi, \ k \geq 0.$$

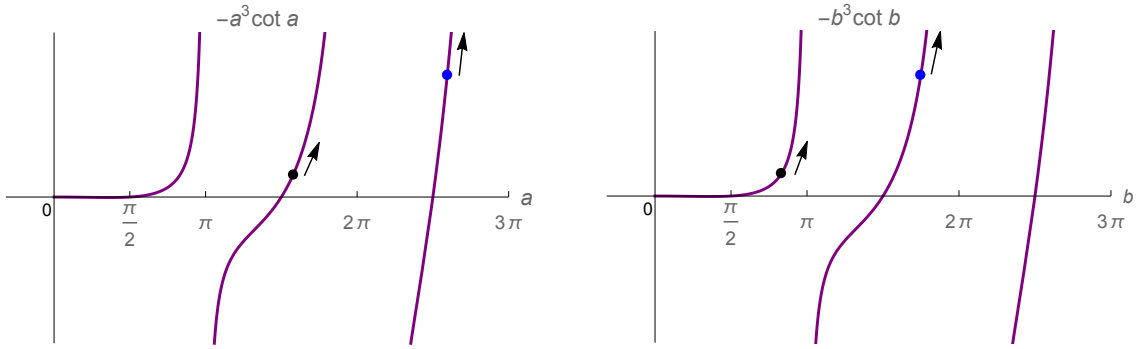

Figure 5.2: By Lemma 5.1 and the definitions of f_{even} and g_{even} in (5.6), the even eigenvalue condition for the super-parabolic region can be written as $f_{\text{even}}(a) = g_{\text{even}}(b)$. As in the odd case, the points on the curves indicate how to interpret a in terms of b and the branch l, that is, $a = a_{l,\text{even}}(b)$ (defined in (5.7)). The points shown correspond to the case $l = 1$, and the arrows indicate motion of points as a increases.

To understand this family of maps, notice that $f^{-1}_{\text{even}}(b; l)$ *maps*

$$\Big(k\pi, (k+1)\pi\Big] \mapsto \Big((k+l)\pi, (k+l+1)\pi\Big].$$

Likewise, define the map $f^{-1}_{\text{even}}(b; 0)$ *which maps from* $b \in (0, b^*]$ *to* $a \in [a^*, \pi/2)$ *by*

$$f^{-1}_{\text{even}}(b; 0) = (R_0 f_{\text{even}})^{-1}(-b^3 \cot b) \quad \textit{when } b \in (0, b^*].$$

For any integer $l \geq 0$*, we may now express the* l*th branch of the eigenvalues according to* $a = a_{l,\text{even}}(b)$*, where*

$$a_{l,\text{even}}(b) = f^{-1}_{\text{even}}(-b^3 \cot b; l) \quad \textit{for } b > 0. \tag{5.7}$$

See Figure 5.2 for an illustration of this relationships across the branches.

Remark 5.4. The eigenvalue conditions we have derived so far take the form $f(a) = g(b)$. In the upper half-plane, we parameterized the eigenvalue curves in terms of a, inverting $g(b)$. By contrast, we chose b as our parameter for eigenvalue curves in the super-parabolic region, inverting $f(a)$. In this case, the function $f(a) = -a^3 \cot a$ is not one-to-one unless we restrict our domain.

The first branch of f_{even} requires further restriction, taking either the portion to

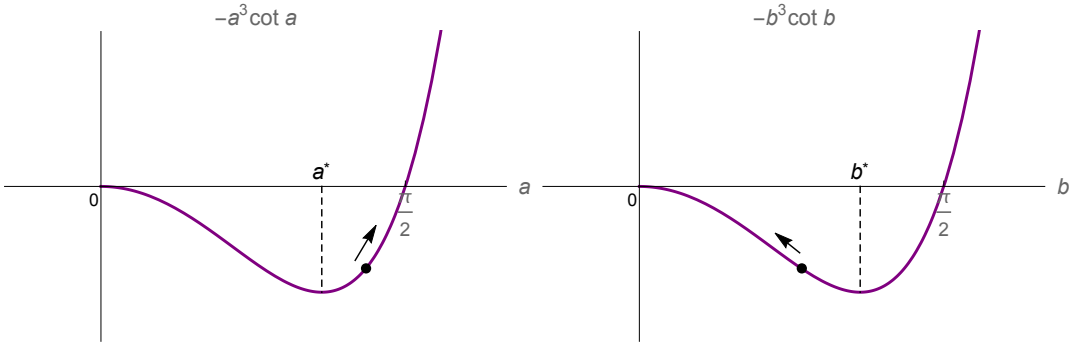

Figure 5.3: Super-parabolic region: the first branch of the even eigenvalue condition $f_{\text{even}}(a) = g_{\text{even}}(b)$ gives $a_{0,\text{even}}(b)$ (see Remark 5.4). The arrows indicate the motion of points as a increases. Here $a^* \leq a < \pi/2$ and $0 < b \leq b^*$, where $a^* = b^*$ are the locations of the minima.

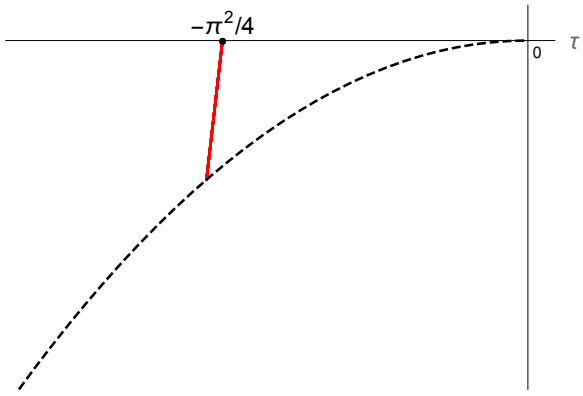

Figure 5.4: The even eigenvalue branch $\mu_0^{\text{even}}(\tau)$ (Remark 5.4), which connects $(-\pi^2/4, 0)$ on the τ-axis with the critical parabola (Theorem 5.5.3).

the left or the right of its minimum at $a = a^*$ (see Figure 5.3). Since a is greater than b, we discard the portion of the first branch of f_{even} on $[0, a^*)$.

The case when the a and b values are on the same branch gives us a little piece of the even eigenvalue curve that connects to a point on the critical parabola (Figure 5.4).

Theorem 5.5 (Eigenvalues of the super-parabolic region)**.** *The eigenvalue curves in the super-parabolic region are indexed by integers l. For each index, there is one odd eigenvalue curve and one even eigenvalue curve.*

1. *Odd: For each $l \geq 1$, the eigenvalue curve $(\tau, \mu_l^{\text{odd}}) = F_2(a_{l,\text{odd}}(b), b)$ is parameterized by $b > 0$ (Figure 5.5).*

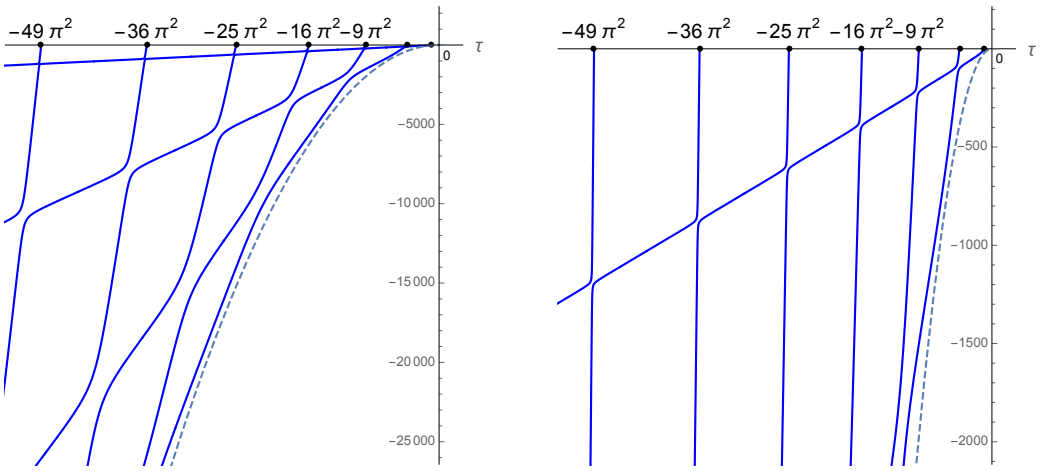

Figure 5.5: The odd eigenvalue branches $\mu_l^{\text{odd}}(\tau)$ in the lower half-plane above the critical parabola $\mu = -\tau^2/4$ (dashed) for $l = 1, \ldots, 7$, and zoomed-in vertically near the τ-axis (Theorem 5.5). The intercepts along the τ-axis are at $-l^2\pi^2$.

2. *Even: For each $l \geq 0$, the eigenvalue curve $(\tau, \mu_l^{\text{even}}) = F_2(a_{l,\text{even}}(b), b)$ is parameterized by $b > 0$ (Figure 5.6).*

3. *Critical parabola: There exists a unique (τ, μ) pair on the critical parabola $\mu = -\tau^2/4$. This eigenvalue is $\mu = -a^4$ with corresponding even eigenfunction $u = C\cos(ax) + Dx\sin(ax)$, where $a \approx 1.13943$.*

Proof. This theorem follows immediately from our work for Lemma 5.1 and our Definitions 5.2 and 5.3. □

Remark 5.6. The parameterization of the eigenvalue curves is quite different in the upper half-plane compared to the super-parabolic region. In the upper half-plane, each eigenvalue branch consists of a single parameterization. In the super-parabolic region, each eigenvalue branch consists of infinitely many pieces. The difference is that for the upper half-plane (Figures 4.1 and 4.2), the functions g_{odd} and g_{even} are monotonic and can be inverted, whereas in the super-parabolic region (Figures 5.1 and 5.2), neither f_{odd} and f_{even} nor g_{odd} and g_{even} are globally invertible. Thus, we must restrict the branches to achieve local invertibility.

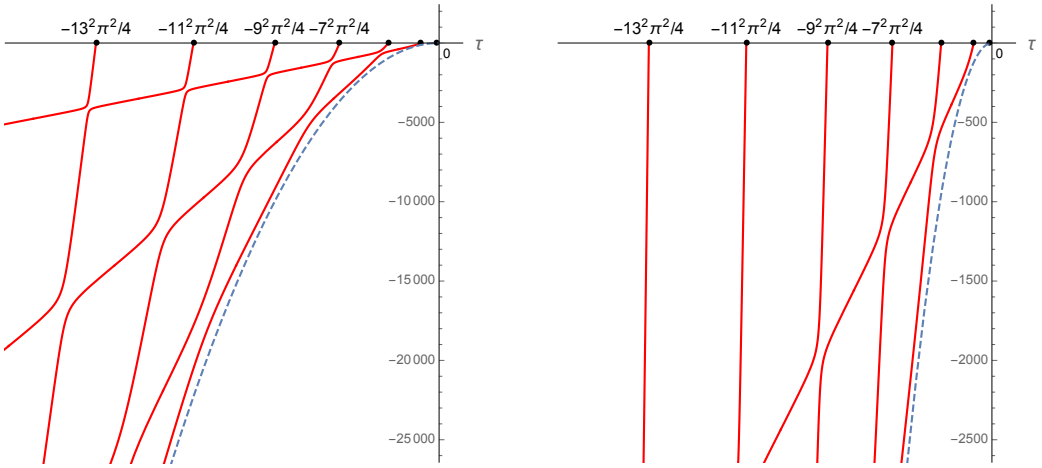

Figure 5.6: The even eigenvalue branches $\mu_l^{\text{even}}(\tau)$ in the lower half-plane above the critical parabola $\mu = -\tau^2/4$ (dashed) for $l = 0, \ldots, 6$, and zoomed-in vertically near the τ-axis (Theorem 5.5). The intercepts along the τ-axis are at $-(l+1/2)^2\pi^2$.

5.3 Some properties of the eigenvalue curves in the super-parabolic region

In this section, we state and prove several properties of the eigenvalue branches lying in the super-parabolic region. We also state some properties which are clear from numerical investigation but for which we do not have rigorous proof.

We begin with a proposition identifying the intersections of eigenvalue branches.

Proposition 5.7. *1. Same-symmetry eigenvalue branches in the super-parabolic do not intersect. That is,*

$$\begin{aligned} &\text{if } l_2 > l_1 > 0, \text{ then} \quad \mu_{l_2}^{\text{odd}}(\tau) > \mu_{l_1}^{\text{odd}}(\tau) \quad \text{for all } \tau \leq -(l_2\pi)^2, \\ &\text{if } l_2 > l_1 \geq 0, \text{ then} \quad \mu_{l_2}^{\text{even}}(\tau) > \mu_{l_1}^{\text{even}}(\tau) \quad \text{for all } \tau \leq -\left((l_2+\frac{1}{2})\pi\right)^2. \end{aligned}$$

2. Different-symmetry eigenvalue branches in the super-parabolic region with the same index l intersect infinitely often. These intersections occur at the points

$$(\tau, \mu) = \left(-\frac{(m^2+l^2)\pi^2}{2}, -\frac{(m^2-l^2)^2\pi^4}{16}\right), \quad \text{for } m \in \mathbb{N}. \tag{5.8}$$

Proof. By the bijection F_2 from Lemma 3.1.2, any intersections of eigenvalue branches

in the super-parabolic region in the (τ, μ) plane are in one-to-one correspondence with intersections in the (a, b) plane. For a given symmetry type, the (a, b) pairs uniquely determine the eigenfunction (up to multiplication by a constant), so the only possible intersections of eigenvalue curves occur when odd and even eigenvalue curves with the same (a, b) meet.

Since we are looking at the same index l for both even and odd branches, we must consider branches j and k of f_{odd} and f_{even}, with $j - k = l$ (Section 5.2). The odd and even eigenvalue curves meet when a and b satisfy the eigenvalue conditions (5.2) and (5.3) simultaneously, which means

$$a^3 \sin a \cos b = b^3 \cos a \sin b,$$
$$a^3 \cos a \sin b = b^3 \sin a \cos b.$$

First, we show that the points (5.8) satisfy the two conditions. In the (a, b) plane, these points correspond to the following two families of points:

$$C_{j,k}^{\text{odd}}(a, b) = \left(\left(j + \frac{1}{2} \right) \pi, \left(k + \frac{1}{2} \right) \pi \right),$$
$$C_{j,k}^{\text{even}}(a, b) = (j\pi, k\pi),$$

where $j - k = l$. It is obvious that two pairs satisfy both eigenvalue conditions simultaneously.

Next we show that these are the only solutions of the two conditions. By adding the two equations and using a trigonometric identity, we obtain

$$a^3 \sin(a + b) = b^3 \sin(a + b).$$

Thus we must have either $a = b$ or $a + b = m\pi, m \in \mathbb{N}$. However, in this case we know that $a \neq b$, since we are not on the critical parabola (see the proof of Lemma 5.1). Similarly, subtracting one eigenvalue condition from the other, we obtain the condition $a - b = n\pi, n \in \mathbb{N}$.

Additionally, the odd condition implies that $a \in ((j - 1/2)\,\pi, (j + 1/2)\,\pi]$ and $b \in ((k - 1/2)\,\pi, (k + 1/2)\,\pi]$ for $j > k$. Hence $a - b \in ((j - k - 1)\,\pi, (j - k + 1)\,\pi)$, or equivalently $((l - 1)\,\pi, (l + 1)\,\pi)$. Similarly, we obtain $a - b \in ((l - 1)\,\pi, (l + 1)\,\pi)$ from the even condition. Hence $a - b = l\pi$. Therefore, $a = (m + l)\pi/2$ and $b =$

$(m-l)\pi/2$.

We have thus identified all points where the odd and even eigenvalue curves meet. We then recover the (τ, μ) values of the points of intersection from the bijection F_2. □

We now list, as observations, some properties of the eigenvalue branches.

1. **Observation of connection between the upper half-plane and super-parabolic regions:** In the upper half-plane, eigenvalue branches (save for the constant zero branch) are indexed by nonnegative integers l; for each l, there is one odd branch and one even branch. In the super-parabolic region, the parameterization of eigenvalue branches depends upon indices j and k. If we have $l = j - k$, then then the lth odd eigenvalue branch in the upper half-plane and the j, kth odd eigenvalue branch in the super-parabolic region have the same horizontal intercept, $\tau = -l^2\pi^2$. The same is true for even branches.

2. **Asymptotic behavior of the eigenvalue branches.**

   Along each branch, as τ tends to $-\infty$, we have

   $$\mu = -\frac{\tau^2}{4} + \mathcal{O}(|\tau|),$$

   where the constant in the "$\mathcal{O}$" term depends on the eigenvalue branch.

   Proof. From Property 1, we may write $a = b + l\pi + (s - t)$, where $s, t \in (-\pi/2, \pi/2]$. Set $\gamma = l\pi + (s - t)$. While γ is variable, it takes values in $((l-1)\,\pi, (l+1)\,\pi)$ and so is bounded. We express τ and μ in terms of b and γ as follows:

   $$\mu = -a^2b^2 = -b^4 - 2\gamma b^3 - \gamma^2 b^2,$$
   $$\tau = -a^2 - b^2 = -2b^2 - 2\gamma b - \gamma^2.$$

   From this, we obtain a relation between τ and μ:

   $$\mu = -\frac{\tau^2}{4} + \frac{(-\gamma^2 \pm 2\gamma\sqrt{-\gamma^2 - 2\tau})^2}{4}$$

Therefore, $\mu = -\tau^2/4 - 2\gamma^2\tau + \mathcal{O}\left(|\tau|^{1/2}\right)$, where γ depends on the branch l as well as s and t. □

3. **Observation of shallow straight lines (Cascading phenomenon)** We observe that the eigenvalue curves in the super-parabolic region consist of a pattern of nearly-linear segments and barely-avoided crossings. If we draw lines through the even-odd points of intersection as in Figure 5.7, we see they are very close to the nearly-linear segments of different branches of the same symmetry type. We will call these lines "phantom spectral lines".

   From Proposition 5.7, we know that the two families of intersection points indexed by the same l can be expressed as

$$C_{j,k}^{\text{odd}}(\tau,\mu) = \left(\frac{-(2j+1)^2-(2k+1)^2}{4}\pi^2, \frac{-(2j+1)^2(2k+1)^2}{16}\pi^4\right),$$
$$C_{j,k}^{\text{even}}(\tau,\mu) = \left(\left(-j^2-k^2\right)\pi^2, -j^2k^2\pi^4\right) \quad \text{where } j-k=l.$$

   The kth phantom spectral line for the odd branches is the line that connects the points $C_{j,k}^{odd}$ with $j > k$. Similarly, the kth phantom spectral line for the even branch connects the points $C_{j,k}^{even}$ with $j \geq k$. The equations of these phantom spectral lines are:

$$P_k^{\text{odd}} : \mu = \left(\frac{(2k+1)\pi}{2}\right)^2\tau + \left(\frac{(2k+1)\pi}{2}\right)^4, \quad \text{for } k \geq 0,$$
$$P_k^{\text{even}} : \mu = (k\pi)^2\tau + (k\pi)^4, \quad \text{for } k \geq 0.$$

Remark 5.8. Figure 5.7 suggests that the phantom spectral lines are tangent to the eigenvalue curves at the $C_{j,k}^{\text{odd}}$'s and $C_{j,k}^{\text{even}}$'s. This is not the case, although as $\mu \to -\infty$, the slopes of the phantom spectral lines approach those of the eigenvalue curves. The details will be in the following subsection.

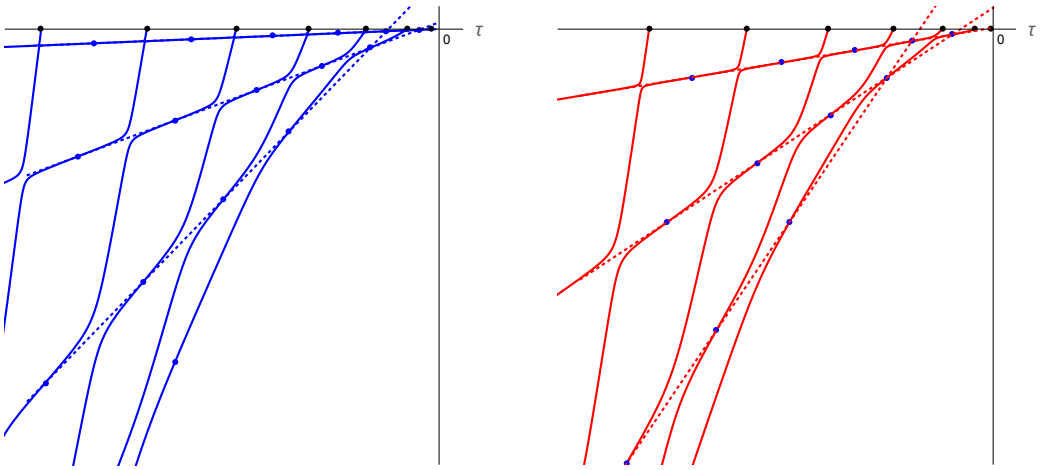

Figure 5.7: Lower half-plane above the critical parabola: dotted "phantom" lines for the odd and even eigenvalue branches (Property 3).

Approximation of the eigenvalue curves in the super-parabolic region by the phantom spectral lines

We see that the phantom spectral lines approximate the eigenvalue curves in the super-parabolic region (see Figure 5.7). To prove this property, we will show that the phantom spectral lines are approximately tangential to the eigenvalue curves at the points $C^{\text{odd}}_{j,k}$ and $C^{\text{even}}_{j,k}$ where different-symmetry eigenvalue branches in the super-parabolic region with the same index l intersect. We will prove that the slopes of the phantom spectral lines approach those of the spectral curves as $\mu \to -\infty$. First, we describe $d\mu/d\tau$ at one family of intersection points $C^{\text{odd}}_{j,k}$ with fixed k where $a = (2j+1)\pi/2$ and $b = (2k+1)\pi/2$ for $j-k > 0$. Remember that in the super-parabolic region μ and τ are defined by

$$\mu = -a^2b^2,$$
$$\tau = -a^2 - b^2.$$

Differentiating each of these in terms of a gives us

$$\frac{d\mu}{d\tau} = \frac{d\mu/da}{d\tau/da} = \frac{-2ab^2 - 2a^2b\frac{db}{da}}{-2a - 2b\frac{db}{da}}. \tag{5.9}$$

We first find db/da. Recall that the eigenvalue condition is $b^3\tan(b) = a^3\tan(a)$ from (5.2) and we take reciprocal of the condition to get rid of problem of infinity:

$$b^{-3}\cot(b) = a^{-3}\cot(a).$$

Call the left-hand side $h(b)$. Since

$$h'\left(\frac{(2k+1)\pi}{2}\right) \neq 0,$$

the function h is invertible near $(2k+1)\pi/2$. Hence, we can express

$$b = h^{-1}(a^{-3}\cot(a)).$$

With some calculations, we obtain

$$\begin{aligned}\frac{db}{da} &= \frac{(a^{-3}\cot(a))'}{h'\big(h^{-1}\left(a^{-3}\cot(a)\right)\big)} \\ &= \frac{-3a^{-4}\cot(a) - a^{-3}\csc^2(a)}{h'(b)} \\ &= \frac{-3a^{-4}\cot(a) - a^{-3}\csc^2(a)}{-3b^{-4}\cot(b) - b^{-3}\csc^2(b)}.\end{aligned}$$

As $a \to (2j+1)\pi/2$ and $b \to (2k+1)\pi/2$, we find

$$\frac{db}{da} \to \left(\frac{2k+1}{2j+1}\right)^3.$$

We use this evaluation to find $d\mu/d\tau$ at $a = (2j+1)\pi/2$ and $b = (2k+1)\pi/2$. From (5.9) we get

$$\frac{d\mu}{d\tau} = \left(\frac{2k+1}{2}\pi\right)^2 \frac{(2j+1)^4 + (2j+1)^2(2k+1)^2}{(2j+1)^4 + (2k+1)^4}.$$

Note that $j > k$ and so ratio is greater than 1. Hence, $d\mu/d\tau$ at the point $(a,b) = ((2j+1)\pi/2, (2k+1)\pi/2)$ is greater than $((2k+1)\pi/2)^2$. Also, as

$j \to \infty$ with k fixed, we see

$$\frac{d\mu}{d\tau} \to \left(\frac{2k+1}{2}\pi\right)^2,$$

which is the slope of one family of phantom spectral lines P_k^{odd} of Property 3 in Section 5.3.

With a similar calculation, we could obtain $d\mu/d\tau$ at the other family of intersection points $C_{j,k}^{\text{even}}$ with fixed k where $a = j\pi$ and $b = k\pi$ for $j - k \geq 0$. That is,

$$\frac{d\mu}{d\tau} = (k\pi)^2 \frac{j^4 + j^2k^2}{j^4 + k^4}.$$

The quantity $j^4 + j^2k^2/j^4 + k^4$ is greater than or equal to 1 since $j \geq k$, and so $d\mu/d\tau$ at $(a, b) = (j\pi, k\pi)$ is greater than the slope $(k\pi)^2$ of the family of phantom spectral lines P_k^{even}. Also, as j tends to ∞, $d\mu/d\tau$ tends to $(k\pi)^2$.

Therefore, we have shown that the phantom spectral lines better approximate the actual spectral curves as $\mu \to -\infty$.

CHAPTER 6

THE LOWER HALF-PLANE: SUB-PARABOLIC REGION

In this chapter, which is the most technically difficult of the first part of the thesis, we treat the case of eigenvalue branches lying in the lower half-plane below the critical parabola, that is, $\{(\tau, \mu) : \tau < 0, \mu < -\tau^2/4\}$. We will see that this region corresponds to the case where the characteristic equation $r^4 - \tau r^2 - \mu = 0$ has non-real, non-purely-imaginary complex roots. Note that since a nonnegative τ guarantees nonnegative eigenvalues, we need only consider $\tau < 0$. When μ and τ are both negative and satisfy $\mu < -\tau^2/4$, we may factor the eigenvalue equation as

$$\left(\frac{d^2}{dx^2} + (a - ib)^2\right)\left(\frac{d^2}{dx^2} + (a + ib)^2\right) u = 0, \tag{6.1}$$

for $a > b > 0$, where $\mu = -(a^2 + b^2)^2$ and $\tau = 2(b^2 - a^2)$, as in the bijection Lemma 3.1.3.

The behavior of the eigenvalue branches is quite different in this region from that in the upper half-plane or the super-parabolic region. We cannot find an explicit parameterization, so instead we develop an "implicit parameterization" to describe the odd and even eigenvalue branches. In particular, we will show that there are only two eigenvalue branches (one odd and one even), and they cross infinitely many times. The eigenfunctions have a more complicated form than in previous cases.

We will also discuss in Section 6.3 the question of intersections of the family of parabolas $\mu = -c\tau^2$ with the first two eigenvalue branches, which has applications to the second part of the thesis (Theorem 8.7 in Section 8.2 of Chapter 8).

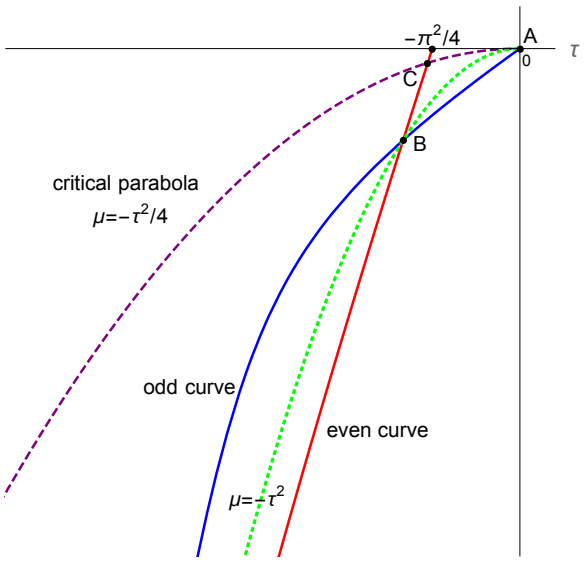

Figure 6.1: Only two spectral curves penetrate below the critical parabola. They intersect infinitely often along the dotted parabola $\mu = -\tau^2$. The points A, B, C, and $(-\pi^2/4, 0)$ are significant for the discussion in Chapter 6.

6.1 Eigenfunctions and eigenvalue conditions

Lemma 6.1 (Sub-parabolic region)**.** *For all $\tau < 0$ and all eigenvalues μ satisfying $\mu < -\tau^2/4$, at least one of the following must hold:*

1. *The eigenvalue μ is associated with an odd eigenfunction u_o of the form*

$$u_o(x) = A\cos(ax)\sinh(bx) + B\sin(ax)\cosh(bx),$$

where A and B are nonzero constants, and $a > b > 0$ are positive numbers such that $\mu = -(a^2+b^2)^2$, $\tau = 2(b^2-a^2)$, and satisfy the additional condition

$$(3a^2 - b^2)\frac{\sin(2a)}{2a} = (3b^2 - a^2)\frac{\sinh(2b)}{2b}. \tag{6.2}$$

2. *The eigenvalue μ is associated with an even eigenfunction u_e of the form*

$$u_e(x) = C\sin(ax)\sinh(bx) + D\cos(ax)\cosh(bx),$$

where C and D are nonzero constants, and $a > b > 0$ are positive numbers such

that $\mu = -(a^2+b^2)^2$, $\tau = 2(b^2-a^2)$, *and satisfy the additional condition*

$$(3a^2-b^2)\frac{\sin(2a)}{2a} = (a^2-3b^2)\frac{\sinh(2b)}{2b}. \tag{6.3}$$

Proof. Since we are considering the case of $\mu < -\tau^2/4$ and $\tau < 0$, by Lemma 3.1.3, we may express the eigenvalue equation in terms of a and b as (6.1), and so the characteristic equation has four distinct non-real, non-purely-imaginary complex roots $r = \pm ia \pm b$. As usual, we consider only even and odd solutions, so we express the solutions $e^{\pm iax \pm bx}$ of the differential equation as $\cos(ax)\sinh(bx)$, $\sin(ax)\sinh(bx)$, $\cos(ax)\cosh(bx)$, and $\sin(ax)\cosh(bx)$. Our possible solutions are then linear combinations of these, chosen according to symmetry. We then see the odd and even eigenfunctions have the forms

$$\begin{aligned} u_o(x) &= A\cos(ax)\sinh(bx) + B\sin(ax)\cosh(bx), \\ u_e(x) &= C\sin(ax)\sinh(bx) + D\cos(ax)\cosh(bx). \end{aligned}$$

The boundary conditions (2.2) and (2.3) in terms of a and b say that:

$$\begin{cases} u'' = 0 & \text{when } x = \pm 1, \\ u''' - 2(b^2-a^2)u' = 0 & \text{when } x = \pm 1. \end{cases}$$

We consider the odd eigenfunction first. We wish to determine which values of a and b (and hence τ and μ) yield a solution to the boundary value problem. Applying the two boundary conditions yields

$$\begin{cases} A[(b^2-a^2)\cos a\sinh b - 2ab\sin a\cosh b] \\ \qquad = -B[(b^2-a^2)\sin a\cosh b + 2ab\cos a\sinh b], \\ A[(b^3+a^2b)\cos a\cosh b + (a^3+ab^2)\sin a\sinh b] \\ \qquad = -B[(b^3+a^2b)\sin a\sinh b - (a^3+ab^2)\cos a\cosh b]. \end{cases}$$

We require that our linear combination coefficients A, B be nontrivial, so the system's determinant must vanish. We can express this determinant condition as

$$(4a^2b - 2b^3 + 2a^2b)\sin a\cos a = (2ab^2 - 2a^3 + 4ab^2)\sinh b\cosh b.$$

Since a, b are nonzero, this formula is equivalent to

$$(3a^2 - b^2)\frac{\sin(2a)}{2a} = (3b^2 - a^2)\frac{\sinh(2b)}{2b},$$

which gives a condition on (a, b) that guarantees existence of an odd solution to the eigenvalue problem.

For the even eigenfunction u_e, applying the boundary conditions gives us

$$\begin{cases} C[(b^2 - a^2)\sin a \sinh b + 2ab \cos a \cosh b] \\ \qquad = -D[(b^2 - a^2)\cos a \cosh b - 2ab \sin a \sinh b], \\ C[(a^2 b + b^3)\sin a \cosh b - (a^3 + ab^2)\cos a \sinh b] \\ \qquad = -D[(a^2 b + b^3)\cos a \sinh b + (a^3 + ab^2)\sin a \cosh b]. \end{cases}$$

Once again, to have nontrivial linear combination coefficients C, D, we require the system's determinant be zero, which leads to

$$(3a^2 - b^2)\frac{\sin(2a)}{2a} = (a^2 - 3b^2)\frac{\sinh(2b)}{2b}. \qquad \square$$

Unlike the prior cases, we cannot solve the eigenvalue conditions (6.2) or (6.3) for a in terms of b (or b in terms of a) explicitly, and so we have not found a smooth parameterization of the eigenvalue curves in this region. Instead, we seek to understand the eigenvalue branches by looking at solutions of the eigenvalue conditions in the (a, b)-plane. We call this method "implicit parameterization" since it relies on implicit functions and does not give us a complete parameterization as we found for the other regions.

In the sections that follow, we describe the behavior of the eigenvalue curves in the (a, b)-plane. We then consider the problem of intersections of parabolas and the eigenvalue curves by considering their images in the (a, b)-plane.

6.2 Image of eigenvalue branches in the (a, b)-plane

In this section, we consider the images of the eigenvalue branches of the sub-parabolic region in the (a, b)-plane. From Lemma 6.1, we know that the odd and even eigenvalue

curves in the (a, b)-plane are given by the following equations:

$$\begin{aligned} \text{odd}: \quad & (3a^2 - b^2)\frac{\sin(2a)}{2a} = (3b^2 - a^2)\frac{\sinh(2b)}{2b}, \\ \text{even}: \quad & (3a^2 - b^2)\frac{\sin(2a)}{2a} = -(3b^2 - a^2)\frac{\sinh(2b)}{2b}. \end{aligned}$$

The shapes of the eigenvalue curves are not clear from the equations themselves. We analyze their properties near the origin in the next two lemmas.

Define the functions

$$\begin{aligned} F_o(a, b) &= (3a^2 - b^2)\frac{\sin(2a)}{2a} - (3b^2 - a^2)\frac{\sinh(2b)}{2b}, \\ F_e(a, b) &= (3a^2 - b^2)\frac{\sin(2a)}{2a} + (3b^2 - a^2)\frac{\sinh(2b)}{2b}. \end{aligned}$$

We restrict our domain to be the triangle

$$\{(a, b) : 0 \le a \le \pi/2, 0 \le b \le \pi/\sqrt{12}, b < a\},$$

continuously extending $\sin(2a)/2a$ and $\sinh(2b)/2b$ to $a = 0$ and $b = 0$ respectively.

First, we will show that $F_o(a, b) = 0$ has a unique solution $b(a)$ for each $a \in (0, \pi/2)$. We then use the Implicit Function Theorem to conclude that these solutions form a continuous function of a, and so the graph is a single connected curve in the (a, b)-plane. We argue the analogous result is also true for the even case: that $F_e(a, b) = 0$ has a unique solution $a(b)$ for each $b \in (0, \pi/\sqrt{12})$, which can be considered a continuous function.

We first prove existence and uniqueness of the solutions.

Lemma 6.2 (Existence and uniqueness of the solutions)**.**

1. *For each $a \in (0, \pi/2)$, there exists a unique $b \in (a/\sqrt{3}, a)$ such that $F_o(a, b) = 0$, and furthermore, the equation has no solutions when $b \in (0, a/\sqrt{3}]$.*

2. *For each $b \in (0, \pi/\sqrt{12})$, there exists a unique $a \in (\sqrt{3}b, \pi/2)$ such that $F_e(a, b) = 0$, and furthermore, the equation has no solutions when $a \in (b, \sqrt{3}b]$.*

Proof. Let $f(a) = \sin(2a)/2a$ and $g(b) = \sinh(2b)/2b$. Note that $f(a) > 0$ for $a \in (0, \pi/2)$ and $f(a) < 1 < g(a)$ for all $a > 0$.

We begin with the odd case. We fix $a \in (0, \pi/2)$ and show existence of b satisfying $F_o(a, b) = 0$.

For any such a, it is obvious that $F_o(a, \cdot)$ is a continuous function on $b \in [a/\sqrt{3}, a]$. At the left endpoint $b = a/\sqrt{3}$, we have $F_o(a, a/\sqrt{3}) = 8a^2 f(a)/3 > 0$, since $a \in (0, \pi/2)$. At the right endpoint $b = a$, we have $F_o(a, a) = 2a^2(f(a) - g(a)) < 0$, since $a > 0$. Then by the Intermediate Value Theorem, there exists a $b \in (a/\sqrt{3}, a)$ such that $F_o(a, b) = 0$.

To show uniqueness of the b for the odd case, we fix the value a and write the equation $F_o(a, b) = 0$ in the form

$$g(b) = f(a)h(b), \qquad \text{where } h(b) = \frac{3a^2 - b^2}{3b^2 - a^2},$$

and consider the behavior of both sides. The left-hand side $g(b)$ is positive and increasing in b. On the other hand, $f(a)$ is a fixed positive number and $h(b)$ is positive and decreasing when $b \in (a/\sqrt{3}, a)$. Therefore, there is only one $b \in (a/\sqrt{3}, a)$ that satisfies the equation.

Note also that if $0 < b \leq a/\sqrt{3}$, there is no solution for $F_o(a, b) = 0$. On this interval, the function $h(b)$ is negative, but $g(b)$ remains positive.

The even case proceeds similarly. In this case, we fix $b \in (0, \pi/\sqrt{12})$ and consider $F_e(\cdot, b)$ as the continuous function on $a \in [\sqrt{3}b, \pi/2]$. It is easy to show $F_e(\sqrt{3}b, b) > 0$ and $F_e(\pi/2, b) < 0$.

To show uniqueness of that a-value for the even case, we fix the value b and write the equation $F_e(a, b) = 0$ in the form

$$f(a) = g(b)h(a), \qquad \text{where } h(a) = -\frac{3b^2 - a^2}{3a^2 - b^2},$$

and consider the behavior of both sides. The left-hand side $f(a)$ is positive and decreasing. On the other hand, $g(b)$ is a fixed positive number and $h(a)$ is positive and increasing when $a \in (\sqrt{3}b, \pi/2)$. Therefore, there is only one $a \in (\sqrt{3}b, \pi/2)$ that satisfies the equation.

Similarly, if $b < a \leq \sqrt{3}b$, there is no solution for $F_e(a, b) = 0$. On this interval, the quantity $h(a)$ is now negative, but $f(a)$ remains positive. □

Remark 6.3. This method of proof can be extended to show existence of $b(a)$ for all $a > 0$ in the odd case, with $b \in (a/\sqrt{3}, a)$ whenever $a \in (k\pi, (2k+1)\pi/2)$ and

$b \in [0, a/\sqrt{3}]$ whenever $a \in [(2k+1)\pi/2, (k+1)\pi]$, where k is an integer. Existence of $a(b)$ for all $b \geq 0$ in the even case can likewise be obtained. The functions involved do not have the desired behaviors on the intervals in question, so other methods are necessary to establish uniqueness.

We next show that eigenvalue conditions $F_o(a,b) = 0$ and $F_e(a,b) = 0$ actually have continuous solutions $b(a)$ and $a(b)$, respectively. For what follows, we find it useful to define the quantity a^* such that $\sin(2a^*)/2a^* = 1/3$, which corresponds to $F_e(a^*, 0) = 0$. Numerically, we have

$$a^* \approx 1.13943. \tag{6.4}$$

Lemma 6.4 (Continuity and smoothness of the solutions)**.**

1. *The solution $b(a)$ of $F_o(a,b) = 0$ is continuous for $a \in [0, \pi/2]$, smooth for $a \in (0, \pi/2)$, and satisfies $b(0) = 0$, $b'(0^+) = 1$, and $b(a) < a$ for $a \in (0, \pi/2)$.*

2. *The solution $a(b)$ of $F_e(a,b) = 0$ is continuous for $b \in [0, \pi/\sqrt{12}]$ and smooth for $b \in (0, \pi/\sqrt{12})$.*

Proof. By Lemma 6.2, there exist unique solutions of $F_o(a,b) = 0$ for each $a \in (0, \pi/2)$ and of $F_e(a,b) = 0$ for $b \in (0, \pi/\sqrt{12})$. We will use the Implicit Function Theorem to establish these solutions depend continuously on a or b as appropriate. In order to prove smoothness and properties of the solution, we break into two pieces: "away from the origin" and "near the origin".

Claim 1: The solution $b(a)$ of $F_o(a,b) = 0$ is smooth for $a \in (0, \pi/2)$ (away from the origin) and $b(a) < a$ for all $a \in (0, \pi/2)$.

From Lemma 6.2.1, it is obvious that the solution $b(a) < a$ for $a \in (0, \pi/2)$. We will use the Implicit Function Theorem to show the solution is smooth for $a \in (0, \pi/2)$.

1. First, we show the function F_o is continuously differentiable for $(a,b) \in [0, \pi/2] \times [0, \pi/\sqrt{12}]$.

   Note that F_o is analytic as a function of $(a,b) \in \mathbb{R}^2$, by using the standard power series expansions for $\sin(z)$ and $\sinh(z)$. That is, the function F_o can be written as

$$F_o(a,b) = (3a^2 - b^2)\left(1 - \mathcal{O}(a^2)\right) - (3b^2 - a^2)\left(1 + \mathcal{O}(b^2)\right).$$

Since F_o is an analytic function on $(a,b) \in \mathbb{R}^2$, it is easy to see that the partials $\partial F_o/\partial a$ and $\partial F_o/\partial b$ are continuous for $(a,b) \in [0,\pi/2] \times [0,\pi/\sqrt{12}]$.

2. Next, we show $\partial F_o/\partial b$ is nonzero for $(a,b) \in (0,\pi/2] \times (0,\pi/\sqrt{12}]$. Recall from (6.2) that for the odd eigenvalue branch $F_o(a,b) = 0$, we have

$$\frac{\partial F_o}{\partial b} = -\frac{b}{a}\sin(2a) - \left(\frac{a^2}{2b^2} + \frac{3}{2}\right)\sinh(2b) + \left(\frac{a^2}{b} - 3b\right)\cosh(2b).$$

The first and second terms are obviously negative for $a \in (0,\pi/2]$ and $b \in (0,\pi/\sqrt{12}]$. The third term is also negative, since by Lemma 6.2 the solution curve $F_o(a,b) = 0$ lies in the portion of the plane where $a < \sqrt{3}b$. Therefore, $\partial F_o/\partial b < 0$.

Therefore, by the Implicit Function Theorem, there exist neighborhoods $U_a \subseteq \mathbb{R}$ and $V_b \subseteq \mathbb{R}$ such that $a \in U_a, b \in V_b$, and a unique function $g_{a,b} : U_a \to V_b$ exists such that $b = g_{a,b}$ and $F_o(x, g_{a,b}(x)) = 0$ for all $x \in U_a$. Furthermore, the function $g_{a,b}$ is infinitely differentiable on U_a.

We cannot apply the Implicit Function Theorem at the origin because $\partial F_o/\partial b = 0$ there. To understand the behavior of the curve near the origin, we introduce a change of variable.

Claim 2: The solution $b(a)$ of $F_o(a,b) = 0$ is smooth on a neighborhood of the origin, and $b(0) = 0$, $b'(0^+) = 1$, and $b(a) < a$ for a near 0.

We express $F_o(a,b)$ near the origin using the standard power series expansions for $\sin(2a)$ and $\sinh(2b)$, obtaining

$$F_o = (3a^2 - b^2)\left(1 - \frac{2}{3}a^2 + \mathcal{O}(a^4)\right) - (3b^2 - a^2)\left(1 + \frac{2}{3}b^2 + \mathcal{O}(b^4)\right).$$

Expressing F_o as a function of the new variables $\alpha = a^2$ and $\beta = b^2$, we obtain a series expansion:

$$F_o = (3\alpha - \beta)\left(1 - \frac{2}{3}\alpha + \mathcal{O}(\alpha^2)\right) - (3\beta - \alpha)\left(1 + \frac{2}{3}\beta + \mathcal{O}(\beta^2)\right)$$

Note that $\partial F_o/\partial\beta = -4 \neq 0$ at $(\alpha,\beta) = (0,0)$. Hence by the Implicit Function Theorem applied to $F_o = 0$ in the (α,β)-plane, we obtain a unique smooth solution

$\beta = \beta(\alpha)$. The condition $F_o = 0$ implies that

$$4(\alpha - \beta) = \frac{2}{3}(\alpha + \beta)^2 + \frac{4}{3}(\alpha - \beta)^2 + \mathcal{O}(\rho^3),$$

where $\rho = \sqrt{\alpha^2 + \beta^2}$. The right-hand side of the above equation is positive near $(\alpha, \beta) = (0, 0)$, so we conclude $\alpha > \beta$ near the origin on the curve defined by $F_o = 0$. Moreover, we know that at $(\alpha, \beta) = (0, 0)$,

$$\frac{\partial \beta}{\partial \alpha} = -\frac{\partial F_o/\partial \alpha}{\partial F_o/\partial \beta} = 1.$$

Therefore, we have a smooth curve $\beta(\alpha) = \alpha + \mathcal{O}(\alpha^2)$ that passes through the origin in the (α, β)-plane with slope 1, and $\alpha > \beta$. By reverting to the original variables, we obtain $b^2 = a^2 + \mathcal{O}(a^4)$. That is, $b = a + \mathcal{O}(a^3)$ and so $b(0) = 0$, $b'(0^+) = 1$, and $b(a) < a$ for a near the origin.

We now repeat this argument for the even branch. We consider the equation $F_e(a, b) = 0$ for all $a \in [a^*, \pi/2]$ and $b \in [0, \pi/\sqrt{12}]$, where a^* is as defined previously (see (6.4)). We need $\partial F_e/\partial a$ to be nonzero at each point (a, b) along the solution curve.

Recall that for the even eigenvalue branch $F_e(a, b) = 0$, we have

$$\frac{\partial F_e}{\partial a} = \left(\frac{3}{2} + \frac{b^2}{2a^2}\right)\sin(2a) + \left(3a - \frac{b^2}{a}\right)\cos(2a) - \frac{a}{b}\sinh(2b).$$

For convenience, we divide $\partial F_e/\partial a$ by $a > 0$ and show that is always a negative quantity for the restricted range. After rewriting this expression, we have

$$\frac{1}{a}\frac{\partial F_e}{\partial a} = \left(3 + \frac{b^2}{a^2}\right)\frac{\sin(2a)}{2a} + \left(3 - \frac{b^2}{a^2}\right)\cos(2a) - \frac{\sinh(2b)}{b}. \tag{6.5}$$

Solving $F_e(a, b) = 0$ for the expression $\sin(2a)/2a$, we obtain

$$\frac{\sin(2a)}{2a} = -\left(\frac{3b^2 - a^2}{3a^2 - b^2}\right)\frac{\sinh(2b)}{2b}.$$

We substitute this expression into (6.5), obtaining

$$\frac{1}{a}\frac{\partial F_e}{\partial a} = -\left(\frac{3(a^2 + b^2)^2}{a^2(3a^2 - b^2)}\right)\frac{\sinh(2b)}{2b} + \left(\frac{3a^2 - b^2}{a^2}\right)\cos(2a).$$

The first term is negative for $a \in [a^*, \pi/2]$ and $b \in [0, \pi/\sqrt{12}]$, since $\sinh(2b)/2b > 0$ for all $b \in [0, \pi/\sqrt{12}]$ and the curve $F_e(a,b) = 0$ lies in the region $a > \sqrt{3}b$ by Lemma 6.2. The second term is also negative since we consider $a \in [a^*, \pi/2]$ and $a^* \approx 1.13943 > \pi/4$. Therefore, we obtain that $\partial F_e/\partial a$ is negative (and so nonzero) at each point (a,b) with $a \in [a^*, \pi/2]$ and $b \in [0, \pi/\sqrt{12}]$.

By the Implicit Function Theorem, there exist neighborhoods $U_a \subseteq \mathbb{R}$ and $V_b \subseteq \mathbb{R}$ such that $a \in U_a, b \in V_b$, and a unique function $g_{a,b} : V_b \to U_a$ exists such that $a = g_{a,b}(b)$ and $F_e(g_{a,b}(y), y) = 0$ for all $y \in V_b$. Furthermore, the function $g_{a,b}$ is infinitely differentiable on V_b. □

Now that we have achieved smooth curves $F_o(a,b) = 0$ and $F_e(a,b) = 0$ in the (a,b)-plane, the bijection F_3 gives us a homeomorphism of these curves onto smooth curves in the (τ, μ)-plane. These are the odd eigenvalue curve connecting the points $A(0,0)$ and $B(-\pi^2/3, -\pi^4/9)$, and the even eigenvalue curve connecting the points $B(-\pi^2/3, -\pi^4/9)$ and $C(-2(a^*)^2, -(a^*)^4)$, the latter of which lies on the critical parabola (see Figure 6.1).

In the sections which follow, we will use the notation $\mu_o(\tau)$ and $\mu_e(\tau)$ to denote the odd and even eigenvalue branches in the sub-parabolic region.

6.3 Intersections of a family of parabolas and the lowest eigenvalues $\mu_o(\tau)$ and $\mu_e(\tau)$

Our goal is now to prove the following proposition:

Proposition 6.5 (Intersection between parabola and the eigenvalues $\mu_o(\tau)$ or $\mu_e(\tau)$)**.** *Each parabola $\mu = -c\tau^2$ with $c > 0$ intersects at least one eigenvalue branch in the third quadrant.*

In other words, we wish to demonstrate that for each $c > 0$, there exists a point (τ, μ) on the parabola $\mu = -c\tau^2$ which is an eigenvalue pair. We build up the proof in several steps.

When $0 < c \leq 1/4$, the parabola lies on or above the critical parabola, and we will be able to work directly with our parameterizations from the super-parabolic region. When $c > 1/4$, this parabola lies in the sub-parabolic region, and we will find it more convenient to work in the (a,b)-plane. We will show the image of this parabola under

our bijection F_3^{-1} is a line through the origin in the (a,b)-plane. We then show this line intersects at least one of the curves $F_o(a,b)=0$ and $F_e(a,b)=0$. Using these results, we can then prove Proposition 6.5 later in the section.

We begin by establishing that the images of the parabolas are lines under F_3^{-1}:

Lemma 6.6 (Transformation of quadratics from the (τ,μ)-plane into the (a,b)-plane)**.** *For each $c>1/4$, the parabola $\mu=-c\tau^2$ is mapped to the line $b=m(c)a$ in the (a,b)-plane, where the slope $m(c)$ satisfies*

$$0<m(c)=\frac{\sqrt{4c-1}}{\sqrt{4c}+1}<1,$$

and $m(c)\to 1$ as $c\to\infty$.

Proof. Since $\tau<0$ we have $\sqrt{\tau^2}=|\tau|$, and so by the bijection Lemma 3.1.3,

$$\begin{aligned}(a,b)&=F_3^{-1}(\tau,-c\tau^2)\\&=\left(\frac{\sqrt{|\tau|}\sqrt{1+\sqrt{1+|1-4c|}}}{2},\frac{\sqrt{|\tau|}\sqrt{-1+\sqrt{1+|1-4c|}}}{2}\right).\end{aligned}$$

From this, since $c>1/4$, we obtain a linear relationship $b=m(c)a$ with $m(c)$ as above.

□

Next, we examine the intersections of lines with the eigenvalue curves.

Lemma 6.7 (Intersections of eigenvalue curves $F_o(a,b)=0$ and $F_e(a,b)=0$ with a line)**.** *For each slope $0<m<1$, the line $b=ma$ intersects at least one of the curves $F_o(a,b)=0$ or $F_e(a,b)=0$ when $a\in(0,\pi/2)$ and $b\in(0,\pi/\sqrt{12})$.*

In particular, when $1/\sqrt{3}\le m<1$, the line intersects $F_o(a,b)=0$ at least once. If $0<m\le 1/\sqrt{3}$, the line intersects $F_e(a,b)=0$ at least once.

Proof. Following Lemma 6.2, we take $b(a)$ to be the solution of $F_o(a,b)=0$ for $a\in(0,\pi/2)$ and likewise take $a(b)$ to be the solution of $F_e(a,b)=0$ for $b\in(0,\pi/\sqrt{12})$. We shall use the Intermediate Value Theorem together with continuity of the solutions $b(a)$ and $a(b)$ (Lemma 6.4) to obtain existence of an intersection of the line and the curves $F_o(a,b)=0$ or $F_e(a,b)=0$.

We consider three cases for m.

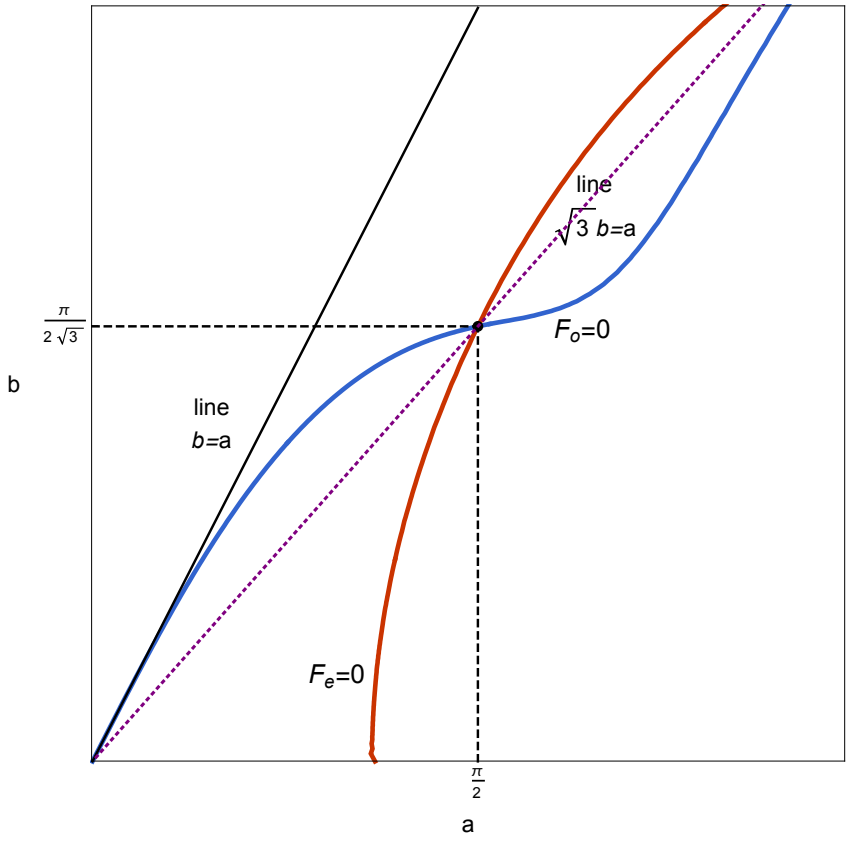

Figure 6.2: Two eigenvalue branches in the sub-parabolic region are transformed in the (a, b)-plane. The odd eigenvalue branch $F_o(a, b) = 0$ (blue curve) and even eigenvalue branch $F_e(a, b) = 0$ (red curve) intersect repeatedly along the dotted purple line $b = a/\sqrt{3}$.

(i) *For each* $1/\sqrt{3} < m < 1$, *the line* $b = ma$ *intersects the curve* $F_o(a, b) = 0$. We showed in Lemma 6.4 that $b'(0^+) = 1$, so the line $b = ma$ lies below the graph of $b(a)$ near the origin. By direct computation, the line also lies above $b(a)$ at $a = \pi/2$ (see Figure 6.2). By continuity, there exists some $a' \in (0, \pi/2)$ such that $b(a') = ma'$.

(ii) *For each* $m = 1/\sqrt{3}$, *the line* $b = a/\sqrt{3}$ *intersects the curves* $F_e(a, b) = 0$ *and* $F_o(a, b) = 0$. By Proposition 6.8, the eigenvalue curves intersect at $(a, b) = (\pi/2, \pi/\sqrt{12})$, which lies on the desired line.

(iii) *For each* $0 < m < 1/\sqrt{3}$, *the line* $b = ma$ *intersects the curve* $F_e(a, b) = 0$. The line $a = b/m$ lies below the curve $a(b)$ at $b = 0$ and lies above the curve at $b = \pi/\sqrt{12}$ (see Figure 6.2). By continuity, there exists some $b' \in (0, \pi/\sqrt{12})$ such that $a(b') = b'/m$.

Finally, from Lemma 6.6, we see $m_1 = 1/\sqrt{3}$; when $1 < c < \infty$, we have $1/\sqrt{3} < m < 1$; and when $1/4 < c < 1$, we have $0 < m < 1/\sqrt{3}$. □

Proof of Proposition 6.5. For every $0 < c \leq 1/4$, the parabola $\mu = -c\tau^2$ lies on or above the critical parabola. In the super-parabolic region, by Theorem 5.5.2, there is a continuous eigenvalue curve that connects the point $(-\pi^2/4, 0)$ on the τ-axis with the point $C(-2(a^*)^2, -(a^*)^4)$ on the critical parabola. This curve is in fact the first even eigenvalue curve in the super-parabolic region. At the upper point $(-\pi^2/4, 0)$, we have $-c\tau^2 < \mu$. At the lower point $C(-2(a^*)^2, -(a^*)^4)$, we have $-c\tau^2 > \mu$. Therefore, since μ and τ are continuous along the curve, there exists some point at which $-c\tau^2 = \mu$.

For the case of $c > 1/4$, the parabola lies in the sub-parabolic region and we work in the (a, b)-plane. By Lemma 6.6, we have that the parabola $\mu = -c\tau^2$ maps to the line $b = m(c)a$, with $1 < c < \infty$ corresponding to $1/\sqrt{3} < m(c) < 1$, with $1/4 < c < 1$ corresponding to $0 < m(c) < 1/\sqrt{3}$, and with $m(1) = 1/\sqrt{3}$. By Lemma 6.7, we showed that each line intersects at least one of the curves $F_o(a, b) = 0$ and $F_e(a, b) = 0$, which corresponds to eigenvalue curves in the sub-parabolic region by using the homeomorphism F_3. □

6.4 Properties of the eigenvalue curves in the sub-parabolic region

We end with a result on the intersections of the eigenvalue curves with each other.

Proposition 6.8 (Intersections of Eigenvalue Curves)**.** *The odd and even eigenvalue branches in the sub-parabolic region intersect infinitely often along the parabola* $\mu = -\tau^2$.

Proof. The odd and even eigenvalue curves intersect when a and b both satisfy eigenvalue conditions (6.2) and (6.3) simultaneously. By adding the two equations, we obtain

$$2(3a^2 - b^2)\frac{\sin(2a)}{2a} = 0.$$

Hence the equation gives us (i) $3a^2 = b^2$ or (ii) $\sin(2a) = 0$. Case (i) is not possible since $a > b$ by properties of F_3. When (ii) is satisfied, we have $a = m\pi/2$ for some $m \in \mathbb{N}$, and furthermore,

$$0 = (3b^2 - a^2)\frac{\sinh(2b)}{2b}.$$

But since $\sinh(2b)/2b > 0$ for all $b > 0$, the above reduce to $3b^2 = a^2$. The (a, b) values at the points of intersection correspond to

$$\tau = -\frac{4}{3}a^2, \quad \mu = -\frac{16}{9}a^4, \qquad \text{where } a = \frac{m}{2}\pi,\ m \in \mathbb{N}.$$

These (τ, μ) all lie on the parabola $\mu = -\tau^2$, as desired (see Figure 6.3). □

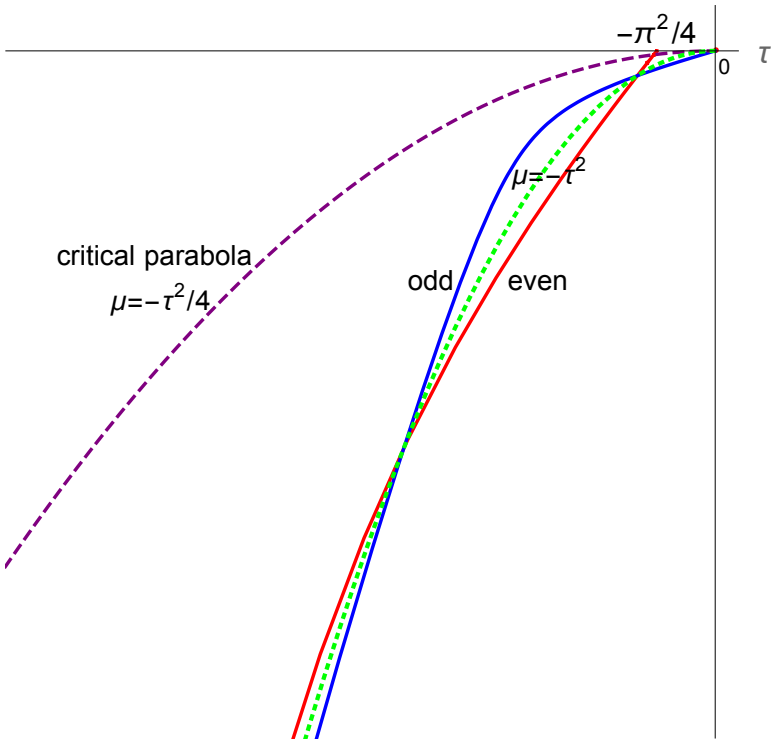

Figure 6.3: Sub-parabolic region: the odd and even eigenvalue curves intersect on the parabola $\mu = -\tau^2$ at the points $(\tau, \mu) = (-m^2\pi^2/3, -m^4\pi^4/9)$. See Proposition 6.8 in Section 6.4.

Part II

Diffusion-driven instability of fourth order system

CHAPTER 7

INTRODUCTION TO TURING INSTABILITY

7.1 History and motivation

This part of the thesis characterizes the Turing space of two-species reaction-diffusion mechanisms with fourth order bi-Laplacian type diffusion. Alan Turing conjectured a mathematical mechanism which explains how two diffusing morphogen populations interact to generate patterns in biology [31]. This mechanism is now known as Turing instability or diffusion-driven instability. The idea is that two quantities, the activator and inhibitor, satisfy coupled reaction-diffusion equations. These equations admit a linearly stable spatially homogeneous steady state when diffusion is absent, but this homogeneous steady state becomes linearly unstable in the presence of diffusion, initiating a spatially varying inhomogeneous state, or pattern. The space of parameters for which Turing instability occurs is called the Turing space. The field of Turing's theory has been broadened analytically and numerically by many researchers producing applications of the mathematical model to closely represent patterns in biology [9, 22, 23, 25].

In standard Turing analysis, the Laplacian operator acts for diffusion of the activator and inhibitor and the domain is fixed. Recent work in Turing's theory has extended applicability of the method, such as by considering growing domains, which are biologically relevant since actual organisms are growing as patterns are forming [16, 21, 27]. In this part of the thesis, we will consider a fixed domain but allow the activator and inhibitor to diffuse according to a bi-Laplacian type operator that includes both fourth order and second order terms whose relative importance is determined by the tension coefficient. The analysis applies in all dimensions.

7.2 Overview of results

We characterize the parameter values forming the Turing space (Theorem 8.3), meaning the parameter values for which Turing instability occurs for a given domain. The fourth order situation is different from the standard second order situation because two different types of diffusion, fourth order and second order terms, can compete. The fourth order term stabilizes the system whereas the second order term destabilizes the system, when the tension parameter is negative. Negative tension parameter is considered as destabilization since the backwards Laplacian is ill-posed. This competing situation leads to negative eigenvalues of the diffusion operator, which was not considered in the Laplacian Turing analysis. We show that when competition of two diffusions happens, Turing instability always occurs if we are willing to vary the domain (Corollary 8.5). One might think it is obvious instability occurs simply because of negative eigenvalues. However, it actually relies upon properties of the spectrum established in the first part of the thesis, as we now explain.

To refine our understanding of the Turing space, we identify a cross-section of Turing space in terms of domain and tension parameter (Theorem 9.3). We certify for which length of the domain we obtain Turing instability, at least in the one-dimensional case. We fix the reaction parameters but vary the size of domain and tension parameter, and investigate how these changes affect occurrence of Turing instability. This investigation can be done since in Part I of the thesis we analyzed properties of the spectrum of the bi-Laplacian type operator with the natural (free) boundary conditions in one dimension. We find new phenomena when the fourth order and second order terms are competing. Having negative eigenvalues for the diffusion operator does not by itself make Turing instability occur. Additional conditions need to be satisfied.

To conclude the second part of the thesis, we apply an analogous cross-sectional Turing analysis to the periodic boundary condition case in one dimension. Even though the periodic boundary condition is not so biologically relevant, it is worth to consider in a sense of providing motivation and insight. The periodic case can be analyzed exactly because the spectrum of the bi-Laplacian type operator for the periodic boundary conditions can be computed exactly. Therefore, we also treat this case and compare the two situations (free and periodic). We find that overall shape of the cross-sectional Turing space for periodic situation is similar to the free case

(Figures 9.3 and 10.1), which provides insight into the shape of cross-sectional Turing space for the more difficult free case.

7.3 Related literature

Although Turing's theory is mostly considered as biological pattern formation, the idea of diffusion-driven instability is not restricted to biology. The mathematical framework can be generally applied wherever the populations can be considered as random moving reactive materials. For instance, researchers have identified Turing-like patterns in the distribution of species in ecological systems, such as the predator-prey model, where the prey acts as activator while the predator acts as inhibitor [1, 18, 20, 24, 28].

Growing domain

It is a natural question to ask how the reaction-diffusion model produces spatial patterns via Turing instability on "growing" domains. Crampin *et al.* were the first researchers to consider the domain growth effects in the reaction-diffusion models [8]. Plaza *et al.* [27], Madzvamuse *et al.* [21] investigated the role of growth in pattern formation considering Turing instability. For instance, they found that an activator-activator model may give Turing patterns in the presence of domain growth. Such choice of kinetics cannot exhibit Turing instability on fixed domains. Furthermore, a recent paper by Klika and Gaffney [16] pointed out that analysis of Turing instability on growing domains is even more complicated than Madzvamuse *et al.* [21] have considered. They emphasized the history dependence of the stability conditions and the transient nature of the unstable modes with faster growth. An interesting future direction is to apply these conditions for growing domains to the bi-Laplacian type diffusion considered in this thesis.

Plate problems

This part of the thesis includes analysis using properties of the spectrum of the free rod under tension and compression. The rod is the one-dimensional case of the

plate. Plate problems are fourth order analogues of membrane problems, with the bi-Laplacian operator taking the place of the Laplacian. The fourth order problems with appropriate boundary conditions have modeled a number of plates with physically relevant conditions. For example, Sweers recently gave a survey of sign- and positivity-preserving properties of rod and plate problems with certain boundary conditions [30]. More recently, Ashbaugh *et al.* proved an isoperimetric inequality for the first eigenvalue of the clamped plate under compression for a small range of compression $\tau < 0$ [2]. Our investigation in this part of the thesis connects the analysis of fourth order plate problem (Part I of the thesis) to Turing's model of pattern formation in biology.

Lewis employed the fourth order type diffusion in a plant-herbivore model [19]. He showed that the coupling of herbivore dispersal with plant and herbivore dynamics gives rise to both persistent and transient spatial patterns.

7.4 Positivity preservation and thin fluid film diffusion

Turing instability for fourth order diffusion with a second order term is comprehensively analyzed in this part of the thesis. A disadvantage of the fourth order diffusion is that it does not satisfy the minimum principle. Initial data that is positive can evolve to become negative at some point, at a later time, which is not biologically reasonable.

However, the fourth order nonlinear "thin fluid film equation" that preserves positivity gives a way to solve this problem. For example,

$$h_t = -(h^n h_{xxx})_x \pm \tau (h^m h_x)_x \tag{7.1}$$

is known to have a "weak minimum principle" for a sufficiently large value n, in that interior finite-time singularities in (7.1) are forbidden for $n \geq 3.5$ [4]. Furthermore, Bertozzi and Pugh proved global positivity preservation when $n \geq 3.5$ [5]. Linearizing such a PDE around a constant steady state gives a linear fourth order PDE of the type considered in my research. Hence the nonlinear "thin fluid film" PDE with additional reaction terms may be an interesting question for future research in 4th order pattern formation.

CHAPTER 8

TURING SPACE FOR FOURTH ORDER DIFFUSION

8.1 Reaction-diffusion system, boundary conditions and Turing space

The interaction of two chemicals, activator u and inhibitor v, gives a reaction-diffusion system of equations

$$\frac{\partial u}{\partial t} = (-\Delta^2 u + \tau\Delta u) + f(u,v) \tag{8.1}$$

$$\frac{\partial v}{\partial t} = k(-\Delta^2 v + \tau\Delta v) + g(u,v), \tag{8.2}$$

where f and g model the reaction kinetics, $k > 0$ is a proportionality constant of diffusion (call it "diffusivity"), and τ is tension coefficient. The bi-Laplacian Δ^2 was defined in (2.5). We fix the homogeneous steady state $(u_0, v_0) \in \mathbb{R}^2$ of (8.1)–(8.2) to be the solution of

$$f(u_0, v_0) = 0, \quad g(u_0, v_0) = 0,$$

and the partial derivatives of f and g to be evaluated at the steady state (u_0, v_0), so that

$$f_u = f_u(u_0, v_0), \quad f_v = f_v(u_0, v_0),$$

throughout this part of the thesis, and similarly for g_u and g_v.

The bi-Laplacian type operator $\Delta^2 - \tau\Delta$ includes both 4th order and 2nd order terms whose relative importance is determined by the "tension" coefficient τ. Even though the terminology "tension" is related to the vibrating plate model [6, Section 2] and it is not relevant to diffusion operation, we still call τ the tension coefficient. For the domain $\Omega \subset \mathbb{R}^n$, we work with the natural (free) boundary conditions associated with the diffusion operator $\Delta^2 - \tau\Delta$. In dimension $n = 2$, this means u and v satisfy

boundary conditions of the type

$$\frac{\partial^2 \phi}{\partial n^2} = 0 \qquad \text{on } \partial\Omega, \tag{8.3}$$

$$\tau \frac{\partial \phi}{\partial n} - \frac{\partial(\Delta\phi)}{\partial n} - \frac{\partial}{\partial s}\left(\frac{\partial^2 \phi}{\partial s \partial n} - K(s)\frac{\partial \phi}{\partial s}\right) = 0 \qquad \text{on } \partial\Omega, \tag{8.4}$$

where n denotes outward unit normal derivative, s the arclength, and K the curvature of $\partial\Omega$. For n-dimension, the natural (free) boundary conditions for $\Delta^2 - \tau\Delta$ are stated in [6, Proposition 5]. The natural boundary condition (8.4) with $\phi = u$ and $\phi = v$ imply that mass is conserved by the diffusion operator.

The eigenvalues $\mu_j = \mu_j(\Omega, \tau)$ of the operator $\Delta^2 - \tau\Delta$ are governed by the differential equation

$$\Delta^2 u - \tau \Delta u = \mu u \tag{8.5}$$

together with the natural boundary conditions (8.3)–(8.4) on Ω, and are listed in increasing order as

$$\mu_1 \leq \mu_2 \leq \mu_3 \leq \cdots \to \infty.$$

There is always a zero eigenvalue, with constant eigenfunction. When $\tau \geq 0$, this zero eigenvalue is the lowest eigenvalue. When $\tau < 0$, there is at least one negative eigenvalue. For more on the spectrum and the relevant Sobolev spaces and bilinear forms, see [6] and Part I of the thesis.

Remark 8.1. Imposing Dirichlet boundary conditions would cause a flux of u and v through the boundary, so there might be some loss of spatial patterns. Therefore we do not consider Dirichlet conditions. On the other hand, we will investigate a simpler boundary condition at the end of the second part of the thesis, that is, the periodic boundary conditions in one dimension.

Notice we have the same diffusion operator for both activator and inhibitor, up to constant multiple. Hence we can expand both u and v in terms of the same eigenfunctions, to carry out the Turing instability analysis, in the proof of Theorem 8.3.

In the next definition, we need a system of ordinary differential equations

$$\frac{\partial u}{\partial t} = f(u, v) \tag{8.6}$$

$$\frac{\partial v}{\partial t} = g(u, v), \tag{8.7}$$

which is same as the system (8.1)–(8.2) without the diffusion terms.

Definition 8.2 (Turing space)**.** *Consider a smoothly bounded domain $\Omega \subset \mathbb{R}^n$. The reaction diffusion system (8.1)–(8.4) admits* Turing instability *if the homogeneous steady state (u_0, v_0) is linearly asymptotically stable to small perturbations in the absence of diffusion (meaning for the ODE system (8.6)–(8.7)), but linearly unstable to small* spatial *perturbations when diffusion is present (meaning for the PDE system (8.1)–(8.4)).*

The Turing space *for Ω is the space of parameters giving* Turing instability*:*

$$TS(\Omega) = \{(f_u, f_v, g_u, g_v, k, \tau) \in \mathbb{R}^6 : \textit{the homogeneous steady state } (u_0, v_0) \textit{ is linearly asymptotically stable in the absence of diffusion but unstable when diffusion is present}\}.$$

For convenience, we use notation $\vec{p} = (f_u, f_v, g_u, g_v, k) \in \mathbb{R}^5$ as vector of reaction-diffusion parameters. With fixed τ, the Turing space *for Ω and τ is the cross-section*

$$TS(\Omega, \tau) = \{\vec{p} \in \mathbb{R}^5 : (\vec{p}, \tau) \in TS(\Omega)\}.$$

8.2 Characterization of Turing space for fixed domain

In this section, we will fix τ and find conditions for the reaction-diffusion parameter vector $\vec{p}$ to get a Turing instability on the domain Ω.

We define three quantities which will be used in the following discussion:

$$A(\vec{p}) = \frac{f_u + g_v}{1 + k}, \tag{8.8}$$

$$a(\vec{p}), b(\vec{p}) = \frac{(kf_u + g_v) \pm \sqrt{(kf_u + g_v)^2 - 4k(f_u g_v - f_v g_u)}}{2k}, \tag{8.9}$$

where a corresponds to the minus root and b corresponds to the plus root.

(The roots $a(\vec{p})$ and $b(\vec{p})$ in Part II of the thesis are not the same as the parameters a and b in Part I of the thesis.)

Recall that $\mu_j = \mu_j(\Omega, \tau)$ denotes the jth eigenvalue of the diffusion operator $\Delta^2 - \tau\Delta$ with natural boundary conditions (8.3)–(8.4) on the domain Ω. Define

$$\text{Spec}(\Omega, \tau) = \text{spectrum} = \{\mu_j(\Omega, \tau) : j = 1, 2, 3, \dots\}.$$

Theorem 8.3 (Characterization of Turing space for fixed domain)**.** *Given the domain Ω, if $\tau \geq 0$ then the Turing space is*

$$TS(\Omega, \tau) = \{\vec{p} \in \mathbb{R}^5 : \text{ (8.10)–(8.13) hold, and } \text{Spec}(\Omega, \tau) \cap (a(\vec{p}), b(\vec{p})) \neq \emptyset\},$$

and if $\tau < 0$ then the Turing space is

$$TS(\Omega, \tau) = \{\vec{p} \in \mathbb{R}^5 : \text{either (8.10)–(8.12) hold and } \text{Spec}(\Omega, \tau) \cap (a(\vec{p}), b(\vec{p})) \neq \emptyset, \\ \text{or (8.10)–(8.11) hold and } \mu_1 < A(\vec{p})\},$$

where the conditions are

$$f_u + g_v < 0, \tag{8.10}$$
$$f_u g_v - f_v g_u > 0, \tag{8.11}$$
$$(kf_u + g_v)^2 - 4k(f_u g_v - f_v g_u) > 0, \tag{8.12}$$
$$kf_u + g_v > 0. \tag{8.13}$$

Note condition (8.10) implies $A(\vec{p}) < 0$.

Proof. When $\tau \geq 0$ we get the same conditions for Turing instability as when Laplacian diffusion is used [23, Section 2.3], namely conditions (8.10)–(8.13). We give this proof below, since the later parts of the proof must be modified when $\tau < 0$.

Conditions (8.10) and (8.11) come from requiring linear stability of the ODE system in the absence of any spatial variation, as we now explain. Without spatial variation u and v satisfy

$$u_t = f(u, v), \quad v_t = g(u, v).$$

First, we linearize the system about the constant steady state (u_0, v_0): set $\vec{w} =$

$\begin{pmatrix} u-u_0 \\ v-v_0 \end{pmatrix}$, so that for small $|\vec{w}|$,

$$\vec{w}_t = \begin{pmatrix} f_u & f_v \\ g_u & g_v \end{pmatrix} \vec{w}$$

where the derivative matrix is evaluated at $u = u_0, v = v_0$. Look for solution of the form $\vec{w} \propto e^{\lambda t}$. The steady state $\vec{w} = 0$ is linearly stable if $\operatorname{Re} \lambda < 0$ for each eigenvalue λ of the derivative matrix. That is, where λ satisfies the quadratic equation

$$\det \left[\begin{pmatrix} f_u & f_v \\ g_u & g_v \end{pmatrix} - \lambda I \right] = \lambda^2 - (f_u + g_v)\lambda + ^2 (f_u g_v - f_v g_u) = 0.$$

Hence linearly stability of the constant steady state for the ODE system is guaranteed if (8.10) and (8.11) hold:

$$\begin{aligned} f_u + g_v &< 0, \\ f_u g_v - f_v g_u &> 0. \end{aligned}$$

We assume these conditions throughout the rest of the proof.

Conditions (8.12) and (8.13) come from requiring linear instability of the PDEs (including the diffusion term) at the constant steady state, as we now explain. Consider the full reaction-diffusion system (8.1)–(8.2) and again linearize about (u_0, v_0) to get

$$\vec{w}_t = \begin{pmatrix} 1 & 0 \\ 0 & k \end{pmatrix} (-\Delta^2 + \tau\Delta)\vec{w} + \begin{pmatrix} f_u & f_v \\ g_u & g_v \end{pmatrix} \vec{w}. \tag{8.14}$$

Define $\phi_j(x)$ to be the time-independent solution of the eigenvalue problem:

$$\Delta^2 \phi_j - \tau\Delta\phi_j = \mu_j \phi_j,$$

with the free boundary conditions (8.3)–(8.4), where μ_j is the eigenvalue.

We look for a solution $\vec{w}(x,t)$ of (8.14) in the separated form

$$\vec{w}(x,t) = \sum_j \begin{pmatrix} c_j \\ d_j \end{pmatrix} e^{\lambda_j t}\phi_j(x),$$

where c_j's and d_j's are constants. Note that the growth rate λ_j informs us about the stability of the homogeneous steady state with respect to the perturbation ϕ_j. If the real part of λ_j is negative for all j, then any perturbations will tend to decay exponentially quickly. However, in the case that the real part of λ_j is positive for any value of j, our expansion suggests that the amplitude of these modes will grow exponentially quickly and so the homogeneous steady state is linearly unstable. Substitution gives us for each j,

$$\lambda\phi_j = -\mu_j D\phi_j + M\phi_j \tag{8.15}$$

where $D = \begin{pmatrix} 1 & 0 \\ 0 & k \end{pmatrix}$ is the diffusivity matrix and $M = \begin{pmatrix} f_u & f_v \\ g_u & g_v \end{pmatrix}$ is the stability matrix. To get a nontrivial ϕ_j, formula (8.15) says λ must be an eigenvalue of the matrix $-\mu_j D + M$, and so

$$\det[\lambda I + \mu_j D - M] = 0.$$

Hence we get the eigenvalues $\lambda(\mu_j)$ as functions of the wavenumber μ_j, as the two roots of

$$\begin{aligned} \lambda^2 + F(\mu_j)\lambda + H(\mu_j) &= 0, \\ F(\mu_j) &\stackrel{\text{def}}{=} \mu_j(1+k) - (f_u + g_v) < 0, \\ H(\mu_j) &\stackrel{\text{def}}{=} k\mu_j^2 - (kf_u + g_v)\mu_j + (f_u g_v - f_v g_u). \end{aligned} \tag{8.16}$$

For the steady state to be unstable to spatial perturbation, we require

$$\mathrm{Re}\,[\lambda(\mu_j)] > 0 \qquad \text{for some } j \neq 0.$$

Recall that a quadratic equation with real coefficients has a root with positive real part if and only if either the sum of the roots is positive or the product of the roots

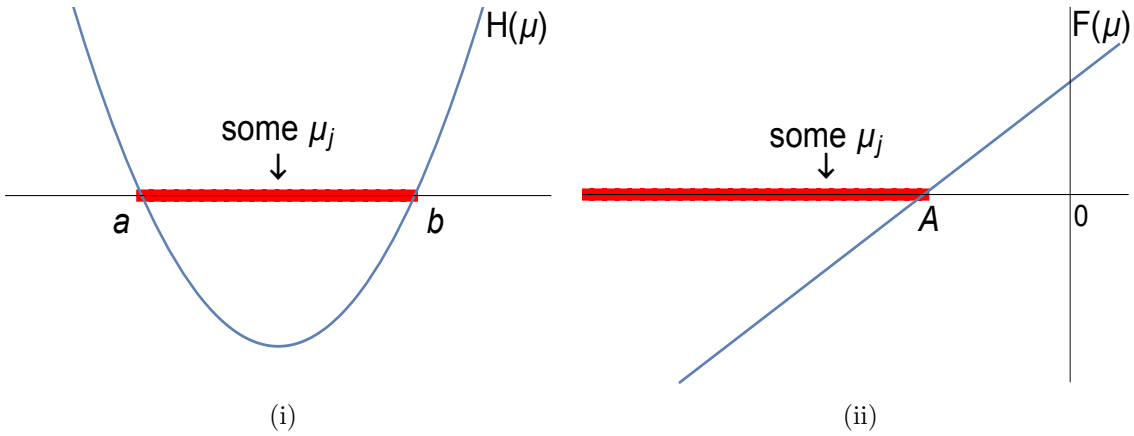

(i) (ii)

Figure 8.1: There are two different ways that we can get instability. For the steady state to be unstable to spatial perturbation, we require $\mathrm{Re}\,[\lambda(\mu_j)] > 0$ for some $j \neq 0$. This can happen if either (i) $H(\mu_j) \stackrel{\text{def}}{=} k\mu_j^2 - (kf_u + g_v)\mu_j + (f_u g_v - f_v g_u) < 0$ or (ii) $F(\mu_j) \stackrel{\text{def}}{=} \mu_j(1+k) - (f_u + g_v) < 0$ for some $j \neq 0$, where a, b, A in the graphs are the intercepts along the μ-axis. The figure shows general possible ways where instability can occur. Obviously, case (ii) cannot happen if all the eigenvalues μ_j are positive.

is negative. Applied to the quadratic (8.16), that means we want $F(\mu_j) < 0$ or $H(\mu_j) < 0$, for some $j \geq 1$. See Figure 8.1.

Now, we will consider the cases $\tau \geq 0$ and $\tau < 0$ separately. When $\tau < 0$, the 2nd order "backwards" diffusion $\dfrac{\partial u}{\partial t} = \tau \Delta u$ is ill-posed, meaning the 2nd order term destabilizes the system whereas the 4th order term $\Delta^2 u$ stabilizes the system. In other words, two different types of diffusion compete when the tension parameter τ is negative. However, such competition does not happen in $\tau \geq 0$ case. The 4th and 2nd order diffusion operators are each well-posed when $\tau \geq 0$. The case $\tau \geq 0$ is very similar to the traditional Turing analysis with the Laplacian diffusion, since all eigenvalues μ_j of (8.5) are positive by the Rayleigh Quotient in Definition 8.6. On the other hand, the case $\tau < 0$ is different from the traditional Turing instability since there are some negative eigenvalues.

Case $\tau \geq 0$. When $\tau \geq 0$, the fact that μ_j is always positive (from Rayleigh Quotient in Definition 8.6) and $f_u + g_v < 0$ from the stability condition (8.10) mean $F(\mu_j) \geq 0$. So $\mathrm{Re}\,[\lambda(\mu_j)] > 0$ if and only if $H(\mu_j) < 0$ for some j. See Figure 8.2(ii). Since $f_u g_v - f_v g_u > 0$ by (8.11), we see $H(\mu_j) < 0$ if and only if (8.12)–(8.13) hold,

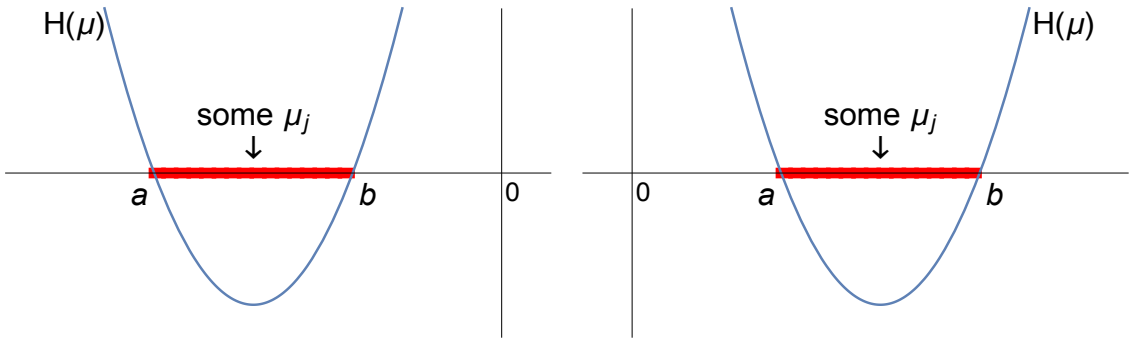

(i) (ii)

Figure 8.2: The two ways to get $H(\mu_j) < 0$. The distinct roots a and b of $H(\mu) = 0$ must have the same sign since the vertical intercept is $f_u g_v - f_v g_u > 0$ from the condition (8.11). When $\tau \geq 0$, figure (ii) is the only possibility, because all μ_j are nonnegative. When $\tau < 0$, there exists negative eigenvalues of $\Delta^2 u - \tau \Delta u = \mu u$ and so both (i) and (ii) are possible.

meaning $H(\mu_j) = 0$ has distinct positive roots:

$$\begin{aligned} (kf_u + g_v)^2 - 4k(f_u g_v - f_v g_u) &> 0, \\ kf_u + g_v &> 0, \end{aligned}$$

since $\mu_j \geq 0$ for all j. The first condition is a discriminant requirement. Hence, to be in Turing space, conditions (8.12)–(8.13) are necessary and sufficient, when (8.10)–(8.11) hold.

Case $\tau < 0$. Now, we will consider $\tau < 0$. The difference from $\tau \geq 0$ comes from the fact that μ_j can be positive or negative and so both cases in Figure 8.1 can happen in order to get $\mathrm{Re}\,[\lambda(\mu_j)] > 0$. Therefore, to be in Turing space, either $F(\mu_j) < 0$ (which is $\mu_j < A(\vec{p})$ hence $\mu_1 < A(\vec{p})$) or $H(\mu_j) < 0$ are necessary to hold.

For $H(\mu_j) < 0$, $H(\mu_j) = 0$ must have distinct roots that have the same sign since the vertical intercept of the quadratic $H(\mu_j)$ is $f_u g_v - f_v g_u > 0$ by (8.11) and this gives a further necessary condition (8.12):

$$(kf_u + g_v)^2 - 4k(f_u g_v - f_v g_u) > 0.$$

Also, the spectrum must intersect the interval $(a(\vec{p}), b(\vec{p}))$:

$$\mu_j \in (a(\vec{p}), b(\vec{p}))\,,$$

where $a(\vec{p})$ and $b(\vec{p})$ are the distinct roots of $H(\mu_j) = 0$, that is, the quantities defined in (8.9):

$$a, b = a(\vec{p}), b(\vec{p}) = \frac{(kf_u + g_v) \pm \sqrt{(kf_u + g_v)^2 - 4k(f_u g_v - f_v g_u)}}{2k}.$$

Note that we have two possibilities depending on the sign of μ_j (see Figure 8.2). We do not have to satisfy (8.13) because we are allowed to have negative wavenumber μ_j of $\Delta^2 - \tau\Delta$. We have shown that when $\tau < 0$, in addition to conditions (8.10)–(8.11), either condition (8.12) and $\mathrm{Spec}(\Omega, \tau) \cap (a(\vec{p}), b(\vec{p})) \neq \emptyset$ are necessary to hold, or else $\mu_1 < A(\vec{p})$ is necessary, for belonging to the Turing space.

Until now, we have showed necessary conditions to be in the Turing space, when $\tau < 0$. To finish proving the theorem, we have to show the conditions are sufficient. We show that $\vec{p}$ belongs to the Turing space if

$$\begin{aligned}&\text{either (8.12) holds and } \mathrm{Spec}(\Omega, \tau) \cap (a(\vec{p}), b(\vec{p})) \neq \emptyset,\\ &\text{or } \mu_1 < A(\vec{p}),\end{aligned}$$

when $\tau < 0$ and (8.10)–(8.11) are assumed.

Assume first we are in situation of Figure 8.1(i), meaning (8.10)–(8.12) hold and there exists at least one eigenvalue μ_j such that $\mu_j \in (a(\vec{p}), b(\vec{p}))$. Since $H(\mu_j) < 0$, Turing instability occurs.

Assume now that we are in situation of Figure 8.1(ii), meaning (8.10)–(8.11) hold and

$$\mu_1 < \frac{f_u + g_v}{1 + k} = A(\vec{p}).$$

Since $F(\mu_1) < 0$ and so $\mathrm{Re}\,[\lambda(\mu_1)] > 0$, Turing instability occurs. These prove the theorem when $\tau < 0$.

□

Remark 8.4. When $\tau \geq 0$, conditions (8.10) and (8.13) imply $k \neq 1$, meaning one of the activator and inhibitor must diffuse faster than the other. When $\tau < 0$, since the

condition (8.13) need not be assumed in Theorem 8.3, we see k can equal 1, meaning the activator and inhibitor possibly diffuse at the same rate.

8.3 Varying the domain

We characterized the Turing space for a fixed domain Ω in Theorem 8.3. When $\tau \geq 0$, all four conditions (8.10)–(8.13) are the same as the standard Turing space for the Laplacian. When $\tau < 0$, only the first two or three of these conditions are required to be in the Turing space, so the Turing space for the fourth order operator $\Delta^2 - \tau\Delta$ is larger than standard Turing space.

In the following corollary, we show that we can always get Turing instability when $\tau < 0$, provided we are willing to vary the domain.

Corollary 8.5. *If $\tau < 0$ and $\vec{p}$ satisfies (8.10) and (8.11), then Turing instability occurs for some domain Ω.*

Corollary 8.5 depends on a certain fact about the minimum of the lowest eigenvalue of $\Delta^2 - \tau\Delta$, which we state below as Theorem 8.7.

Write D^2u for the Hessian matrix of u, and $|D^2u|^2 = \sum_{i,j} u_{x_i,x_j}^2$.

Definition 8.6. *Define μ_1 = lowest eigenvalue of $(\Delta^2 - \tau\Delta)u = \mu u$ with natural (free) boundary conditions (8.3)–(8.4). That is (see [6, Section 2]),*

$$\mu_1(\Omega, \tau) = \min_{u \in H^2(\Omega)} \frac{\int_\Omega \left(|D^2u|^2 + \tau|\nabla u|^2\right) dx}{\int_\Omega u^2 \, dx}. \tag{8.17}$$

Denote the "smallest possible" first eigenvalue by

$$\mu_1^*(\tau) = \inf_\Omega \mu_1(\Omega, \tau).$$

The ratio on the right of (8.17) is called the Rayleigh quotient. It is obtained formally by multiplying the eigenvalue equation (8.5) by u and integrating by parts, using the natural boundary conditions (8.3)–(8.4).

Observe that $\mu_1^*(\tau) < 0$ when $\tau < 0$, by choosing a linear trial function. We show $\mu_1^*(\tau) = -\infty$, which is the key to proving Corollary 8.5.

Theorem 8.7. *If $\tau < 0$ then the first eigenvalue can be arbitrarily negative:*

$$\mu_1^*(\tau) = -\infty.$$

Proof. Step 1: Fix $\tau < 0$. We will prove the theorem first on a one-dimensional interval. Let $\Omega = (-R, R)$; an interval of length $2R$ centered at the origin. We start by finding a rescaling relation. Let $\tilde{x} = x/R$ and $v(\tilde{x}) = u(x)$. Then v is defined on the interval $(-1, 1)$. From the transformation, the differential equation (8.5) and the one-dimensional natural boundary conditions of the type (8.3)–(8.4) are converted into

$$v'''' - \tau R^2 v'' = R^4 \mu\,(\Omega, \tau)\, v,$$

and

$$\begin{cases} v'' = 0 & \text{at } \tilde{x} = \pm 1, \\ v''' - \tau R^2 v' = 0 & \text{at } \tilde{x} = \pm 1. \end{cases}$$

Changing variable like this leads to the rescaling relation:

$$\mu_j(\Omega, \tau) = R^{-4} \mu_j((-1, 1), \tau R^2). \tag{8.18}$$

(We rescaled since we know from Part I of the thesis how the eigenvalue $\mu_j((-1, 1), \tau R^2)$ behaves with respect to the parameter τR^2 when the domain $(-1, 1)$ is fixed.)

Notice the following equivalent conditions, when $c > 0$ is fixed:

$$\begin{aligned} & \mu_j((-R, R), \tau) = -c\tau^2 \\ \iff & R^{-4} \mu_j((-1, 1), \tau R^2) = -c\tau^2 \qquad \text{from the rescaling} \\ \iff & \mu_j((-1, 1), \tau R^2) = -c(\tau R^2)^2 \\ \iff & \mu_j((-1, 1), \tilde{\tau}) = -c\tilde{\tau}^2, \end{aligned} \tag{8.19}$$

where $\tilde{\tau} = \tau R^2$. There is at least one value $\tilde{\tau} < 0$ and one index j such that (8.19) holds, since we know from Proposition 6.5 there is at least one intersection between the eigenvalue curves $\mu_j((-1, 1), \tilde{\tau})$ for $\tilde{\tau} < 0$ and the parabola $y = -c\tilde{\tau}^2$. From the equivalent conditions, there is at least one value R and one index j such that

$$\mu_j((-R, R), \tau) = -c\tau^2.$$

Hence $\mu_1((-R,R),\tau) \le -c\tau^2$. We have shown that

$$\text{for arbitrary } c>0, \text{ there exists } R \text{ such that } \mu_1((-R,R),\tau) \le -c\tau^2.$$

So

$$\mu_1^*(\tau) = \inf_{\Omega} \mu_1(\Omega,\tau) \le -c\tau^2.$$

Letting $c \to \infty$ shows $\mu_1^*(\tau) = -\infty$.

Step 2: Extend to n-dimensional cube in $\mathbb{R}^n$. Firstly we show extension to a 2-dimensional square domain. Let $\Omega_1 = (-R,R)$ and $\Omega_2 = (-R,R)\times(-R,R)$. The first eigenvalue μ_1 is the minimum of Rayleigh quotient over the space of all functions $u \in H^2$, by using the Rayleigh-Ritz variational formula, that is,

$$\begin{aligned}
\mu_1(\Omega_1) &= \min_{u\in H^2(\Omega_1)} Q[u] = \min_{u\in H^2(\Omega_1)} \frac{\int_{-R}^{R} (|u''|^2 + \tau|u'|^2)\, dx}{\int_{-R}^{R} u^2\, dx}, \\
\mu_1(\Omega_2) &= \min_{v\in H^2(\Omega_2)} Q[v] = \min_{v\in H^2(\Omega_2)} \frac{\int_{-R}^{R}\int_{-R}^{R} (|D^2 v|^2 + \tau|\nabla v|^2)\, dxdy}{\int_{-R}^{R}\int_{-R}^{R} v^2\, dxdy}.
\end{aligned} \tag{8.20}$$

We can take a function $u(x)$ of one variable in $H^2(\Omega_1)$ and regard it as a function of two variables, for instance, $v(x,y) = u(x) \in H^2(\Omega_2)$. Hence we obtain $H^2(\Omega_1) \subset H^2(\Omega_2)$. By taking minimum of each Rayleigh quotient Q we get

$$\mu_1(\Omega_2) = \min_{v\in H^2(\Omega_2)} Q[v] \le \min_{u\in H^2(\Omega_1)} Q[u] = \mu_1(\Omega_1),$$

where the second integral of the right side of (8.20) is cancelled because nothing depends on y and so it comes down to the case of the first eigenvalue in one-dimensional domain. After taking infimum of μ_1 and together with the above observation of one-dimensional case, we conclude that

$$\mu_1^*(\tau) = \inf_{\Omega_2} \mu_1(\Omega_2) = -\infty.$$

It is straightforward to generalize 2-dimensional square case to n-dimensional cubes. □

Proof of Corollary 8.5. The point of Theorem 8.7 is that if $\tau < 0$ then there exist

domains that have arbitrarily negative value of μ_1. Hence the condition

$$\mu_1(\Omega, \tau) < A(\vec{p})$$

in Theorem 8.3 holds for some domain Ω. Together with the hypotheses that $\vec{p}$ satisfies conditions (8.10)–(8.11), we conclude by Theorem 8.3 that Turing instability occurs for the domain Ω. □

CHAPTER 9

INSTABILITY REGIONS OF THE FOURTH ORDER DIFFUSION OPERATOR $\Delta^2 - \tau\Delta$ IN ONE DIMENSION

In this chapter, we consider a different cross-section of Turing space: we will look at which combinations of the size of domain and the tension parameter τ produce Turing instability when the reaction-diffusion parameters are fixed.

In this chapter we restrict attention to one dimension, since earlier work in Part I of the thesis gives detailed information on the spectrum of the diffusion operator $\Delta^2 - \tau\Delta$ in one dimension. The domain is the interval

$$\Omega(R) = (-R, R).$$

9.1 The cross-section of Turing space

We introduce the Turing spaces with fixed $\vec{p}$:

Definition 9.1 (Turing space with fixed parameter)**.**

$$TS(\vec{p}) = \{(R, \tau) \in \mathbb{R}^2 : \vec{p} \in TS\left(\Omega(R), \tau\right), R > 0\}.$$

This definition produces a region in (R, τ)-plane and our goal is to determine the shape of this region (see Figure 9.3) and to understand some of its properties. We have seen in Part I of the thesis that the spectrum of the operator $\Delta^2 - \tau\Delta$ can be split into eigenvalue branches $\mu_l^{\text{odd}}(\tau)$ and $\mu_l^{\text{even}}(\tau)$ depending on τ and an index $l \geq 0$ and also depending on the evenness and oddness of the underlying eigenfunction. See details in Part I of the thesis and Figure 2.2. For each corresponding eigenvalue branch we will define two regions in (R, τ)-plane and then we will prove in Theorem 9.3 that those regions are the instability regions. That is, pairs (R, τ) in these regions are the length and tension parameters which give points in the Turing space, for the fixed reaction-diffusion parameter vector $\vec{p}$.

Definition 9.2 (Instability region)**.** *Fix a reaction-diffusion parameter vector $\vec{p}$ that satisfies condition (8.10), and recall the number $A = A(\vec{p})$ from (8.8), noting $A < 0$ by (8.10). Define regions*

$$E_-(l) = \{(R,\tau) : R^{-4}\mu_l^{even}(\tau R^2) < A \text{ and } \tau < 0\},$$
$$O_-(l) = \{(R,\tau) : R^{-4}\mu_l^{odd}(\tau R^2) < A \text{ and } \tau < 0\},$$

for $l \geq 0$. If in addition $\vec{p}$ satisfies condition (8.12) then the numbers $a = a(\vec{p})$ and $b = b(\vec{p})$ in (8.9) make sense, and we define

$$E_+(l) = \{(R,\tau) : R^{-4}\mu_l^{even}(\tau R^2) \in (a,b)\},$$
$$O_+(l) = \{(R,\tau) : R^{-4}\mu_l^{odd}(\tau R^2) \in (a,b)\}.$$

(The "$+$" and "$-$" notation refers to the sign of the unstable eigenvalues in the proof of Theorem 9.3 below.) Let $E = E_+ \cup E_-$ and $O = O_+ \cup O_-$, for each l.

Figure 9.1 shows the instability regions $E(0)$ and $O(0)$ associated to the zero-th even and odd eigenvalue branches, respectively. These figures were formed using implicit parameterizations of the eigenvalue branches μ_0^{even} and μ_0^{odd}, respectively, as described at the end of the chapter.

In the next theorem, we will show that the instability regions we have found make up the whole Turing space $TS(\vec{p})$. Remember that E_+ intersects both first and fourth quadrants in the (R,τ)-plane, while E_- lies in the lower (fourth) quadrant, and similarly for O_+ and O_-. Recall $E = E_+ \cup E_-$ and $O = O_+ \cup O_-$.

Theorem 9.3 (Instability region associated to each eigenvalue branch)**.**

1. *If the reaction-diffusion vector $\vec{p}$ satisfies (8.10)–(8.13), then the regions E and O generate Turing instability and fill the Turing space $TS(\vec{p})$:*

$$TS(\vec{p}) = \bigcup_{l\geq 0} \big(E(l) \cup O(l)\big).$$

2. *If the reaction-diffusion vector $\vec{p}$ satisfies (8.10)–(8.11), then the regions E_- and O_- generate Turing instability:*

$$E_-(l) \cup O_-(l) \subset TS(\vec{p}), \quad l \geq 0.$$

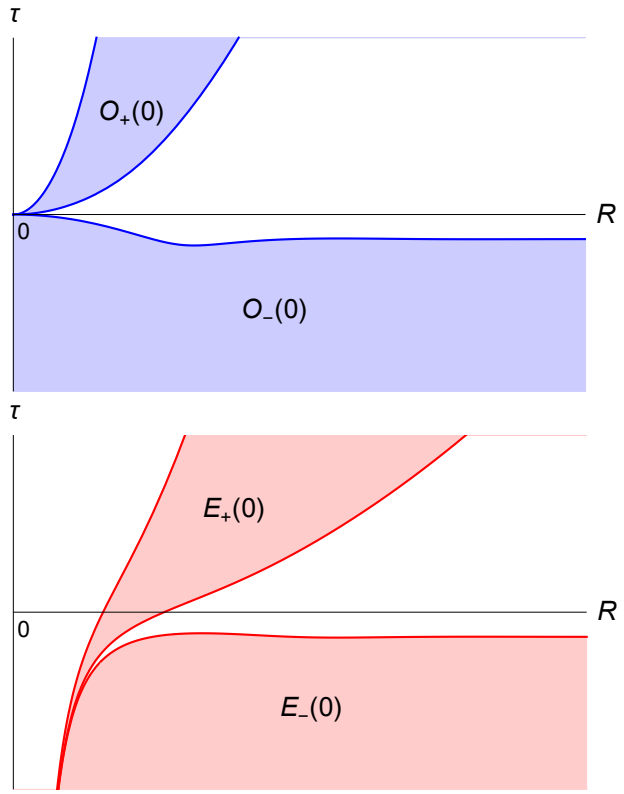

Figure 9.1: Points (R, τ) in shaded regions mean that for the interval $\Omega(R) = (-R, R)$, the stable homogeneous steady state of the reaction system becomes unstable in the presence of diffusion. Here we assume the reaction-diffusion vector $\vec{p}$ satisfies conditions (8.10)–(8.13). (The figure uses the Gierer–Meinhardt system [23, Section 2.2] and parameter values $\vec{p} = (0.4, -0.16, 5, -1, 30)$.) The first (resp. second) figure describes the instability region associated to the zero-th odd (resp. even) eigenvalue branch of $\Delta^2 u - \tau \Delta u = \mu u$, as explained immediately after Definition 9.2. See also Figure 9.3.

In other words, if a pair (R,τ) belongs to the instability region $E(l)$ or $O(l)$, $l \geq 0$, then Turing instability occurs for the domain $\Omega(R) = (-R,R)$ with the tension parameter τ. That is, the spatially homogeneous linearly asymptotically stable steady state (u_0, v_0) of (8.6)–(8.7) becomes unstable under diffusion.

Before we start the proof, we explain why we use the " $+$ " and " $-$ " notation for the sets $E_\pm$ and $O_\pm$. For $E_+(l)$ and $O_+(l)$ in Definition 9.2, the eigenvalues μ_l^{even} and μ_l^{odd}, which lie between positive constants by the condition (8.13), are positive. Hence, the sets E_+ and O_+ relate to eigenvalues that are in the upper half of the spectral plane. For $E_-(l)$ and $O_-(l)$ in Definition 9.2, the eigenvalues μ_l^{even} and μ_l^{odd} are negative because they are less than the negative constant $A(\vec{p})$, by assumption (8.10). Hence, the sets E_- and O_- relate to eigenvalues that are in the lower half of the spectral plane.

Proof of Theorem 9.3. 1. "$\supset$": Pick one case $E_+(1)$ as an example, since the other cases are similar. If conditions (8.10)–(8.13) on the reaction-diffusion vector $\vec{p}$ are assumed, then we can apply Theorem 8.3 to show $E_+(1) \subset TS(\vec{p})$, as follows. Suppose $(R,\tau) \in E_+(1)$, so that by Definition 9.2, the eigenvalue branch μ_1^{even} satisfies

$$R^{-4}\mu_1^{\text{even}}((-1,1),\tau R^2) \in (a(\vec{p}),b(\vec{p}))\,.$$

Recall the domain $\Omega(R)$ is the interval $(-R,R)$. Together with the rescaling relation:

$$\mu((-R,R),\tau) = R^{-4}\mu((-1,1),\tau R^2)$$

from (8.18), we have

$$\mu_1^{\text{even}}(\Omega(R),\tau) \in (a(\vec{p}),b(\vec{p}))\,.$$

Hence by Theorem 8.3, the reaction-diffusion vector $\vec{p}$ belongs to the Turing space $TS(\Omega(R),\tau)$, and so $(R,\tau) \in TS(\vec{p})$. We have shown

$$TS(\vec{p}) \supset \bigcup_{l\geq 0}\big(E(l)\cup O(l)\big).$$

"$\subset$": We will prove

$$TS(\vec{p}) \subset \bigcup_{l\geq 0}\big(E(l)\cup O(l)\big)$$

in the following. Suppose $(R,\tau) \in TS(\vec{p})$, where $\vec{p} \in TS\left(\Omega(R),\tau\right), R>0$. If $\tau \geq 0$, from Theorem 8.3, there exist some eigenvalue $\mu_j(\Omega(R),\tau)$ such that

$$\mu_j(\Omega(R),\tau) \in \left(a(\vec{p}),b(\vec{p})\right).$$

From the analysis of the spectrum in Part I of the thesis we know that eigenvalues correspond to some lth branch of the spectrum μ_l (see Figure 2.2). Note that $a(\vec{p})>0$ from the condition (8.13) and so such $\mu_j(\Omega(R),\tau)$ are positive. Equivalently, there exist some lth even or odd eigenvalue branches μ_l^{even} or μ_l^{odd} such that

$$\mu_l^{\text{even}}(\Omega(R),\tau) \text{ or } \mu_l^{\text{odd}}(\Omega(R),\tau) \in \left(a(\vec{p}),b(\vec{p})\right).$$

Together with the rescaling relation, it is equivalent to

$$\mu_l^{\text{even}}\left((-1,1),\tau R^2\right) \text{ or } \mu_l^{\text{odd}}\left((-1,1),\tau R^2\right) \in \left(a(\vec{p})R^4,b(\vec{p})R^4\right).$$

Therefore, (R,τ) belongs to some instability regions $E_+(l)$ or $O_+(l)$. The fact that $\mu_j(\Omega(R),\tau)$ is positive tells us (R,τ) is in the " $+$ " regions. We have shown that if $(R,\tau) \in TS(\vec{p})$ with $\tau \geq 0$ then

$$(R,\tau) \in \bigcup_{l\geq 0}\big(E_+(l) \cup O_+(l)\big).$$

Now if $\tau<0$, from Theorem 8.3, either there exists some eigenvalue $\mu_j(\Omega(R),\tau)$ such that

$$\mu_j(\Omega(R),\tau) \in \left(a(\vec{p}),b(\vec{p})\right), \tag{9.1}$$

or else

$$\mu_1(\Omega(R),\tau) < A(\vec{p}). \tag{9.2}$$

The first case (9.1) is the same as we showed when $\tau \geq 0$. For the second case, recall from Chapter 6 that the first eigenvalue μ_1 corresponds to the zero-th even or odd eigenvalue branch μ_0^{even} or μ_0^{odd} (shown in Figure 2.2). Note that $A(\vec{p})<0$ from the condition (8.10) and so $\mu_1(\Omega(R),\tau)$ is negative. The second case (9.2) is equivalent to

$$\mu_0^{\text{even}}(\Omega(R),\tau) \text{ or } \mu_0^{\text{odd}}(\Omega(R),\tau) < A(\vec{p}).$$

From the rescaling relation,

$$\mu_0^{\text{even}}\left((-1,1),\tau R^2\right) \text{ or } \mu_0^{\text{odd}}\left((-1,1),\tau R^2\right) < A(\vec{p})R^4.$$

Hence, (R,τ) belongs to the instability regions $E_-(0)$ or $O_-(0)$. By combining when $\tau \geq 0$ and the first and second cases of $\tau < 0$, we have shown

$$(R,\tau) \in \bigcup_{l\geq 0}\big(E(l)\cup O(l)\big),$$

where recall $E = E_+ \cup E_-$, $O = O_+ \cup O_-$.

2. The proof is similar to part 1. "$\supset$", except using $E_-(1)$ as the typical case instead of $E_+(1)$.

□

We found infinitely many instability regions $E_\pm(l)$, $O_\pm(l)$ in Theorem 9.3. We will discuss some properties of these instability regions in the following section.

9.2 Properties of Turing space

We will discuss how instability regions behave as l increases in the following Proposition 9.4.

Proposition 9.4 (Movement of instability regions as index l increases)**.**

1. *Assume (8.12) holds. The regions $E_+(l)$ and $O_+(l)$ move downwards as the index l increases, in the sense that the top (resp. bottom) boundary curve of region $E_+(l)$ lies above the top (resp. bottom) boundary curve of region $E_+(l+1)$.*

2. *Assume (8.10) holds. The regions $E_-(l)$ and $O_-(l)$ are nested as l increases:*

$$E_-(0) \supset E_-(1) \supset E_-(2) \supset \cdots,$$
$$O_-(0) \supset O_-(1) \supset O_-(2) \supset \cdots.$$

Figure 9.3 shows some of these regions, and the nesting behavior.

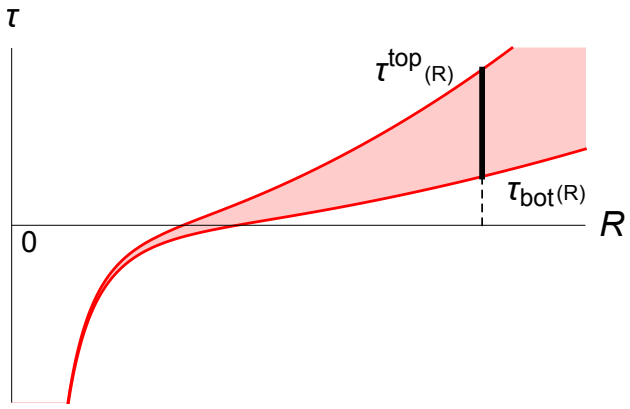

Figure 9.2: For given R, there is a single interval of τ being in the instability region E_+. The top and bottom boundary curves of region E_+ are given by functions $\tau^{\text{top}}(R)$ and $\tau_{\text{bot}}(R)$.

Proof. 1. Fix $\vec{p}$ and l, and write $a = a(\vec{p}), b = b(\vec{p})$. We will prove the even case $E_+(l)$ and the odd case $O_+(l)$ is similarly obtained. Define two sets from the definition of the instability region $E_+(l)$ by the following:

$$\text{Top} = \{(R, \tau) : R^{-4}\mu_l^{\text{even}}(\tau R^2) = b\}, \tag{9.3}$$

$$\text{Bot} = \{(R, \tau) : R^{-4}\mu_l^{\text{even}}(\tau R^2) = a\}. \tag{9.4}$$

We will prove that these sets are graphs of functions of R. First, we show that for given R there is a single interval of τ-values that satisfies the condition

$$R^{-4}\mu_l^{\text{even}}(\tau R^2) \in (a, b)$$

for being in the instability region $E_+(l)$ in Definition 9.2. The condition is equivalent to

$$\tau \in \left(R^{-2}(\mu_l^{\text{even}})^{-1}(aR^4), R^{-2}(\mu_l^{\text{even}})^{-1}(bR^4)\right),$$

which is a single interval since $\mu_l^{\text{even}}(\tau)$ is a strictly increasing function by Proposition 4.6 so that the inverse is uniquely defined. See Figure 9.2. Hence the sets (9.3) and (9.4) are the graphs of the function:

$$\tau^{\text{top}}(R; l) = R^{-2}(\mu_l^{\text{even}})^{-1}(bR^4),$$
$$\tau_{\text{bot}}(R; l) = R^{-2}(\mu_l^{\text{even}})^{-1}(aR^4)$$

It is clear from Definition 9.2 that these are the top and bottom boundary curves of region $E_+(l)$.

Now, we will prove that $E_+(l)$ moves downward as l increases, in the sense that

$$\tau^{\text{top}}(R;l) > \tau^{\text{top}}(R;l+1) > \tau^{\text{top}}(R;l+2) > \cdots,$$
$$\tau_{\text{bot}}(R;l) > \tau_{\text{bot}}(R;l+1) > \tau_{\text{bot}}(R;l+2) > \cdots.$$

Notice that for all $\tau \in \mathbb{R}$,

$$\mu_l^{\text{even}}(\tau) < \mu_{l+1}^{\text{even}}(\tau)$$

as proved in Proposition 4.5. Since the eigenvalue branches $\mu_l^{\text{even}}(\tau)$ are strictly increasing to infinity, we know that the inverse functions satisfy

$$\left(\mu_{l+1}^{\text{even}}\right)^{-1}(b) < \left(\mu_l^{\text{even}}\right)^{-1}(b),$$

for fixed b. Therefore, we obtain

$$\tau^{\text{top}}(R;l+1) = R^{-2}\left(\mu_{l+1}^{\text{even}}\right)^{-1}(bR^4) < R^{-2}\left(\mu_l^{\text{even}}\right)^{-1}(bR^4) = \tau^{\text{top}}(R;l),$$

and similarly for the bottom curves.

2. Now we consider $E_-(l)$ and $O_-(l)$, assuming conditions (8.10)–(8.11) hold. We will prove the even case $E_-(l)$ and the odd case $O_-(l)$ is similarly obtained. We will show the regions $E_-(l)$ are nested as l increases in the sense that the boundary curve of $E_-(l)$ is nested as l increases. We can express the boundary curve of $E_-(l)$ as the function of R in a similar way to part 1:

$$\tau^{\text{top}}(R;E_-(l)) = R^{-2}(\mu_l^{\text{even}})^{-1}(AR^4).$$

We will show that as l increases,

$$\tau^{\text{top}}(R;E_-(l)) > \tau^{\text{top}}(R;E_-(l+1)) > \tau^{\text{top}}(R;E_-(l+2)) > \cdots.$$

For all $\tau \in \mathbb{R}$, like above we have

$$\mu_l^{\text{even}}(\tau) < \mu_{l+1}^{\text{even}}(\tau)$$

and so

$$\left(\mu_{l+1}^{\text{even}}\right)^{-1}(A) < \left(\mu_{l}^{\text{even}}\right)^{-1}(A),$$

for fixed A. Therefore, we obtain

$$\tau^{\text{top}}(R; E_-(l+1)) = R^{-2}\left(\mu_{l+1}^{\text{even}}\right)^{-1}(AR^4) < R^{-2}\left(\mu_{l}^{\text{even}}\right)^{-1}(AR^4) = \tau^{\text{top}}(R; E_-(l)).$$

□

Remark 9.5. One might think it is obvious that we get Turing instability if $\tau < 0$ because of existence of negative eigenvalues for $\Delta^2 - \tau\Delta$. However, we show in the next corollary that having negative eigenvalue is not always enough to get instability. We have some region in the (R, τ)-plane with $\tau < 0$ which corresponds to homogeneous steady states of the reaction-diffusion system staying stable. This stability relies upon a certain fact about the growth rate of the spectrum of $\Delta^2 - \tau\Delta$ with free boundary conditions when τ is small negative.

Corollary 9.6 (Existence of region outside the Turing space)**.** *If the reaction-diffusion vector $\vec{p}$ satisfies (8.10)–(8.13), then there exists some region in (R, τ)-plane where $\tau < 0$ that is outside the union $\bigcup_{l\geq 0}\left(E(l) \cup O(l)\right)$ of the instability regions.*

Figure 9.3 shows these regions. The corollary says there is some unshaded part in the lower half plane.

Proof. To prove there exists stable region with $\tau < 0$, for each fixed $\vec{p}$ satisfying (8.10)–(8.13), we study the region near the origin in Figure 9.3. We will show:

1. The bottom boundary of $O_+(0)$ lies above the horizontal axis $\tau = 0$.
2. The boundary of $O_-(0)$ lies below the horizontal axis $\tau = 0$.
3. The boundary curves of $E_+(0)$, $E_-(0)$, and $O_+(1)$ have $\tau \to -\infty$ as $R \to 0$.

Since the instability regions $E_\pm(l)$ and $O_\pm(l)$ move downwards as l increases, by Proposition 9.4, there exist some regions near the origin that are not covered by any instability regions in $\{(R, \tau) : R > 0 \text{ and } \tau < 0\}$.

Step 1: the bottom boundary of $O_+(0)$ lies above the horizontal axis $\tau = 0$.

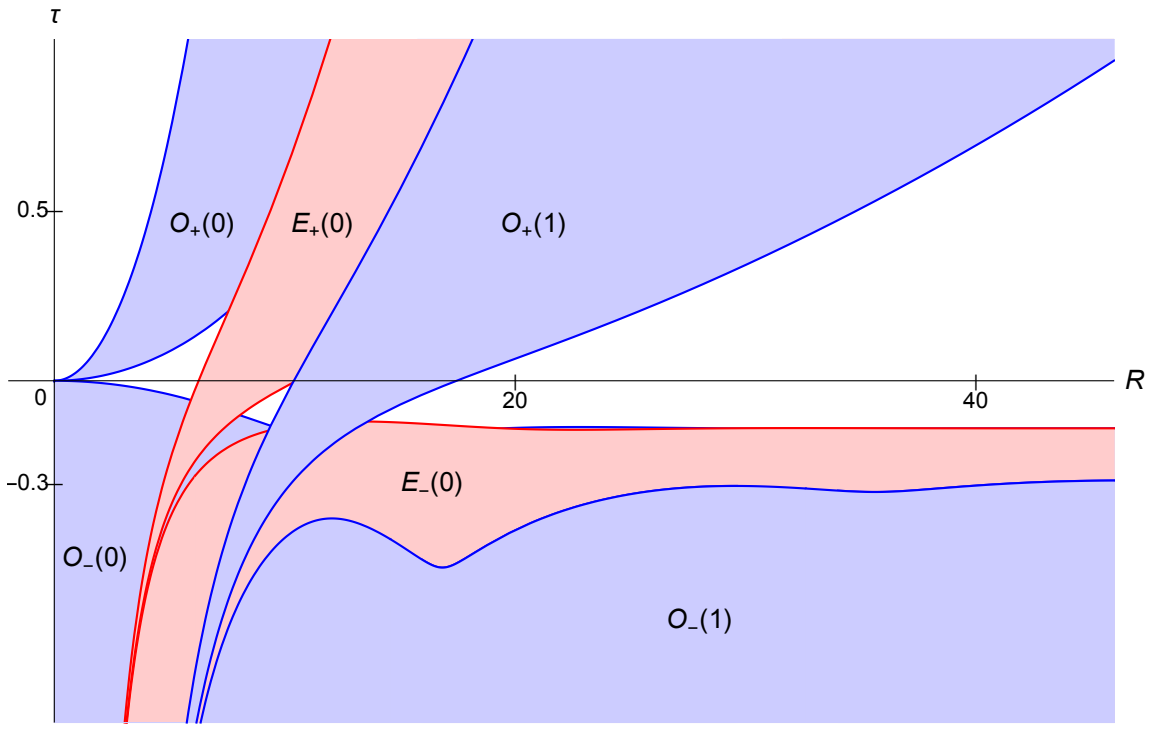

Figure 9.3: The instability regions $O_{\pm}(0)$, $E_{\pm}(0)$, and $O_{\pm}(1)$, assuming conditions (8.10)–(8.13) hold for the reaction-diffusion vector $\vec{p}$. (The figure uses parameter values $\vec{p} = (0.4, -0.16, 5, -1, 30)$.) Observe some parts of the lower half plane are not covered by any instability regions.

Recall the number $a = a(\vec{p}) > 0$ from (8.13). Since $\mu_0^{\text{odd}}(\tau)$ is strictly increasing with $\mu_0^{\text{odd}}(0) = 0$ from Proposition 4.6 and Chapter 4, we have $(\mu_0^{\text{odd}})^{-1}(aR^4) > 0$. Hence,

$$\tau_{\text{bot}}(R; O_+(0)) > 0,$$

which means the bottom boundary of $O_+(0)$ lies above the horizontal axis $\tau = 0$.

Step 2: the boundary of $O_-(0)$ lies below the horizontal axis $\tau = 0$.

We know from the spectrum, the eigenvalue branch μ_0^{odd} is approximately a straight line $\mu_0^{\text{odd}}(\tau) \simeq \pi^2\tau/4$ near the origin (see Section 4.3). Hence the boundary curve of $O_-(0)$ satisfies

$$\lim_{R\to 0^+} \frac{\tau^{\text{top}}(R; O_-(0))}{R^2} = \lim_{R\to 0^+} \frac{(\mu_0^{\text{odd}})^{-1}(AR^4)}{R^4} = \frac{4A}{\pi^2} < 0$$

because $A < 0$ by (8.10). Since the number $4A/\pi^2$ is negative, the limit shows that the curve $\tau^{\text{top}}(R; O_-(0))$ lies below some negative quadratic, near the origin.

Step 3: the boundary curves of $E_+(0)$, $E_-(0)$, and $O_+(1)$ have $\tau \to -\infty$ as $R \to 0$.

As $R \to 0^+$, the limit of the upper boundary curve of $E_+(0)$ is

$$\lim_{R\to 0^+} \tau^{\text{top}}(R; E_+(0)) = \lim_{R\to 0^+} R^{-2}(\mu_0^{\text{even}})^{-1}(bR^4) = -\infty,$$

since the inverse function $(\mu_0^{\text{even}})^{-1}(0) = -\pi^2/4$ from the spectrum of $\Delta^2 u - \tau\Delta u = \mu u$ (see Chapters 4 and 5). The same is true for $O_+(1)$, since $(\mu_1^{\text{odd}})^{-1}(0) = -\pi^2$.

As $R \to 0^+$, the limit of the boundary curve of $E_-(0)$ is

$$\lim_{R\to 0^+} \tau^{\text{top}}(R; E_-(0)) = \lim_{R\to 0^+} R^{-2}(\mu_0^{\text{even}})^{-1}(AR^4) = -\infty,$$

since the inverse function $(\mu_0^{\text{even}})^{-1}(0) = -\pi^2/4$.

□

Corollary 9.6 tells us that there is some region that does not belong to any of Turing space $TS(\vec{p})$, as shown by the unshaded regions in Figure 9.3.

9.3 Extra instability regions when $\tau < 0$

In this section, we describe some additional instability regions when $\tau < 0$. From Theorem 8.3, there are two cases for the reaction-diffusion vector $\vec{p}$ belonging to the Turing space when $\tau < 0$:

$$\text{either (8.10)–(8.12) hold and } \mathrm{Spec}(\Omega, \tau) \cap (a(\vec{p}), b(\vec{p})) \neq \emptyset, \tag{9.5}$$

$$\text{or (8.10)–(8.11) hold and } \mu_1 < A(\vec{p}). \tag{9.6}$$

The instability regions E_- and O_- arise from the case (9.6), as shown in Definition 9.2 and Theorem 9.3. In addition to these regions shown in Figure 9.3, in this section we will describe what the instability regions arising from the case (9.5) look like.

In the traditional Turing analysis with the Laplacian, the Turing space would be empty if (8.13) fails (that is, if $kf_u + g_v < 0$), because $a(\vec{p})$ and $b(\vec{p})$ are negative while the spectrum of the Laplacian is positive. But $\Delta^2 - \tau\Delta$ permits negative eigenvalues when $\tau < 0$. This introduces extra instability regions (as shown in Figure 9.4), i.e., creates some Turing space.

Assume the reaction-diffusion vector $\vec{p}$ satisfies (8.10)–(8.12) and $kf_u + g_v < 0$ (meaning (8.13) fails). Define

$$\widetilde{E}(l) = \{(R, \tau) : R^{-4}\mu_l^{\mathrm{even}}(\tau R^2) \in (a, b) \text{ and } \tau < 0\},$$
$$\widetilde{O}(l) = \{(R, \tau) : R^{-4}\mu_l^{\mathrm{odd}}(\tau R^2) \in (a, b) \text{ and } \tau < 0\}.$$

Note that (8.12) guarantees the numbers $a = a(\vec{p})$ and $b = b(\vec{p})$ in (8.9) make sense, and these numbers are negative because $kf_u + g_v < 0$. We present the regions $\widetilde{E}(l)$ and $\widetilde{O}(l)$ numerically in Figure 9.4. The regions are obtained in a similar way to regions $E_\pm$ and $O_\pm$. We use an implicit parameterization for μ_l^{even} and μ_l^{odd} in terms of two other parameters (see Theorem 5.5 and Lemma 6.1), but now we only need to consider eigenvalue branches in the lower half of the spectral plane.

Unlike the instability regions $E_-(l)$ and $O_-(l)$ in Definition 9.2 that only have upper boundary curves, the regions $\widetilde{E}(l)$ and $\widetilde{O}(l)$ have upper and lower boundary curves. To sum up, negative τ values introduce negative eigenvalues for the diffusion operator $\Delta^2 - \tau\Delta$ which lead to the appearance of some instability regions. These are relatively smaller than the regions $E_-(l)$ and $O_-(l)$ in Definition 9.2.

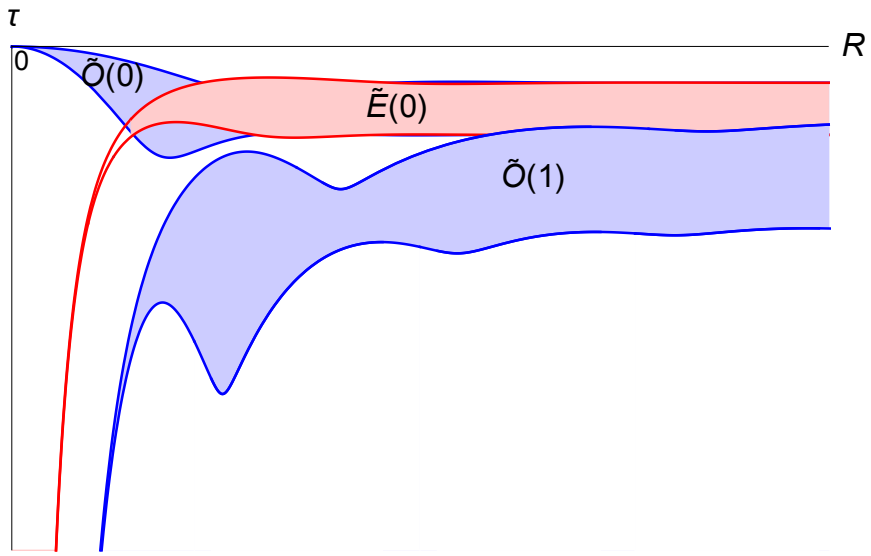

Figure 9.4: New phenomenon: the negative eigenvalues of $\Delta^2 u - \tau\Delta u = \mu u$ permit Turing instability even when $kf_u + g_v < 0$ (meaning (8.13) fails), whereas in the traditional Turing analysis with the Laplacian governing diffusion, the Turing space would be empty. In the pictured situation, conditions (8.10)–(8.12) hold for the reaction-diffusion vector $\vec{p}$ and condition (8.13) fails. (The figure uses parameter values $\vec{p} = (0.1, -0.01, 20, -1, 1)$.) The regions of $\widetilde{O}(0)$, $\widetilde{E}(0)$, and $\widetilde{O}(1)$ are associated to the eigenvalue branches μ_0^{odd}, μ_0^{even}, and μ_1^{odd}, respectively, in the lower half of the spectral plane (see earlier explanation in the section).

9.4 Numerical experiments.

We do some numerical simulations, to see beyond the linear predictions from spectral theory to what is happening in the genuinely nonlinear regime. We modify Gierer and Meinhardt's reaction kinetics [11, Equation (15)], [23, Section 2.2], to use the fourth order diffusion $\Delta^2 - \tau\Delta$ on the interval $\Omega(R) = (-R, R)$ in 1-dimension. The Gierer–Meinhardt reaction system is

$$f(u,v) = k_1 - k_2 u + \frac{k_3 u^2}{v}, \quad g(u,v) = k_4 u^2 - k_5 v. \tag{9.7}$$

We fix constants $(k_1, k_2, k_3, k_4, k_5) = (0, 0.4, 1, 1, 1)$ for our numerical simulations. Hence the homogeneous steady state (u_0, v_0) is

$$(u_0, v_0) = (2.5, 6.25),$$

and the partial derivatives of f and g evaluated at the steady state (u_0, v_0) are

$$(f_u, f_v, g_u, g_v) = (0.4, -0.16, 5, -1).$$

We also take the diffusivity $k = 30$. Figures 9.5 and 9.6 illustrate inhomogeneous steady states corresponding to points in the instability regions $O_+(1)$ and $E_-(0)$ in Theorem 9.3 part 1. An unstable steady state for $\tau \geq 0$ is illustrated in Figure 9.5, which shows a slightly perturbed constant steady state evolving into a stripe pattern. The initial growth of the pattern takes place in the linear regime. The persistence of the pattern as it grows larger is due to the nonlinear effects (reaction). Figure 9.6 illustrates an unstable steady state for $\tau < 0$. Again a perturbed steady state evolves into a stripe pattern. However, the experiment only gives patterns like Figure 9.6 for about $10 - 20\%$ of random initial conditions. The rest of the simulations give irregular cycles of blow up, which might be due to numerical instabilities when $\tau < 0$.

Moreover, it is possible to get stability of the perturbed steady state when $\tau < 0$ even though there is an unstable mode ($\mu < 0$) in the linearized equation, as Corollary 9.6 shows. In about 80% of our simulations (not shown), the initial perturbation decayed and the solution remained near the steady state until time $t = 50$, as predicted qualitatively by Corollary 9.6. In the other 20% of simulations, the solution blew up chaotically, which again we think is due to numerical instabilities.

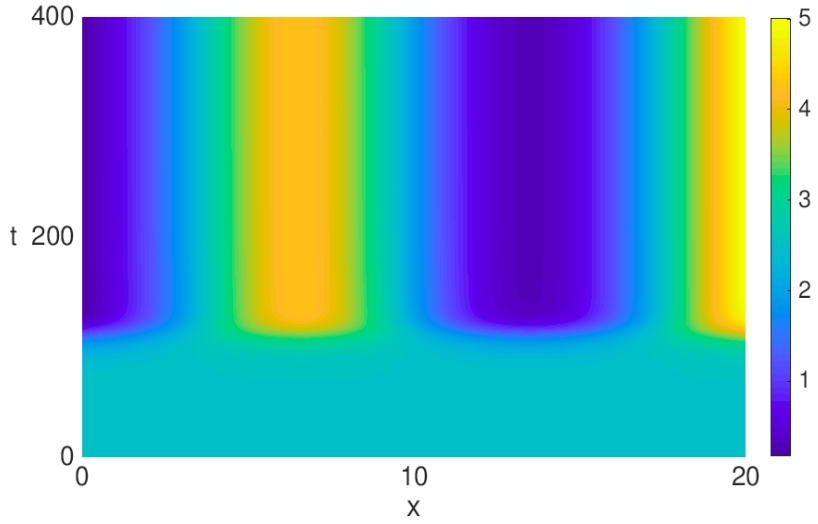

Figure 9.5: Regular stripe pattern of modified fourth order Gierer–Meinhardt system (9.7) with $(k_1, k_2, k_3, k_4, k_5) = (0, 0.4, 1, 1, 1)$ when $\tau \geq 0$: the figure shows a contour plot of the activator u. The pattern corresponds to the point $(R, \tau) = (20, 0.5)$ in the instability region $O_+(1)$ (shown in Figure 9.3) associated to the first odd eigenvalue branch μ_1^{odd} in Figure 2.2. (The figure uses parameter values $\vec{p} = (0.4, -0.16, 5, -1, 30)$.)

9.5 Plotting the instability regions

We end the chapter explaining how we create the instability regions in Figures 9.1 and 9.3. For instance, the direct formula for the bottom boundary curve of the instability region $O_+(l)$ is

$$\tau = R^{-2}(\mu_l^{\text{odd}})^{-1}\left(a(\vec{p})R^4\right)$$

from Definition 9.2. However, it is not straightforward to obtain the curve since we do not have have an explicit formula for μ_l^{odd} as a function of τ. Instead we have the parameterized curves in terms of two other parameters (see Theorem 4.4). Hence, it is easy to work with a parameterized formula for Figures 9.1 and 9.3:

$$R(\alpha) = \sqrt[4]{\frac{\alpha^2\beta^2}{a(\vec{p})}},$$
$$\tau(\alpha) = \frac{\beta^2 - \alpha^2}{\alpha\beta}\sqrt{a(\vec{p})},$$

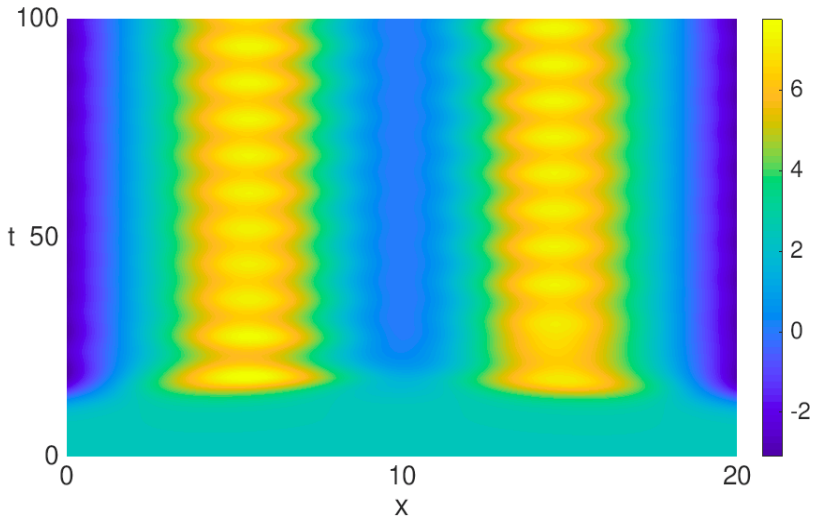

Figure 9.6: Regular stripe pattern of modified fourth order Gierer–Meinhardt system (9.7) with $(k_1, k_2, k_3, k_4, k_5) = (0, 0.4, 1, 1, 1)$ when $\tau < 0$: the figures shows a contour plot of the activator u corresponding to the point $(R, \tau) = (20, -0.3)$ in the instability region $E_-(0)$ (shown in Figure 9.3) associated to the zero-th even eigenvalue branch μ_0^{even} in Figure 2.2. (The figure uses parameter values $\vec{p} = (0.4, -0.16, 5, -1, 30)$.) The simulation only gives a stable pattern for about $10 - 20\%$ of random initial conditions. The rest of the simulations give irregular cycles of blow up. Also, even in the stable pattern shown in the figure, the pattern seems to be slightly temporally periodic.

where α and β are related by $\alpha^3 \tan(\alpha) = \beta^3 \tanh(\beta), l\pi \leq \alpha < (2l+1)\pi/2$ from Lemma 4.1. The point is that

$$\tau(\alpha)R(\alpha)^2 = \beta^2 - \alpha^2,$$
$$a(\vec{p})R(\alpha)^4 = \alpha^2\beta^2,$$

and so by the parameterization in Theorem 4.4 we see that $a(\vec{p})R(\alpha)^4$ equals the μ-value corresponding to the τ-value $\tau(\alpha)R(\alpha)^2$, which means

$$a(\vec{p})R(\alpha)^4 = \mu_l^{\text{odd}}\left((-1,1), \tau(\alpha)R(\alpha)^2\right)$$

as we want.

The " $-$ " regions are special since each eigenvalue branch in the lower half of the spectral plane consists of infinitely many different parameterizations (see Theorem 5.5 and Lemma 6.1), whereas " $+$ " regions are given by eigenvalue branches in the upper half of the spectral plane which consist of a single parameterization in Theorem 4.4. So the boundary curves of $O_-(l)$ and $E_-(l)$ are made up with infinitely many parameterizations.

CHAPTER 10

PERIODIC BOUNDARY CONDITIONS IN ONE DIMENSION

In this chapter, we will illustrate the Turing instability region of the periodic boundary conditions, which has similar shape with the region for the free boundary conditions. The eigenvalue problem is

$$u'''' - \tau u'' = \mu u$$

for $-R < x < R$. We can explicitly express the spectrum of periodic case in one dimension for $-1 < x < 1$ as

$$\mu_l^{\text{per}}(\tau) = (l\pi)^4 + \tau(l\pi)^2, \quad l \geq 0,$$

where eigenfunctions can be taken as the even function $u_{\text{e}}(x) = \cos(l\pi x)$ or the odd function $u_{\text{o}}(x) = \sin(l\pi x)$. Note that all the eigenvalues have multiplicity 2, except for $l = 0$. In the periodic case, we do not need to separate the even and odd instability regions since these regions are the same because eigenvalues associated to even and odd eigenfunctions are the same. We illustrate the spectrum in (τ, μ)-plane, as shown in Figure 2.1. Each branch is a straight line. We see there is a parabola $\mu = -(\tau + \pi^2)^2/4$ on which the intersections of consecutive eigenvalue branches lie. The same parabola occurs also in the spectrum of the free boundary conditions as the parabola on which the intersections of the first even and odd eigenvalue branch μ_1^{even} and μ_1^{odd} lie (see Proposition 5.7). On top of that, we see the spectrum of periodic boundary conditions and the spectrum of free boundary conditions behave in asymptotically similar way: compare Figure 2.1 and Figure 2.2. Actual crossings occur in the spectrum of periodic boundary conditions, whereas there are barely-avoided crossings along eigenvalue branches for free boundary conditions. A pattern of barely-avoided crossings leads to a pattern of nearly-linear segments in the free case, while the periodic spectrum contains actual line segments. Similar spectral behavior of periodic and free boundary conditions should generate similar shape of

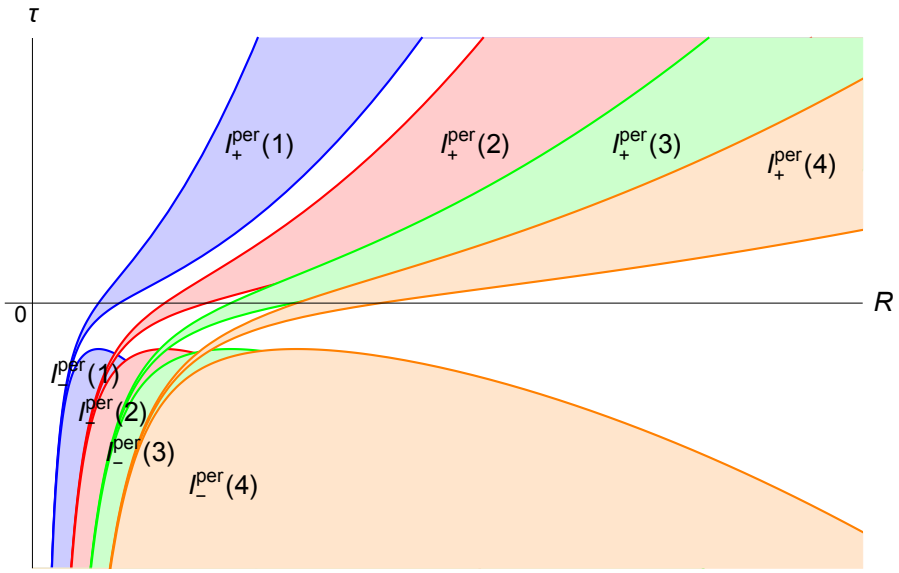

Figure 10.1: The instability regions associated to periodic boundary conditions on the interval $(-R, R)$, for eigenvalue branches $l = 1, \ldots, 4$, assuming conditions (8.10)–(8.13) for the reaction-diffusion vector $\vec{p}$. (The figure uses parameter values $\vec{p} = (0.4, -0.16, 5, -1, 30)$.) Each colored region describes the instability region associated to the corresponding colored eigenvalue branch in Figure 2.1. Points (R, τ) in shaded regions belong to the Turing space $TS(\vec{p})$.

the instability regions (Figure 9.3 and Figure 10.1).

Assume conditions (8.10)–(8.13) hold on the reaction-diffusion vector $\vec{p}$. With a Turing analysis similar to Definition 9.2 and Theorem 9.3, we can express the instability region of periodic boundary conditions explicitly as follows, for the interval $(-R, R)$:

$$I_+^{\text{per}}(l) = \{(R, \tau) : aR^4 < (l\pi)^4 + \tau R^2 (l\pi)^2 < bR^4\},$$
$$I_-^{\text{per}}(l) = \{(R, \tau) : (l\pi)^4 + \tau R^2 (l\pi)^2 < AR^4 \text{ and } \tau < 0\}.$$

The instability regions of the first four eigenvalue branches of periodic case are illustrated in Figure 10.1 in the (R, τ)-plane.

REFERENCES

[1] S. Aly, I. Kim and D. Sheen. *Turing instability for a ratio-dependent predator-prey model with diffusion.* Appl. Math. Comput. 217 (2011) 7265–7281.

[2] M. S. Ashbaugh, R. D. Benguria and R. Mahadevan. *Minimization of the lowest eigenvalue of the vibrating clamped plate under compression.* Forthcoming 2018.

[3] K. Bay, W. Lay and A. Akopyan. *Avoided crossings of the quartic oscillator.* J. Phys. A 30 (1997), no. 9, 3057–3067.

[4] A. L. Bertozzi, M. P. Brenner, T. F. Dupont and L. P. Kadanoff. *Singularities and similarities in interface flows.* Trends and perspectives in applied mathematics, Appl. Math. Sci., 100, Springer, New York (1994), pp. 155–208.

[5] A. L. Bertozzi and M. C. Pugh. *Long-wave instabilities and saturation in thin film equations.* Comm. Pure Appl. Math. 51 (1998), no. 6, 625–661.

[6] L. M. Chasman. *An isoperimetric inequality for fundamental tones of free plates.* Comm. Math. Phys. 303 (2011), no. 2, 421–449.

[7] L. M. Chasman and J. Chung. *Spectrum of the free rod under tension and compression.* Appl. Anal., to appear (2018). doi:10.1080/00036811.2018.1451639

[8] E. J. Crampin, E. A. Gaffney and P. K. Maini. *Reaction and diffusion on growing domains: scenarios for robust pattern formation.* Bull. Math. Biol. 61(6) (1999), 1093–1120.

[9] R. Dillon, P. K. Maini and H. G. Othmer. *Pattern formation in generalized Turing systems. I. Steady-state patterns in systems with mixed boundary conditions.* J. Math. Biol. 32 (1994), no. 4, 345–393.

[10] F. Gesztesy, D. Gurarie, H. Holden, M. Klaus, L. Sadun, B. Simon and P. Vogl. *Trapping and cascading of eigenvalues in the large coupling limit.* Comm. Math. Phys. 118 (1988), no. 4, 597–634.

[11] A. Gierer and H. Meinhardt. *A theory of biological pattern formation.* Biol. Cybern (1972). 12, 30–39.

[12] R. Gilmore. *Elementary Quantum Mechanics in One Dimension.* Johns Hopkins University Press, 2004.

[13] H.-C. Grunau. *Positivity, change of sign and buckling eigenvalues in a one-dimensional fourth order model problem.* Adv. Differential Equations 7 (2002), no. 2, 177–196.

[14] J. L. Hineman and J. M. Neuberger. *GNGA for general regions: semilinear elliptic PDE and crossing eigenvalues.* Commun. Nonlinear Sci. Numer. Simul. 12 (2007), no. 4, 447–464.

[15] B. Kawohl, H. A. Levine and W. Velte. *Buckling eigenvalues for a clamped plate embedded in an elastic medium and related questions.* SIAM J. Math. Anal. 24 (1993), no. 2, 327–340.

[16] V. Klika and E. A. Gaffney. *History dependence and the continuum approximation breakdown: the impact of domain growth on Turing's instability.* Proc. A. 473 (2017), no. 2199, 20160744, 19 pp.

[17] I. V. Komarov and S. Y. Slavyanov. *The two Coulomb centres problem at large centre separation.* Journal of Physics B: Atomic and Molecular Physics, Volume 1 (1968), no. 6, 1066–1072.

[18] J. M. Lee, T. Hillen and M. A. Lewis. *Pattern formation in prey-taxis systems.* J. Biol. Dyn. 3 (2009), no. 6, 551–573.

[19] M. A. Lewis. *Spatial coupling of plant and herbivore dynamics: the contribution of herbivore dispersal to transient and persistent "waves" of damage.* Theor. Popul. Biol. 45 (1994), 277–312.

[20] M. A. Lewis, P. K. Maini and S. Petrovskii. *Dispersal, Individual Movement and Spatial Ecology: A Mathematical Perspective.* Lecture Notes in Mathematics, 2071. Springer, Heidelberg, 2013.

[21] A. Madzvamuse, E. A. Gaffney and P. K. Maini. *Stability analysis of non-autonomous reaction-diffusion systems: the effects of growing domains.* J. Math. Biol. 61 (2010), no. 1, 133–164.

[22] P. K. Maini, T. E. Woolley, R. E. Baker, E. A. Gaffney and S. S. Lee. *Turing's model for biological pattern formation and the robustness problem.* Interface Focus 2, 487 (2012).

[23] J. D. Murray. *Mathematical biology. II. Spatial models and biomedical applications. Third edition. Interdisciplinary Applied Mathematics, 18.* Springer-Verlag, New York, 2003.

[24] M. Neubert, M. Kot and M. A. Lewis. *Dispersal and pattern formation in a discrete-time predator-prey model.* Theoretical Population Biogy, 48(1) (1995): 7–43.

[25] H. F. Nijhout, P. K. Maini, A. Madzvamuse, A. J. Wathen and T. Sekimura. *Pigmentation pattern formation in butterflies: experiments and models.* Comptes Rendus Biologies 2003; 326(8): 717–727. PMID: 14608692

[26] L. E. Payne. *New isoperimetric inequalities for eigenvalues and other physical quantities.* Comm. Pure Appl. Math. 9 (1956), 531–542.

[27] R. G. Plaza, F. Sánchez-Garduño, P. Padilla, R. A. Barrio and P. K. Maini. *The effect of growth and curvature on pattern formation.* J. Dynam. Differential Equations 16 (2004), no. 4, 1093–1121.

[28] J. A. Sherratt, B. T. Eagan and M. A. Lewis. *Oscillations and chaos behind predator-prey invasion: mathematical artifact or ecological reality?* Philos Trans. R. Soc. London Ser. B 352 (1997) 21–38.

[29] S. Y. Slavyanov and N. A. Veshev. *Structure of avoided crossings for eigenvalues related to equations of Heun's class.* J. Phys. A 30 (1997), no. 2, 673–687.

[30] G. Sweers. *On sign preservation for clotheslines, curtain rods, elastic membranes and thin plates.* Jahresber. Dtsch. Math.-Ver. 118 (2016), no. 4, 275–320.

[31] A. M. Turing. *The chemical basis of morphogenesis.* Philos. Trans. Roy. Soc. London Ser. B 237 (1952), no. 641, 37–72.